Style Definition: Normal: Font: English (United Kingdom), Justified, Line spacing: 1,5 lines

Style Definition: Header: Font: English (United Kingdom), Justified, Line spacing: 1,5 lines, Tab stops: 8 cm, Centred + 16 cm, Right + Not at 8,25 cm + 16,51 cm

Style Definition: List Paragraph: Font: (Default) Times New Roman, 10 pt, English (United Kingdom), Justified, Space After: 0 pt, Line spacing: 1,5 lines

Style Definition: Affiliation: Font: 10 pt, English (United Kingdom), Justified, Don't add space between paragraphs of the same style

Style Definition: Placeholder Text: Font colour: Grey

Style Definition: Balloon Text: Font: (Default) Tahoma, 8 pt, English (United Kingdom), Justified

Style Definition: Footer: Font: English (United Kingdom), Justified, Tab stops: 7,96 cm, Centred + 15,92 cm, Right + Not at 8,25 cm + 16,51 cm

Style Definition: Authors: Font: Not Bold, English (United Kingdom), Justified, Space Before: 9 pt, After: 0 pt, Don't add space between paragraphs of the same style

Style Definition: Unresolved Mention: Font colour: Custom Colour (RGB(96;94;92)), Pattern: Clear (Custom Colour (RGB(225;223;221)))

Style Definition: Title: Font: +Headings (Times New Roman), 28 pt, Not Bold, English (United Kingdom), Left, Space After: 4 pt

Style Definition: Reference: English (United Kingdom)

Style Definition: Text: English (United Kingdom)

Style Definition: Figure or Table Caption: English (United Kingdom)

Style Definition: Heading-Main: English (United Kingdom)

Style Definition: Key Points: English (United Kingdom)

Style Definition: Abstract: English (United Kingdom)

Style Definition: Note: English (United Kingdom)

Style Definition: Normal (Web): English (United Kingdom)

Style Definition: Comment Text: English (United Kingdom)

Style Definition: Bibliography: English (United Kingdom), Indent: Left: 0 cm, Hanging: 1,27 cm, Line spacing: Double

Style Definition: Revision

~~Budgets of~~Dissecting particulate organic carbon budgets in the mesopelagic ~~layer across contrasting~~ North Atlantic ~~Ocean biomes: a model study with~~: Mechanistic diagnosis using PISCESv2_RC and observations

M. A. Orihuela – García[1,2,3], Y. Ruprich-Robert, V. Lapin[1], S. Loosveldt[1], Raffaele Bernardello[1], M. Samsó-Cabré[1], P.A. Bretonnière[1], Miguel Castrillo[1] and M. Galí[3]

[1]Barcelona Supercomputing Center (BSC), Plaça d'Eusebi Güell, 1–3, 08034 Barcelona, Catalonia, Spain
[2] Universitat Politècnica de Catalunya (UPC), UPC Campus Nord, Carrer de Jordi Girona, 1-3, Les Corts, 08034 Barcelona, Catalonia, Spain
[3] Institut de Ciències del Mar (ICM), Pg. Marítim de la Barceloneta, 37, Ciutat Vella, 08003 Barcelona, Catalonia, Spain

~~Corresponding author~~*Correspondence to*: Mª Andrea Orihuela García (andrea.orihuela@bsc.es) and Martí Galí (mgali@icm.csic.es)

~~**Key Points:**~~

- ~~We quantify detrital particle budgets (0–1000 m) using NEMO4-PISCESv2_RC and compare results to satellite, Argo float and ship-based data~~
- ~~Gravitational export of large detritus triggers zooplankton ingestion and fragmentation, decreasing transfer efficiency in productive waters~~
- ~~Small detritus, supplemented by aggregate fragmentation and vertical mixing, support ~60% of mesopelagic POC decay across regions~~

Abstract

. Biogeochemical and physical processes in the mesopelagic layer regulate ~~the~~ long-term carbon storage ~~of photosynthetic carbon~~ in the ocean interior. However, ~~persisting~~ uncertainties in ~~the budgets of~~ particulate organic carbon (POC) ~~underscore our limited~~budgets limit quantitative understanding of ~~mesopelagic ecosystem functioning in relation to~~ the biological carbon pump~~. This study examines the drivers of POC variability in the top~~ and its representation in models. Here we analyse POC budgets simulated by NEMO4–PISCESv2_RC in the upper 1000 m of the North Atlantic ~~Ocean~~ over a climatological seasonal cycle~~. Budgets of detrital POC are comprehensively analyzed using the NEMO4-PISCESv2 model, which features two classes of detritus with different sinking speeds, a variable reactivity scheme for POC decay, and diverse modes of zooplankton detritivory and particle aggregation-disaggregation processes. Results reveal a latitudinal shift in detrital POC supply and removal dynamics. In the subtropical area, PISCES depicts relatively simple budgets where gravitational supply is mostly balanced by microbial degradation. By contrast, higher latitudes exhibit marked seasonal succession in supply and removal processes. From February through April, POC diffusion by vertical mixing dominates~~, diagnosing the mechanisms that regulate POC export and transfer efficiency. Gravitational POC export ~~fluxes, supplementing gravitational export (by 37% annually in the~~ and the contribution of large detritus increase poleward, while winter-spring mixing supplies an additional 37% to the subpolar ~~area). During bloom demise in summer, consumption and fragmentation of large aggregates by mesozooplankton explain up to half of the flux attenuation. Interestingly, the lowest~~

Formatted: Font: 14 pt, Condensed by 0,5 pt, Kern at 14 pt
Formatted: Font: 14 pt, Condensed by 0,5 pt, Kern at 14 pt
Formatted: MS title
Formatted: Font: 14 pt, Condensed by 0,5 pt, Kern at 14 pt
Formatted: Font: 14 pt, Condensed by 0,5 pt, Kern at 14 pt
Formatted: Superscript
Formatted: Font colour: Auto
Formatted: Font colour: Auto
Formatted: Font colour: Auto
Formatted: Font colour: Auto

mesopelagic transfer efficiency (11%) occurs in midlatitudes, theregion. Up to 60% of mesopelagic POC supply is intercepted by zooplankton, yet most productive area. Optimal detritus removalis recycled to detritus through fragmentation and trophic processing. This detrital loop modulates particle size, sinking speed, and degradation pathways, and is seasonally reinforced at midlatitudes results from opposed latitudinal gradients inmid-high latitudes. Exported POC becomes more labile toward high latitudes, whereas temperature and particle lability, concurrent with high zooplankton activity. Our results prompt more explicit representation of suspended and slow sinking particle dynamics, and detritus-organism interactions, in biogeochemical models.

Plain Language Summary

Tiny algae absorb dissolved carbon in the sea, using sunlight to transform it into organic material. Some of this material reaches deeper layers as particles, called detritus, including dead organisms and feeding remains. Detritus are consumed by animals or decomposed by bacteria and only a small amount reaches the deep ocean. -driven decay rates decline poleward. These processes, termed theopposing gradients yield maximal mesopelagic POC flux attenuation at midlatitudes, coincident with peak productivity. Small detritus play a central role: they sustain ~55% of mesopelagic POC decay and drive 33–50% of export at 1000 m, reflecting substantial biological supply and a pronounced vertical decline in lability. Evaluation against satellite, Argo-float, shipboard and sediment trap data indicates generally realistic POC stocks and fluxes. Nonetheless, the model overestimates the diatom fraction at mid–high latitudes, exhibits compensation between too-low primary production and excessive epipelagic export in the subtropics, and underestimates mesopelagic POC at mid and low latitudes. We propose POC budget analysis as a mechanistic framework for identifying structural biases and constraining inter-model spread in projections of the biological particulate carbon pump, control how much carbon the ocean can store. Using the NEMO4-PISCESv2 model, we explored how different factors — like particle settling velocities, mixing, microbial degradation rates, and animal feeding — affect this process in the North Atlantic. We found that in warmer, southern waters particles degrade faster at shallow depths, but more of them survive the journey through the twilight zone. Contrastingly, particles in colder northern waters are more affected by animals that feed on them, decreasing the sinking flux and favoring microbial decomposition. Seasons also matter — during winter, deep mixing of water moves organic material downward and provides food for organisms in deeper layers before large particles from algal blooms start sinking during the productive season. Our study shows that all these transformation processes need to be considered to understand how the ocean stores organic carbon and predict how it can evolve in the future..

Short Summary. We use a biogeochemical model to examine how particulate organic carbon (POC) is produced, transformed and transported to the deep ocean. Vertical flux attenuation arises from several interacting processes: export pathways, particle lability, temperature-dependent degradation, and zooplankton transformations, leading to strongest attenuation in the most productive region. Together with extensive comparison to observations, such a budgeting approach can help constrain model projections.

Formatted: Normal, Left

1. Introduction

Through photosynthesis, phytoplankton fix inorganic carbon (C) ~~to create~~into organic matter that fuels ~~the~~ marine food ~~chain~~webs (Lindeman, 1942). This organic matter flows in particulate form through trophic interactions between microbial primary producers (phytoplankton), their protist and metazoan predators (zooplankton), and detrital particles~~. All living and non-living particles are~~ collectively termed particulate organic carbon (POC). A fraction of ~~the~~ primary production is released ~~to the~~as dissolved organic carbon (DOC~~) pool. While most DOC is respired and remineralized by heterotrophic prokaryotes~~); in addition to being remineralised to dissolved inorganic carbon (DIC) and nutrients, ~~a portion of it~~DOC can re-~~enters~~enter the particulate pool via the microbial loop (Pomeroy, 1974).

~~A variable portion of the POC created in surface waters escapes from being recycled in the upper ocean and is exported to deeper layers through gravitational sinking and other transport mechanisms (Boyd et al., 2019), contributing to long-term C storage by the ocean (Eppley & Peterson, 1979; Volk & Hoffert, 1985; Kwon et al., 2009). Additional downward C fluxes are channelled by the gravitational sinking of biogenic particulate inorganic carbon (PIC)~~A portion of surface POC escapes rapid recycling in the upper-ocean and is transferred to depth via gravitational sinking and other transport mechanisms Eppley & Peterson, 1979; Volk & Hoffert, 1985; Kwon et al., 2009; Boyd et al., 2019). Additional vertical fluxes include biogenic particulate inorganic carbon sinking (Honjo, 1980; Neukermans et al., 2023) and ~~by the physical~~ DOC transport ~~of DOC~~ (Jiao et al., 2010)~~. The ensemble of the biology-mediated processes that transfer POC, PIC, and DOC to the deep ocean is known as the biological C pump (Volk & Hoffert, 1985; Legendre, 2024). Here we focus on the POC-driven component of the biological C pump.~~

~~Most of the POC export flux originating from the upper ocean layer is attenuated by biological processes within the mesopelagic or twilight zone~~. The vertical transfer of biogenic carbon pools, and their gradual transformation to DIC and subsequent storage in the ocean interior, constitute the biological carbon pump (Volk & Hoffert, 1985; Marinov et al., 2008; Legendre, 2024; Frenger et al., 2024). Here, we focus on its particulate organic component.

POC export to depth occurs through multiple pathways, including "passive" gravitational sinking (Volk & Hoffert, 1985), turbulent mixing and diffusion (Gardner et al., 1995; Bol et al., 2018), advection (Levy et al., 2013), and "active" transport by diel and seasonal zooplankton migrations (Jónasdóttir et al., 2015; Brun et al., 2019; Gorgues et al., 2019). Once in the mesopelagic, POC is transformed by zooplankton detritivory (Giering et al., 2014) and particle aggregation-disaggregation processes (Mayor et al., 2014; Takeuchi et al., 2019; Briggs et al., 2020), and ultimately removed through bacterial degradation (Belcher et al., 2016). As a result, the vertical POC flux is predominantly attenuated in the mesopelagic zone (~100-1000 m; ~~(Martin et al., 1987), which spans between the bottom of the productive (or epipelagic) layer and ~1000 m depth. Hence, the~~

Formatted: Font: 10 pt
Formatted: Font: 10 pt
Formatted: Left
Formatted: Font: 10 pt
Formatted: Font: 10 pt
Formatted: Font: 10 pt
Formatted: Font: 10 pt
Formatted: Font: 10 pt
Formatted: Font: 10 pt
Formatted: Font: 10 pt
Formatted: Font: 10 pt
Formatted: Font: 10 pt
Formatted: Font: 10 pt
Formatted: Font: 10 pt
Formatted: Left
Formatted: Font: 10 pt
Formatted: Font: 10 pt, English (United Kingdom)
Formatted: Font: 10 pt

~~mesopelagic zone largely controls how much C escapes short-term remineralization and subsequent atmospheric~~Martin et al., 1987). The balance between vertical transfer and remineralisation regulates carbon storage, nutrient regeneration (Rodgers et al., 2024), and sea-air CO_2 exchange (Ricour et al., 2023), ~~helping mitigate global warming~~thereby influencing climate feedbacks (Kwon et al., 2009; Le Quéré et al., 2016). ~~The balance between export and remineralization also regulates nutrient delivery pathways and, thus, upper ocean productivity and its response to global anthropogenic change (Rodgers et al., 2024).~~

~~POC is exported from the epipelagic layer mostly by "passive" gravitational sinking (Volk & Hoffert, 1985), but also by turbulent mixing (Gardner et al., 1995; Bol et al., 2018) and vertical advection. In addition, diel and seasonal zooplankton migrations give rise to the "active" fluxes~~POC spans a broad size spectrum, from hundred nm to ~~(Jónasdóttir et al., 2015; Brun et al., 2019; Gorgues et al., 2019). Within the mesopelagic layer, bacterial degradation (Belcher et al., 2016), zooplankton detritivory (Giering et al., 2014) and particle aggregation-disaggregation processes (Mayor et al., 2014; Takeuchi et al., 2019; Briggs et al., 2020) are key drivers of POC dynamics. Together, these processes determine the vertical fluxes over the seasonal cycle, and the amount, size distribution and biological reactivity of the POC exported below 1000 m.~~

~~POC comprises a wide range of particle sizes, from a hundred nm to a few~~ mm (Stemmann & Boss, 2012). ~~Although most of the POC stock is found in particles smaller than 100 µm (typically >85%; Baker et al., 2017~~Large particles (>100 µm), including phytodetrital aggregates and faecal pellets with their microbial colonisers (Kiørboe et al., 2003) dominate fast gravitational export due to their fast settling velocities in the order of tens to hundreds of m d^{-1} (Stemmann & Boss, 2012). In contrast, small particles (<100 µm), which comprise >85% of the POC stock (Baker et al., 2017; Galí et al., 2022) ~~that are suspended or sink slowly (<10 m d^{-1}), the large particles (roughly >100 µm, including phytodetritus and fecal pellets with their microbial colonizers; Kiørboe et al., 2003), are the main vectors of POC export due to their fast settling velocities in the order of tens to hundreds of m d^{-1} (Stemmann & Boss, 2012). Yet, since suspended POC is more abundant than sinking fractions, small POC is expected to dominate non-gravitational export fluxes, e.g. due to turbulent diffusion (the so-called "mixed layer pump;~~are mostly suspended or sink slowly (<10 m d^{-1}). However, owing to their large standing stocks, small particles contribute substantially to non-gravitational export pathways, such as turbulent diffusion —the so-called "mixed layer pump" (Giering et al., 2016; Lacour et al., 2019)— and advection (Alonso-González et al., 2009).

Formatted: Font: 10 pt

Formatted: Font: 10 pt

Formatted: Font: 10 pt

Formatted: Font: 10 pt

Formatted: Font: 10 pt, English (United Kingdom)

Formatted: Font: 10 pt

Formatted: Left

Formatted: Font: 10 pt

Formatted: Font: 10 pt

Formatted: Font: 10 pt

~~The~~Particle size ~~spectrum of POC~~ is ~~inherently~~ linked to ~~its~~ reactivity, ~~i.e., the mass-specific decay rate of POC, ultimately~~ reflecting variations in ~~the particles'~~ composition, age and bioavailability ~~(Kharbush et al., 2020; Johnson et al., 2020) and bioavailability (Giering et al., 2014). Maximal POC reactivity (or "freshness") is expected in the upper ocean, where living organisms may dominate the total~~ (Walker et al., 2016; Kharbush et al., 2020; Johnson et al., 2020). In surface waters, living organisms may dominate the POC pool, especially in productive settings (Gasol et al., 1997)~~. Although~~, whereas the proportion of detrital POC increases with depth. However, uncertainties in POC apportionment ~~remain~~persist, especially ~~through~~in the mesopelagic zone (Galí et al., 2022; Koestner et al., 2024). As particles undergo biotic and abiotic transformations, their size, sinking velocity and reactivity may vary in concert along the water column. ~~Slow-sinking detritus are more exposed to biological transformation and degradation in the upper ocean owing to their longer residence times. Therefore, sinking-reactivity models (Aumont et al., 2017) predict slow-sinking detritus to become refractory at shallower depths than fast-sinking particles. In fact, several particle injection processes may disrupt such a vertical reactivity continuum~~Slow-sinking detritus experiences longer residence times in the upper ocean and is more exposed to biological transformation. Therefore, sinking-reactivity models (Aumont et al., 2017) predict slow-sinking detritus to become refractory at shallower depths than fast-sinking ones.

~~The~~Observationally, POC export and mesopelagic transformation are difficult to quantify due to the intermittency (Berger & Wefer, 1990) ~~and~~, seasonality ~~associated with POC export events~~ (De Melo Viríssimo et al., 2024), ~~as well as their~~and fine spatial ~~scale~~scales (Bol et al., 2018; Briggs et al., 2020; Lacour et al., 2023)~~, make a thorough observation of POC cycling challenging, especially in the ocean interior. For example,~~ of POC export events. For instance, annual mean export estimates can carry uncertainties of up to ±60% in strongly seasonal regions (Henson et al. ~~(~~2015) ~~quote that significant errors in annual mean export estimates—reaching up to ± 60%—can result from overlooking temporal variability in export efficiency, especially in regions with strong seasonality. Knowledge of the lifestyle and bioenergetics of mesopelagic bacteria and zooplankton, which controls the fate of POC in the mesopelagic layer, is also insufficient~~. Additional challenges arise from limited quantitative knowledge about mesopelagic bacteria and zooplankton activities (Arístegui et al., 2009; Hernández-León et al., 2019)~~. As a consequence, difficulties in closing mesopelagic POC budgets persist (Giering et al., 2014). Potential pitfalls include missing~~, missing or poorly quantified POC inputs (Boyd et al., 2019), biases in metabolic measurements (Burd et al., 2010), and temporal ~~mismatch~~mismatches between POC inputs and losses (Uchimiya et al., 2018). Together, these limitations hinder closure of mesopelagic POC budgets using observations alone (Giering et al., 2014).

Formatted: Font: 10 pt
Formatted: Font: 10 pt
Formatted: Font: 10 pt
Formatted: Font: 10 pt
Formatted: Left
Formatted: Font: 10 pt
Formatted: Font: 10 pt
Formatted: Font: 10 pt
Formatted: Font: 10 pt
Formatted: Font: 10 pt
Formatted: Font: 10 pt
Formatted: Font: 10 pt
Formatted: Font: 10 pt
Formatted: Font: 10 pt
Formatted: Left
Formatted: Font: 10 pt
Formatted: Font: 10 pt
Formatted: Font: 10 pt
Formatted: Font: 10 pt
Formatted: Font: 10 pt, Spanish (Spain)
Formatted: Font: 10 pt
Formatted: Font: 10 pt, Spanish (Spain)
Formatted: Font: 10 pt
Formatted: Font: 10 pt
Formatted: Font: 10 pt

Despite ~~important~~recent advances in ~~the observation of~~observing POC stocks (Claustre et al., 2021), export fluxes (Henson et al., 2024), and biological turnover rates (Bressac et al., 2024), ~~in situ observations still lack the spatial and temporal resolution required for accurate~~comprehensive quantification of ~~key~~POC fluxes~~. Ocean~~ across regions and seasons remains elusive. Therefore, ocean biogeochemistry models are ~~valuable~~essential tools to mechanistically ~~understand the myriad of interacting processes that regulate the biological C pump. Through the simplified mathematical representation of reality~~integrate physical transport, ecosystem structure and biogeochemical transformations (Fennel et al., 2022; Henson et al., 2022), ~~models allow us to access~~ enabling exploration of spatiotemporal scales~~, but also~~ and processes~~, whose measurement cannot be afforded by~~ that are inaccessible to observations alone. Here, we ~~undertake a detailed analysis of~~ investigate mesopelagic POC dynamics ~~in the top 1000 m of the~~ and budgets using the NEMO 4.0.4–PISCESv2_RC coupled model, focusing on the North Atlantic ~~ocean, a~~ data-rich region ~~characterized by~~ with sharp ~~hydrographic and~~ biogeochemical gradients~~, with a detailed focus on the mesopelagic budgets of detrital POC simulated with the NEMO 4.0.4-PISCESv2_RC model~~.

~~In comparison~~Compared to other ~~biogeochemical~~ models participating in the Coupled Model Intercomparison Project (CMIP) (Henson et al., 2022)~~, PISCESv2_RC incorporates unique features like (i) a reactivity continuum (or variable reactivity) scheme (Boudreau & Ruddick, 1991) for POC, reproducing the decrease in mass-specific degradation rates with depth~~ , PISCESv2_RC incorporates several distinctive features relevant to mesopelagic POC cycling: (i) a variable reactivity or reactivity continuum (RC) scheme (Boudreau & Ruddick, 1991) that simulates vertical changes in small and large POC reactivity (Aumont et al., 2017)~~; (ii) zooplankton detritivory via both phagotrophic particle ingestion and flux feeding (sinking flux interception); (iii) fragmentation of large detritus into small ones by mesozooplankton (a function of flux feeding rates and aggregate composition) and bacteria (implicitly representing the solubilization of aggregate-binding polymers); and (iv) abiotic aggregation-disaggregation dynamics that interconvert between DOC and detrital POC. These features improve the simulation of POC abundance and size distribution compared to observational data (Aumont et al., 2017; Galí et al., 2022), while enabling a detailed examination of the interplay between food web and physical processes.~~

; (ii) explicit zooplankton detritivory through both phagotrophic particle ingestion and flux feeding; (iii) parameterisations for fragmentation of large detritus by mesozooplankton and bacterial processes; and (iv) abiotic aggregation-disaggregation dynamics that interconvert between DOC and detrital POC.

Future projections of productivity, export efficiency (EE), and transfer efficiency (TE) under climate change diverge widely in both magnitude and spatial patterns (Wilson et al., 2022; Doney et al., 2024; Wang & Fennel, 2024; Walker & Palevsky, 2025; Doléac et al., 2025). These discrepancies reflect differences in the representation

Formatted: Font: 10 pt
Formatted: Font: 10 pt
Formatted: Font: 10 pt
Formatted: Left
Formatted: Font: 10 pt
Formatted: Font: 10 pt
Formatted: Font: 10 pt
Formatted: Font: 10 pt
Formatted: Font: 10 pt
Formatted: Font: 10 pt
Formatted: Font: 10 pt
Formatted: Font: 10 pt
Formatted: Font: 10 pt
Formatted: Font: 10 pt
Formatted: Font: 10 pt
Formatted: Font: 10 pt
Formatted: Font: 10 pt
Formatted: Font: 10 pt
Formatted: Font: 10 pt
Formatted: Font: 10 pt
Formatted: Font: 10 pt
Formatted: Font: 10 pt

of physical circulation and particle export, remineralisation, and food-web structure (e.g., Walker & Palevsky, 2025; Brabson et al., 2025). As PISCES underpins several CMIP model configurations, a detailed diagnosis of its detrital POC budgets in a relatively well-observed region like the North Atlantic is essential for interpreting inter-model spread and identifying structural and parametric biases relative to observations.

The objectives of this study are to:

- ~~Analyze~~Analyse the variability of ~~model-derived~~modelled POC stocks and fluxes ~~along the water column~~ in the ~~low-, mid- and subpolar latitudes~~upper 1000 m of the North Atlantic, ~~comparing~~from subtropical to subpolar latitudes, and evaluate them ~~to~~against available observations from ~~both~~ satellites, autonomous floats ~~and,~~ shipboard surveys and sediment traps.
- Quantify the budgets of small and large detrital POC ~~within~~in the dynamically consistent framework provided by NEMO–PISCESv2_RC, accounting for the ~~mesopelagic layer of each region, considering the entire~~full suite of simulated food-web and physicochemical process rates (sources and sinks~~),~~) and various physical transport modes.
- ~~Study~~ Dissect the mechanistic drivers of the biological ~~C~~particulate carbon pump ~~efficiency~~ across ~~regions in the~~ contrasting North Atlantic biogeochemical regimes using the epipelagic export efficiency (EE) and mesopelagic transfer efficiency (TE) metrics.

2. ~~Materials and~~ Methods

2.1. ~~Coupled model~~ Model configuration and simulation setup

We use the dynamical ocean model NEMO 4.0.4 ~~(~~Nucleus ~~or~~for European Modelling of the Ocean; Madec, 2008), coupled with the sea-ice model SI^3 (Vancoppenolle et al., 2009) and the biogeochemical model PISCESv2_RC (Pelagic-Interactions Scheme for Carbon and Ecosystem Studies; Aumont et al., 2015, 2017). Hereinafter, we will use the terms NEMO and PISCES ~~as shorthands for~~to refer to NEMO 4.0.4 ~~(released on 29-10-2020)~~ and the version of PISCESv2_RC released alongside it (Table 1). NEMO and PISCES are coupled through the Tracers in Ocean Paradigm (TOP~~), the passive~~) tracer ~~engine of NEMO~~manager ~~(NEMO TOP Working Group, 2018).~~(NEMO TOP Working Group, 2018), which performs advective and diffusive transports of both physical and biogeochemical tracers (see details in SI text S1).

~~We used the same advection scheme, named second order Flux Corrected Transport (FCT), for both biogeochemical and physical tracers to maximize consistency in their dynamics. By default, NEMO uses FCT whereas PISCES uses the Monotonic Upstream centered Scheme for Conservation Laws (MUSCL) (see Lévy et al., 2001). Lateral diffusion is performed with a forward Laplacian operator on both tracers and momentum; vertical mixing (diffusion) is parameterized using the turbulent kinetic energy (TKE) closure scheme; convection triggered by unstable stratification is represented with an enhanced vertical diffusion scheme (NEMO System Team, 2019).~~

Formatted: Font: 10 pt
Formatted: Left
Formatted: Left, Space After: 10 pt
Formatted: Font: 10 pt
Formatted: Font: 10 pt
Formatted: Font: 10 pt
Formatted: Font: 10 pt
Formatted: Left
Formatted: Font: 10 pt
Formatted: Font: 10 pt
Formatted: Font: 10 pt
Formatted: Font: 10 pt
Formatted: Font: 10 pt
Formatted: Font: 10 pt

Table 1. *Abbreviations used in the text and their definitions*

Abbreviations	Description
NEMO	Nucleus for European Modelling of the Ocean (Madec et al., 2008) version 4.0.4
PISCES	Pelagic-Interactions Scheme for carbon and Ecosystem Studies (Aumont et al., 2015) version 2 with POC Reactivity Continuum scheme, PISCESv2_RC (Aumont et al., 2017)
NPP	Vertically integrated Net Primary Production rate
PP	Volumetric Net Primary Production rate
POC	Particulate Organic Carbon
sdetoc[1]	Small detrital particles
ldetoc[1]	Large detrital particles
phydiat[1]	Diatom biomass
phymisc[1]	Miscellaneous small phytoplankton
zmicro[1]	Microzooplankton
zmeso[1]	Mesozooplankton
pkt	Total plankton (phymisc+phydiat+zmicro+zmeso)
DOC	Dissolved Organic Carbon
TOC	Total Organic Carbon
~~PIC~~	~~Particulate Inorganic Carbon~~
DIC	Dissolved Inorganic Carbon
MLD	Mixed Layer depth
EE	Export Efficiency
TE	Transfer Efficiency
Zprod	Bottom of the productive layer
GS	Gravitational Sinking
$ADV_{Z,L}$	Advection: Vertical (Z), Lateral (L)
$DIFF_{Z,L}$	Diffusion: Vertical (Z), Lateral (L)
SPNA	Subpolar North Atlantic
Trans_Area	Transition Area
STNA	Subtropical North Atlantic

[1]~~Fraction~~[1]Biogeochemical model tracer and fraction of POC

~~2.2. Experiment set up~~

~~Global simulations were run on the ORCA1L75 grid, with ca. one-degree horizontal resolution and 75 non-linear vertical levels (of which 24 were in the top 100 m and 22 were between 100-1000 m depth) and with a 45-minute time step for both ocean dynamics and biogeochemistry. The NEMO-PISCES simulation followed the Ocean Model Intercomparison Project (OMIP-2) protocol using JRA-55 reanalysis (Kobayashi et al., 2015) as atmospheric forcing from 1958~~

Formatted ... (repeated 70 times)
Formatted Table ... (repeated 4 times)

~~to 2019. The simulation length is 372 years, repeating six cycles of the 62 year (1958–2019) JRA55 forcing dataset (Tsujino et al., 2018). The first two cycles consisted of NEMO only simulations, and PISCES was coupled at the beginning of the third cycle. A biogeochemical spin-up was performed by cycling 21 times through the same ocean circulation, corresponding to the third cycle (21 cycle x 62 year = 1302 years) while letting the biogeochemical tracers equilibrate. The atmospheric CO_2 concentration was fixed at a preindustrial level corresponding to 1850. At the end of the biogeochemical spin-up, global net primary production (NPP) and gravitational export at 100 m stabilised respectively at 50.8 PgC yr^{-1} and 6.86 PgC yr^{-1} and changed by less than 0.01% over successive cycles. After the spin-up, the simulation proceeded with the remaining three cycles, with a prescribed rise in atmospheric CO_2 concentrations during the last 170 years of the simulation matching the one observed over the 1850–2019 period. Only results from the last cycle (1958–2019), averaged into a monthly climatology, are analysed here, focusing on the North Atlantic.~~

Global simulations were run on the ORCA1L75 grid (~1° horizontal resolution, 75 non-linear vertical levels) with a 45-minute time step for ocean dynamics and biogeochemistry. The simulation followed the Ocean Model Intercomparison Project protocol (OMIP-2; Tsujino et al., 2018) and was forced by the JRA-55 atmospheric reanalysis (Kobayashi et al., 2015). After initialisation, biogeochemistry was spun up for 1302 years under recurring circulation and fixed preindustrial atmospheric CO_2. The subsequent transient simulation included rising atmospheric CO_2 concentrations over 1850-2019. Only results from the final 1958–2019 forcing period are analysed here, focusing on the North Atlantic. For comparison with satellite products, a monthly climatology over 1998–2019 was used. Further details are given in the SI text S1.

~~2.3.~~2.2. Biogeochemical model description

PISCES simulates marine planktonic food webs and the biogeochemical cycling of key elements (carbon, nitrogen, phosphorus, silicon, and iron) using 24 tracers that represent living, detrital and inorganic compartments. Here we ~~provide a brief overview~~briefly describe the representation of POC cycling ~~processes~~ in the model, introducing tracer names in italics.

~~PISCES has~~POC is represented by six tracers: two phytoplankton types ~~that represent~~ —miscellaneous small phytoplankton (~~here called~~ *phymisc*) and diatoms (*phydiat*); two zooplankton types ~~that represent~~ — microzooplankton (*zmicro*) and mesozooplankton (*zmeso*); and two ~~classes of detritus, representing~~ detrital pools —small (*sdetoc*) and large (*ldetoc*) particles. ~~Hence, total POC in PISCES comprises the six tracers listed above. Only the detritus suffer gravitational sinking~~ Of these, only detrital tracers sink, with fixed sinking velocities of 2 and 50 m d^{-1} for *sdetoc* and *ldetoc*, respectively. Phytoplankton growth ~~is controlled by~~ depends on light availability and ~~the~~ uptake of nitrate, ammonium, phosphate, dissolved iron and, ~~in the case of~~for diatoms, silicate. Phytoplankton is lost through zooplankton grazing~~, represented with~~

Formatted: Font: 10 pt
Formatted: Line spacing: 1,5 lines
Formatted: Left
Formatted: Font: 10 pt
Formatted: Font: 10 pt
Formatted: Font: 10 pt
Formatted: Font: 10 pt
Formatted: Font: 10 pt
Formatted: Font: 10 pt
Formatted: Font: 10 pt
Formatted: Font: 10 pt
Formatted: Font: 10 pt
Formatted: Font: 10 pt
Formatted: Font: 10 pt
Formatted: Font: 10 pt

and linear and quadratic mortality terms (, the latter representing aggregation upon bloom demise). Micro- and mesozooplankton predate on the two . Both zooplankton types prey on phytoplankton types and *sdetoc* with different preferences. Mesozooplankton additionally predates on microzooplankton and consumes *sdetoc* and *ldetoc* via flux feeding.

Detritus areis produced mainly through plankton mortality and zooplankton inefficient ("sloppy") feeding, with different partitioning intobetween *sdetoc* and *ldetoc* depending on the plankton typeorganism and process involved. Detrital particles are degraded to DOC according tousing the variable reactivity scheme of (Aumont et al., . (2017), which represents the spatiotemporal variations of detritusallows decay rate constants "(*k*" (also known as C-specific or exponential decay rates, in , d^{-1}).) to vary in space and time. This scheme prescribes a maximalmaximum *k* of 0.035 d^{-1} at 0ºC for freshfreshly produced detritus in the upper mixed layer. Thereafter, the vertical decrease of With increasing depth, *k* changes with space and time and for each detrital tracer, as it depends on the interplaydecreases as sinking particles lose their most reactive components and become increasingly refractory. This decrease is not prescribed explicitly but emerges from the balance between particle sinking, the local supply of fresh detritus inputs, sinking speed, and the rates at which progressive degradation of 15 lability classes (implicitly modelled throughrepresented by a gamma distribution) are progressively degraded along the water column.. As a result, the vertical profile of k varies among regions, seasons, and detrital size classes. Detritus decay rates also increase as a power function of temperature, approximately doubling every 10ºC (Q10 of 1.9). Here we will refer to Following PISCES terminology, degradation of *sdetoc* and *ldetoc* degradation using the term remineralizationis referred to maintain the model's nomenclatureas remineralisation, although remineralization implies conversion of detrital POC is first converted to DOC before reaching dissolved inorganic carbon (DIC, which in PISCES proceeds through DOC.).

The parametrization for mesozooplanktonMesozooplankton flux feeding and fragmentation is aare key featurefeatures in PISCESv2 (Aumont et al., 2017), but its evolution since older model versions . Given that the current parameterisation differs markedly from those previously described (Gehlen et al., 2006) has not been described. In PISCESv2, flux feeding is performed byhere, we provide an updated description. At each time step, a variable fraction of the mesozooplankton thatbiomass engages in flux feeding. This fraction is diagnosed at each model time step as the proportion betweenratio of flux-feeding rates andingestion to total mesozooplankton ingestion rates. In turn, flux. Flux feeding rates are calculated as the product of flux feeder feeding mesozooplankton biomass, thea flux feeding cross-section parameter, and the sinking flux of each detrital tracer (SI text section S1, eq.S2, Eq. S4). The flux-feeding parameter corresponds to a feeding

~~net with a~~ biomass-~~normalized~~normalised area of 3 m^2 (mol C)$^{-1}$, roughly representative of temperate and subpolar ~~pteropods~~flux feeders (Jackson, 1993; Stemmann et al., 2004b; Stukel et al., 2019).

~~Mesozooplankton fragmentation~~ Fragmentation of large detritus by mesozooplankton is expressed as a variable proportion of flux feeding rates, ~~causing~~resulting in additional attenuation of *ldetoc* ~~vertical~~ fluxes and ~~transferring them~~transfer to *sdetoc*. ~~This variable proportion~~ The ratio between fragmentation and flux feeding increases, from 0.2 to around ~~twice the flux feeding rates~~2, as a function of the ratio ~~between the~~of biogenic silica ~~and~~to *ldetoc* ~~tracer~~ concentrations. ~~Modulation of fragmentation by biogenic silica implicitly accounts for the increased~~This dependence is intended to represent the greater fragility of large detritus ~~when they are~~ composed of diatom aggregates ~~(e.g.,~~compared to more compact forms such as ~~opposed to fecal~~faecal pellets~~).~~.

~~2.4.~~2.3. Detrital POC ~~budget equations~~budgets

We ~~output from our simulation all the~~ diagnosed the full budgets of *sdetoc* and *ldetoc* by outputting all individual terms from ~~the~~their prognostic equations ~~for *sdetoc* and *ldetoc*, i.e., their~~, including sources (production processes), sinks (consumption processes) and transports (Fig. 1). Transports include gravitational sinking and tridimensional advection and diffusion ~~(~~, the latter representing subgrid scale ocean dynamics ~~at subgrid scale)~~. Budgets were computed separately for ~~both~~ the epipelagic and mesopelagic layer in three regions outlined in Fig. 2: the Subpolar North Atlantic (SPNA), the Transition Area (Trans_Area) and the Subtropical North Atlantic (STNA). The boundary between the two layers, Zprod, is defined as the depth ~~where~~at which the annual mean vertical profile of primary production ~~profile decreases~~(PP) falls below 1% of its ~~vertical~~ maximum. For each region, Zprod was fixed ~~in each region~~ to ~~avoid computing~~ensure that budgets were computed over ~~different~~a consistent vertical ~~domains each month~~domain over the seasonal cycle.

For a given region and layer, the budget ~~equations take~~equation takes the generic form~~:~~

$$\frac{\delta[X]}{\delta t} = Sources - Sinks - GS - ADV - DIFF \quad \text{~~(eq~~(Eq. 1)}$$

where Sources and Sinks ~~are the~~represent vertically integrated rates averaged over each region. Transport terms, namely gravitational sinking (GS), advection (ADV) and diffusion (DIFF), are ~~included in the budgets~~expressed as the divergence of the fluxes along the lateral and vertical directions ~~across our domain of interest. The divergence is equivalent~~. Divergence corresponds to the net difference between input and output fluxes through the ~~domain's~~domain boundaries, divided by the domain length in the corresponding direction. Hereafter, ~~we use~~ fluxes across a bounding surface are denoted by F followed by a subscript

Formatted ...
Formatted ...
Formatted: Left
Formatted: Font: 10 pt
Formatted: Line spacing: 1,5 lines
Formatted: Left
Formatted ...
Formatted: Font: 10 pt
Formatted ...
Formatted: Left
Formatted: Font: 10 pt
Formatted ...

~~whenever we refer to fluxes through a surface bounding our domain ((~~(e.g., F_{GS}, F_{ADV}, F_{DIFF})~~, and use~~whereas GS, DIFF and ADV ~~to refer to~~denote the ~~divergence of the fluxes. We also~~associated flux divergences. Subscripts Z and L indicate the vertical ~~(Z)~~ and lateral ~~(L) directions with subscripts to flux and divergence terms~~components, respectively (e.g., F_{ADVZ}, F_{ADVL}, $DIFF_Z$, $DIFF_L$).

We verified ~~the budgets~~budget closure by comparing the simulated tracer ~~trend~~tendency $\frac{\delta[X]}{\delta t}$ ~~to~~with the ~~addition~~sum of all ~~individual sources, sinks~~diagnosed source, sink and ~~transports~~transport terms over ~~a given~~each domain. ~~This test confirmed that budgets~~Budgets were closed both over successive model time steps (within ± $6 \cdot 10^{-4}$ % error) and over monthly periods.

Below, we provide ~~only~~ a qualitative ~~description~~representation of the detrital POC budgets (~~equations~~Eq. 2 and 3). Superscript numbers are used as labels to ~~match the visual and text explanations of~~link terms to Table ~~S3~~S2 and Fig. 1

$$\frac{\delta[sdetoc]}{\delta t} = (\text{mortalities}^{1} + \text{zmicro non assimilation}^{2} + \text{bacterial breakdown of ldetoc}^{3} + \text{DOC aggregation}^{4} + \text{zmeso fragmentation of ldetoc}^{5}) - (\text{zmicro ingestion}^{6} + \text{zmeso ingestion \& flux feeding}^{7} + \text{remineralization}^{8} + \text{sdetoc aggregation}^{9}) - (ADV_L^{10} + ADV_Z^{11} + DIFF_L^{12} + DIFF_Z^{13} + GS^{14}) \quad (\text{~~eq~~Eq. 2})$$

$$\frac{\delta[ldetoc]}{\delta t} = (\text{mortalities}^{15} + \text{meso non assimilation}^{16} + \text{sdetoc aggregation}^{9} + \text{DOC aggregation}^{17}) - (\text{zmeso flux feeding}^{18} + \text{zmeso fragmentation of ldetoc}^{5} + \text{remineralization}^{19} + \text{bacterial breakdown of ldetoc}^{3}) - (ADV_L^{20} + ADV_Z^{21} + DIFF_L^{22} + DIFF_Z^{23} + GS^{24}) \quad (\text{~~eq~~Eq. 3})$$

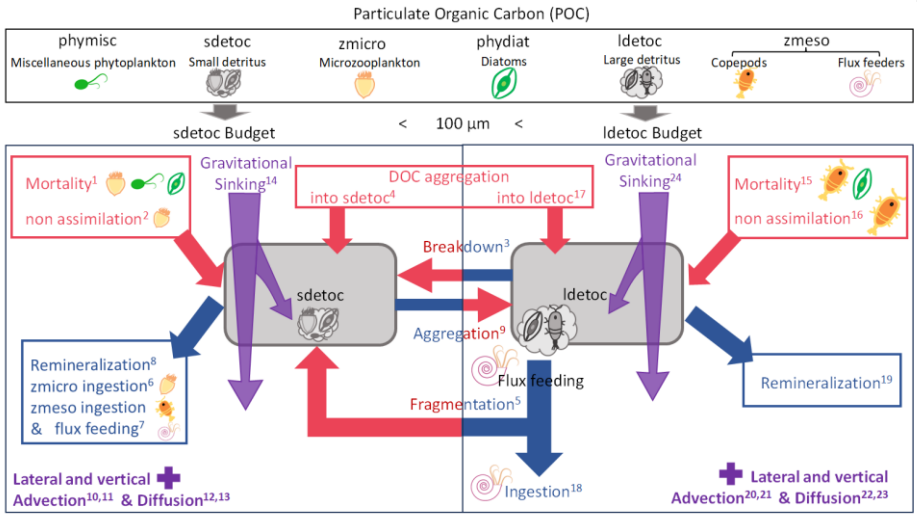

Formatted: Font: 10 pt
Formatted: Font: 10 pt
Formatted: Font: 10 pt
Formatted: Font: 10 pt
Formatted: Font: 10 pt
Formatted: Font: 10 pt
Formatted: Font: 10 pt
Formatted: Font: 10 pt
Formatted: Font: 10 pt
Formatted: Font: 10 pt
Formatted: Font: 10 pt
Formatted: Font: 10 pt
Formatted: Font: 10 pt
Formatted: Font: 10 pt
Formatted: Font: 10 pt
Formatted: Font: 10 pt
Formatted: Font: 10 pt
Formatted: Font: 10 pt
Formatted: Font: 10 pt
Formatted: Font: 10 pt
Formatted: Font: 10 pt
Formatted: Left
Formatted: Font: 10 pt
Formatted: Font: 10 pt
Formatted: Left
Formatted: Font: 10 pt
Formatted: Font: 10 pt

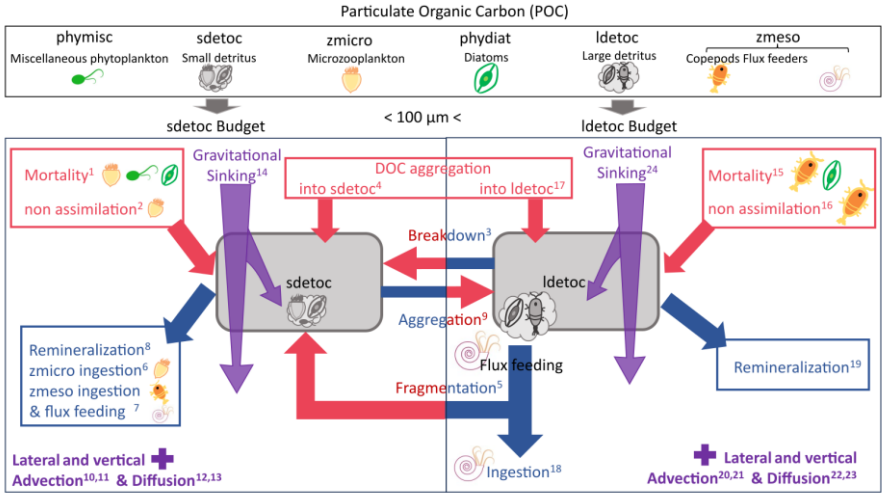

Figure 1. *Schematic of detrital POC dynamics and budgets in the PISCES model. Red arrows represent sources (production processes); blue arrows represent sinks (consumption processes). Purple arrows and tags represent the transport processes, which can supply or remove detritus from the budget. The top panel illustrates the six tracers that form POC in PISCES. Full budgets are ~~analyzed~~analysed only for the detrital tracers (sdetoc and ldetoc), but all POC tracers are included in calculations of vertical non-gravitational fluxes and comparison to observational estimates.*

~~Full model~~The full prognostic equations for *sdetoc* and *ldetoc*, explicitly showing their controlling parameters, are provided in ~~the SI text section S1 because the~~SI Sect. S2, as these equations ~~were already~~have been described previously by Aumont et al. (2015, 2017). ~~Note also that, for simplicity~~For clarity, we lumped together some budget terms that are small and/or follow similar dynamics: (i) *sdetoc* consumption by phagotrophic ingestion and flux feeding; (ii) physical aggregation processes, and (iii) mortality terms. Finally, note that ~~some budget terms~~processes that interconvert between *sdetoc* and *ldetoc* ~~are repeated,~~appear in both budgets with ~~different~~opposite signs~~, in eq. 2 and 3~~.

~~2.5.~~2.4. Export Efficiency (EE) and Transfer Efficiency (TE) metrics

We ~~summarized the~~summarised spatial variations in ~~the functioning of the biological C pump~~vertical POC fluxes using three common metrics. ~~The export~~Export efficiency (EE~~), also known as export ratio, is defined as the ratio between POC export flux through the bottom of the productive~~

~~(epipelagic) layer and the primary production rate integrated over that layer (e.g.,~~; Buesseler, 1998)~~:~~

, also referred to as export ratio, is defined as the ratio between POC export flux through the bottom of the productive (epipelagic) layer and the net primary production rate integrated over that layer (NPP):

$$EE = \frac{F_{Zprod}}{NPP} \quad \text{~~(eq~~(Eq. 4)}$$

Transfer efficiency (TE; François et al., 2002) ~~is calculated as~~quantifies the fractional ~~change in~~transfer of exported POC ~~export fluxes between~~from the ~~bottom~~base of the productive layer ~~and~~to a ~~chosen~~deeper reference depth ~~below it,~~ in our case, the ~~bottom~~base of the mesopelagic layer (1000 m):

$$TE = \frac{F_{Z1000}}{F_{Zprod}} \quad \text{~~(eq~~(Eq. 5)}$$

Vertical POC fluxes at the same two depths bounding the mesopelagic domain were used to calculate Martin's *b* exponent (Martin et al., 1987), often referred to as the flux attenuation coefficient:

$$b = -\frac{ln(F_{Z1000}/F_{Zprod})}{ln(1000/Z_{prod})} \quad \text{~~(eq~~(Eq. 6)}$$

Stronger vertical ~~flux~~ attenuation~~, hence~~ of POC fluxes corresponds to lower TE~~, translates into~~ and larger positive values of *b*. ~~These~~All metrics ~~are~~were calculated ~~only over the~~ using annual~~-~~mean ~~of the~~ climatological ~~vertical~~ fluxes ~~in~~for each region to ~~circumvent~~avoid issues associated with non-steady-state ~~at the~~ seasonal ~~scale~~dynamics (Giering et al., 2017).

To ~~depict the differential~~ assess differences in attenuation ~~of different~~among POC pools, ~~we~~Eq. 4–6 were applied ~~eq. 4–6 to the vertical transports of detritus only~~both to detrital POC fluxes alone (gravitational, diffusive and advective fluxes of *sdetoc* and *ldetoc*) and to ~~the~~ total ~~vertical transport of~~ POC fluxes, which ~~also includes~~ additionally include the diffusive and advective ~~fluxes~~vertical transports of plankton tracers.

~~2.6.~~2.5. Model evaluation

We evaluated ~~**the simulated**~~ model performance using gridded observational products for mixed layer depth (MLD), ~~**NPP and POC against monthly gridded observational estimates**~~vertically integrated net primary production (NPP), phytoplankton carbon biomass, mesozooplankton carbon and small POC (sPOC) stocks, the latter assessed in ~~**each region.**~~both the epi- and mesopelagic layers. After regridding the ~~**observed data**~~observational products onto the ~~**model's**~~model grid (ORCA1_L75), ~~**we computed evaluation**~~model

Formatted: Font: 10 pt
Formatted: Font: 10 pt
Formatted ...
Formatted: Left, Space After: 12 pt
Formatted: Font: 10 pt
Formatted ...
Formatted: Left
Formatted ...
Formatted: Font: 10 pt
Formatted: Left
Formatted: Font: 10 pt
Formatted ...
Formatted: Left
Formatted ...
Formatted: Font: 10 pt
Formatted ...
Formatted: Left
Formatted: Font: 10 pt
Formatted: Line spacing: 1,5 lines
Formatted: Font: 10 pt, Not Bold, Font colour: Auto
Formatted: Font: 10 pt, Not Bold, Font colour: Auto
Formatted ...
Formatted ...

skill was assessed using standard metrics ~~for the~~applied to (i) spatial patterns of annual--mean ~~state~~fields (Fig. 2), and ~~the~~(ii) monthly climatological seasonal ~~cycle~~cycles averaged over each region (Fig. 3). Key characteristics and references for each observational dataset are summarised in Table ~~S4). The model~~ 2. Further evaluation results, including skill metrics (Table S3) and seasonal maps comparing simulated and observed fields (Fig. S2–S3), are presented in the SI.

While some simulated variables have a good correspondence in the observations —most notably MLD and NPP— other comparisons require simplifying assumptions, which are described here. First, modelled phytoplankton is evaluated using a satellite product that resolves three phytoplankton size classes. For this comparison ~~is further illustrated in the SI~~, we assume that satellite microphytoplankton corresponds to model diatoms, and that the sum of pico- and nanophytoplankton corresponds to miscellaneous phytoplankton in the model. This group includes mostly haptophytes and cyanobacteria and, to some extent, dinoflagellates. Although this assumption introduces some uncertainty, it is broadly consistent with wide evidence from size-fractionated biomass measurements, ecophysiological studies, pigment signatures, and bio-optical data, all of which underpin satellite algorithms (Uitz et al., 2006, 2008) and model parameterisations. Second, we assume that the sPOC estimated from bio-optical data corresponds to the sum of four POC tracers with nominal sizes smaller than 100 µm: the two phytoplankton classes, microzooplankton, and small detritus, as previously discussed (Galí et al., 2022). Finally, mesozooplankton is evaluated using an observations-based machine learning product specifically developed for comparison with PISCES mesozooplankton fields (Clerc et al., 2024). No suitable gridded observational products were available for microzooplankton and large detrital POC concentrations.

In the case of sPOC, we used two estimates based on the same observational dataset. The approach of Galí et al. (2022), based on the variable ratio between POC and particulate backscattering, was used to estimate POC between 0–1000 m. For completeness, the method of Koestner et al. (2024), based on the relationship between POC, particulate backscattering and chlorophyll *a*, was used to estimate POC between the surface and the euphotic layer depth (below which gridded chlorophyll *a* data is not available). Hereafter, we refer to these sPOC estimates as G22 and K24, respectively. Additional details on these datasets are provided in SI Sect. S3. ~~seasonal maps (Fig. S2–S5).~~

Simulated export fluxes were ~~also~~ evaluated ~~against observations,~~separately using a ~~match-up (model~~ subsampling~~) strategy because of data sparseness (see 2.6.4).~~ approach designed to account for the sparse and uneven spatiotemporal coverage of the observations. Two complementary data compilations were used (Table 2): (i) Shallow POC export fluxes measured with the ^{234}Th disequilibrium method, mostly at 100–150 m (Le Moigne et al., 2013); (ii) full water-column POC fluxes (Mouw et al., 2016), here restricted to sediment–trap estimates to avoid overlap with the ^{234}Th dataset. Trap deployments longer than 1 month were discarded.

Table 2. *Descriptions of the gridded observational dataset used for the model evaluation.*

Formatted: Font: 10 pt, Not Bold, Font colour: Auto
Formatted: Font: 10 pt, Not Bold, Font colour: Auto
Formatted: Font: 10 pt, Not Bold, Font colour: Auto
Formatted: Font: 10 pt, Not Bold, Font colour: Auto
Formatted: Font: 10 pt, Not Bold, Font colour: Auto
Formatted: Font: 10 pt, Not Bold, Font colour: Auto
Formatted: Font: 10 pt, Not Bold, Font colour: Auto
Formatted: Font: 10 pt, Not Bold, Font colour: Auto
Formatted: Font: 10 pt, Not Bold, Font colour: Auto
Formatted: Font: 10 pt, Not Bold
Formatted: Font: 10 pt, Not Bold
Formatted: Font: 10 pt, Not Bold, Font colour: Auto
Formatted: Font: 10 pt, Not Bold, Font colour: Auto
Formatted: Font: 10 pt, Not Bold, Font colour: Auto
Formatted: Font: 10 pt, Not Bold, Font colour: Auto
Formatted: Heading-Main, Line spacing: 1,5 lines
Formatted: Font: 10 pt, Not Bold, Font colour: Auto
Formatted: Font: 10 pt, Not Bold, Font colour: Auto

Variable	Observational product	Reference	Temporal coverage and resolution	Spatial resolution	Vertical information
MLD	Mixed Layer Depth climatology based on reanalysis observations using a density threshold criterion of 0.03 kg m^{-3} from IFREMER	De Boyer Montégut, (2023)	Climatological fields, monthly	1° global grid	-
NPP	Satellite-derived NPP from the Ocean Colour Climate Change Initiative (OC-CCI) v4.2.	Kulk et al., (2020)	1998–2019, monthly climatology	0.083º global grid	Vertically integrated
Phytoplankton size class carbon biomass (pico-, nano- and microphytoplankton)	Global marine phytoplankton carbon from the ESA BICEP / PHYTO-CCI project, OC-CCI v5-based.	Sathyendranath et al., (2019)	1998–2019, monthly	0.083º global grid	Surface layer
Mesozooplankton biomass	Machine-learning mesozooplankton biomass distribution model (BDM-MAREDAT)	Clerc et al. (2024)	Climatological fields, monthly	1°global grid	Vertically integrated (0–200 m).
sPOC concentration	Global bbp_{700} from the CMEMS MULTIOBS_GLO_BIO_BGC_3D_REP_015_010 product, converted to small POC (sPOC) using the Galí et al. (2022) algorithm (G22).	Sauzède et al., (2016); Galí et al., (2022) Koestner et al., (2024)	1998–2019, monthly 3D fields	0.25° global grid	3D product (36 levels from 0 to 1000 m); vertically integrated (0–200 m and 200-1000 m)
POC export flux	Flux estimates based on ^{234}Th disequilibria and POC/^{234}Th ratios in sinking particles	Le Moigne et al. (2013)	1985-2013	globally distributed sparse	depths <300 m

Variable	Observational product	Reference	Temporal coverage and resolution	Spatial resolution	Vertical information
				measurements	
POC export flux	Flux estimates based on sediment trap deployments	Mouw et al. (2016)	1980-2012	globally distributed sparse measurements	whole water column

Formatted: Font: 10 pt, Font colour: Auto

Formatted: Heading-Main, Line spacing: 1,5 lines

Formatted: Font: 10 pt

~~2.6.1. Results~~

In this section, an overview of ~~Mixed Layer Depth~~

~~A monthly-gridded MLD climatology based on reanalysis of observations was obtained from Ifremer's product (De Boyer Montégut, 2023; last access: July 2023). This MLD climatology uses a density threshold criterion of 0.03 kg m^{-3}. In all regions, the spatially averaged monthly MLD from our simulation shows a strong temporal correlation with the observational product ($R > 0.95$), with minimal relative mean bias (RMB < 6%) and correct timing and amplitude of the annual maxima and minima (Fig. S1 and S2).~~

~~2.6.2. Net primary production~~

~~Satellite-based estimates of net primary production (NPP) were obtained from the Ocean Colour Climate Change Initiative (OC-CCI) v4.2 (last access: October 2021). This dataset offers monthly data from 1998 to 2019 at 9 km resolution (Kulk et al., 2020). The model's NPP (Fig. 3a–c) shows a high correlation ($R \geq 0.95$) with satellite-based estimates in the SPNA and Trans_Area, but with a ~25% annual mean bias in the SPNA that originates mostly from the western subpolar gyre (Fig. S3). Modeled NPP in the Trans_Area shows wider seasonal amplitude than the OC-CCI product, with moderate positive (negative) deviations peaking in late spring (late fall). In the STNA, characterized by narrow seasonal amplitude, the low correlation ($R = -0.01$) and large negative bias (~52.6%) indicate more fundamental model-data discrepancies.~~

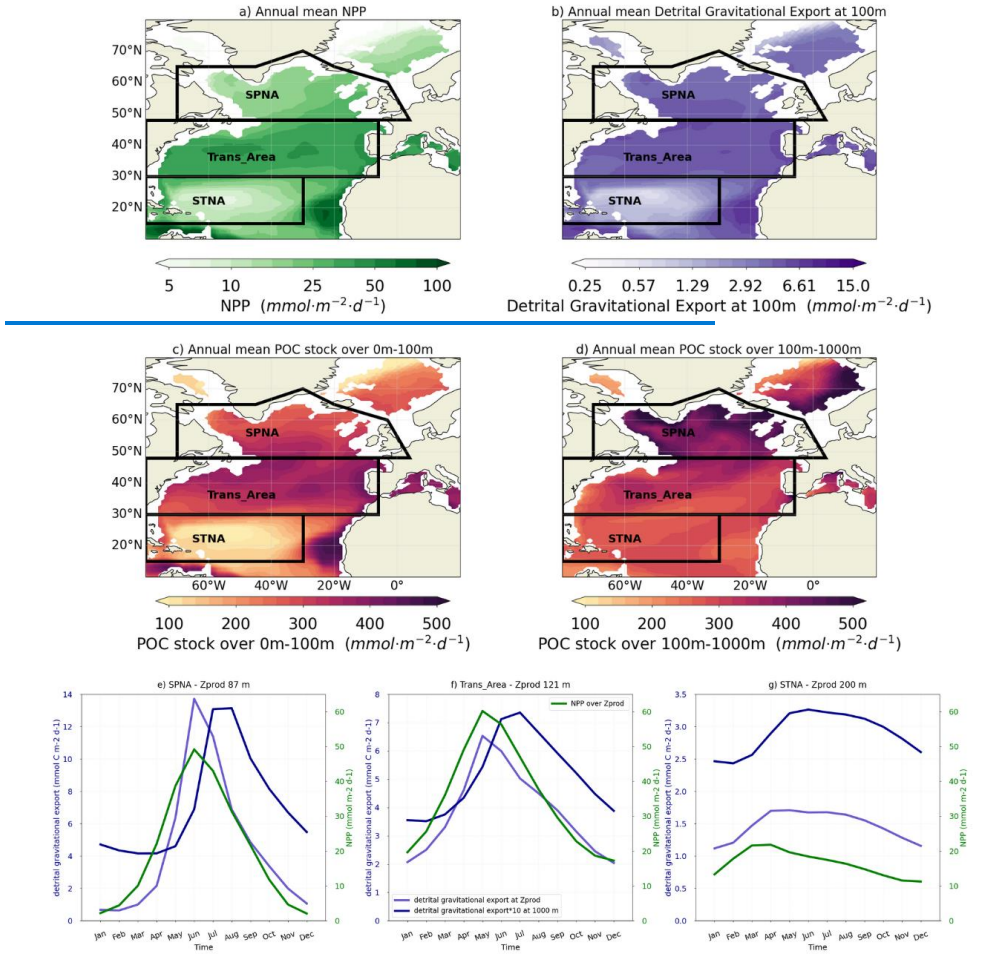

Figure 2: *Annual mean 1998 – 2019 maps of NPP (a), Export flux at 100 m (b), POC stock over the epipelagic layer (0m-100m) (c) and POC stock over the mesopelagic layer (100–1000 m) (d). Region boundaries are indicated with black outlines. Bottom panels (e-g) show, for each region, the seasonal cycle of NPP and the gravitational export flux at the base of the productive layer (Zprod) and at 1000 m.*

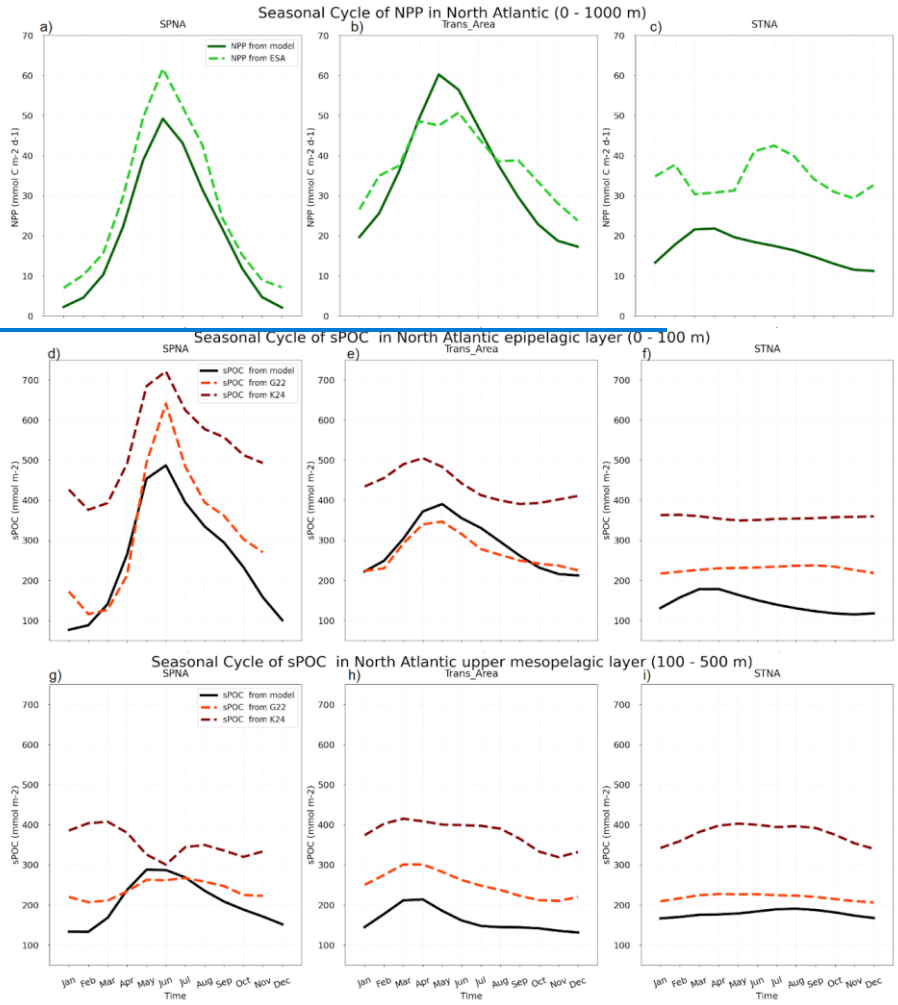

Figure 3. *Seasonal cycle of simulated and satellite-based NPP integrated over the water column (a-c), epipelagic sPOC stock integrated between 0-100 m (d-f), and upper mesopelagic sPOC stock integrated between 100-500m (g-i). Simulations and Earth-observation data are shown with continuous and dashed lines, respectively. Observations-based sPOC stocks are estimated with two different algorithms (see section 2.6.3 for details). Statistics are included in Table S4.*

~~2.6.3. Particulate organic carbon~~

~~3. We compared PISCES output to the MULTIOBS_GLO_BIO_BGC_3D_REP_015_010 product from Copernicus Marine Environmental Monitoring Service (CMEMS; last access: August 2023), based on various Earth observation data as described by Sauzède et al., (2016). Gridded 3D fields of particulate backscattering at 700 nm wavelength ($b_{bp,700}$) provided by CMEMS were used to calculate POC with two different algorithms, hereafter referred as G22 (Galí et al., 2022) and K24 (Koestner et al., 2024). Although the CMEMS dataset includes a POC estimate, here we refrained from using it because it is based on an empirical relationship between POC and $b_{bp,700}$ that tends to overestimate POC in mesopelagic waters, where POC/$b_{bp,700}$ ratios are lower (Bol et al., 2018). The G22 and K24 approaches allow for variations in POC/$b_{bp,700}$ as a function of additional input variables: MLD in the case of G22 (see 2.6.1), and chlorophyll *a* in the case of K24 (obtained from the same CMEMS dataset). Details about the implementation of G22 and K24, including slight modifications to the original methods, are provided in the SI section~~model performance and simulated patterns (3.1), is followed by more detailed descriptions of simulated POC dynamics, including vertical patterns in stocks, export and decay rates (3.2), mesopelagic budgets of detrital POC at annual (3.3) and monthly scales (3.4), and POC export and transfer efficiency metrics (3.4). The data provided in the following text and figures can be found in two summary spreadsheets included in the SI section.

3.1. Model evaluation and overview of spatiotemporal patterns

3.1.1. Mixed Layer Depth (MLD)

Winter mixing depths decrease from the subpolar area (mean MLD of ~240 m in March) to the Trans_Area (~120 m in February) and the subtropical area (~70 m in February). In the three regions, the spatially averaged monthly MLD from the simulation shows a strong temporal correlation with the observations ($r > 0.95$), low relative mean bias (RMB < 6%) and realistic peak timing and amplitude (Fig. S1 and S2, Table S3).

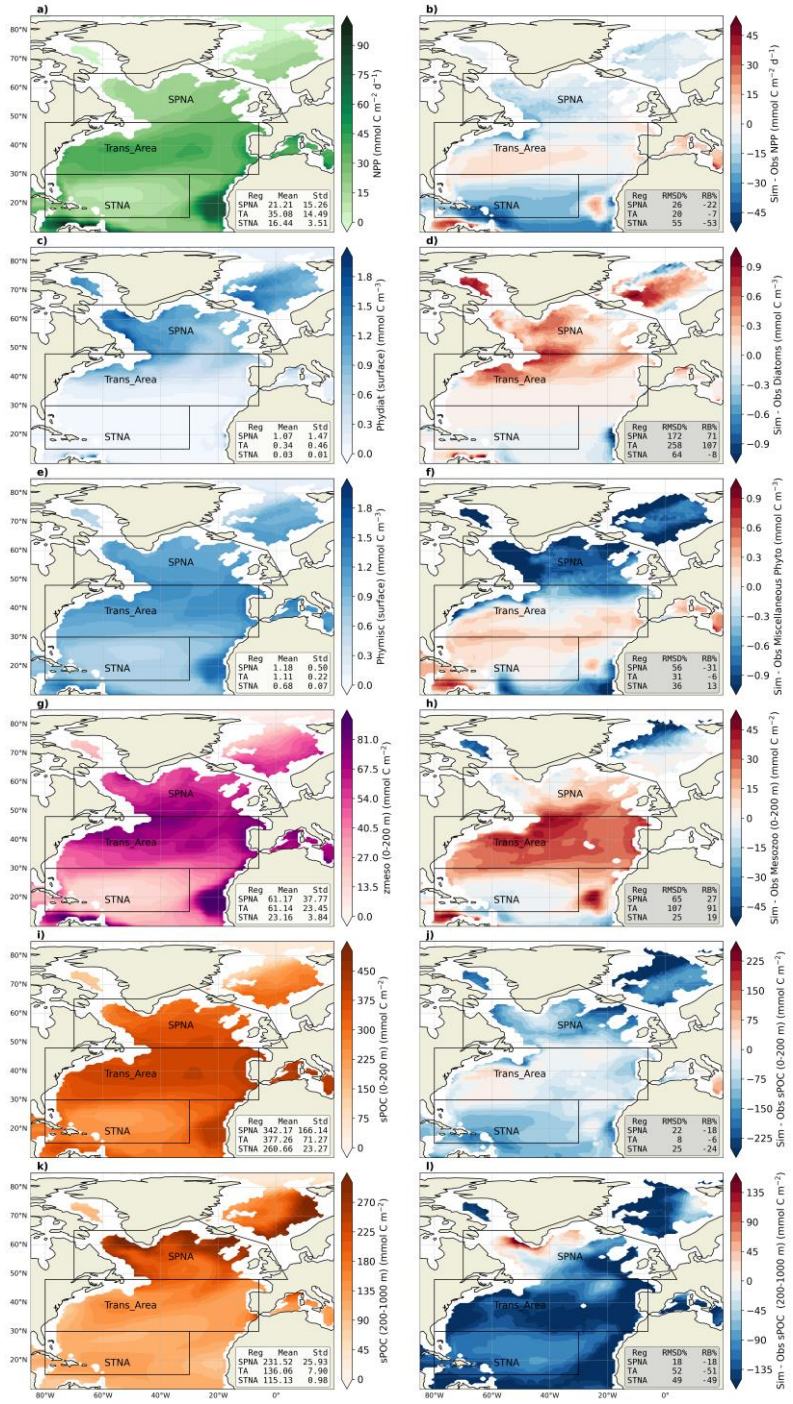
a)
b)
c)
d)
e)
f)
g)
h)
i)
j)
k)
l)
SPNA
Trans_Area
STNA
NPP (mmol C m⁻² d⁻¹)
Sim - Obs NPP (mmol C m⁻² d⁻¹)
Phydiat (surface) (mmol C m⁻³)
Sim - Obs Diatoms (mmol C m⁻³)
Phymisc (surface) (mmol C m⁻³)
Sim - Obs Miscellaneous Phyto (mmol C m⁻³)
zmeso (0-200 m) (mmol C m⁻²)
Sim - Obs Mesozoo (0-200 m) (mmol C m⁻²)
sPOC (0-200 m) (mmol C m⁻²)
Sim - Obs sPOC (0-200 m) (mmol C m⁻²)
sPOC (200-1000 m) (mmol C m⁻²)
Sim - Obs sPOC (200-1000 m) (mmol C m⁻²)
Reg Mean Std
SPNA 21.21 15.26
TA 35.08 14.49
STNA 16.44 3.51
Reg RMSD% RB%
SPNA 26 -22
TA 20 -7
STNA 55 -53
Reg Mean Std
SPNA 1.07 1.47
TA 0.34 0.46
STNA 0.03 0.01
Reg RMSD% RB%
SPNA 172 71
TA 258 107
STNA 64 -8
Reg Mean Std
SPNA 1.18 0.50
TA 1.11 0.22
STNA 0.68 0.07
Reg RMSD% RB%
SPNA 56 -31
TA 31 -6
STNA 36 13
Reg Mean Std
SPNA 61.17 37.77
TA 61.14 23.45
STNA 23.16 3.84
Reg RMSD% RB%
SPNA 65 27
TA 107 91
STNA 25 19
Reg Mean Std
SPNA 342.17 166.14
TA 377.26 71.27
STNA 260.66 23.27
Reg RMSD% RB%
SPNA 22 -18
TA 8 -6
STNA 25 -24
Reg Mean Std
SPNA 231.52 25.93
TA 136.06 7.98
STNA 115.13 0.98
Reg RMSD% RB%
SPNA 18 -18
TA 52 -51
STNA 49 -49
80°W
60°W
40°W
20°W
0°

Figure 2. *The left column includes maps for the annual climatology of the five biogeochemical modelled variables evaluated in this study: NPP (a), surface carbon from phytoplankton biomass; diatoms (c) and miscellaneous phytoplankton (pico and nano-phytoplankton, e), carbon from mesozooplankton integrated over 0-200m, (g) the small POC (particulate organic carbon, i) integrated over 0-200m and (k) the small POC integrated over 200-1000m. The right column shows the mean spatial bias of the simulated variables compared to observational datasets.*

3.1.2. Net Primary Production (NPP)

The model reproduces the meridional NPP gradient, with the largest annual production in the Trans_Area (Fig. 2). In the SPNA and the Trans_Area, the seasonal cycles are well correlated with satellite estimates and capture the timing of the spring–summer production peak (Fig. 3a–b and S3). In the SPNA, however, NPP is systematically lower than satellite estimates year-round, with a -22% mean deviation. The Trans_Area shows the smallest annual mean deviation (-7%), which results from the compensation between moderate seasonal biases. In the STNA, the model underestimates NPP year-round and produces almost no seasonal variability, resulting in a weak temporal correlation with the satellite product (Fig. 3c).

3.1.3. Phytoplankton carbon biomass

Surface phytoplankton carbon is evaluated separately for diatoms (*phydiat*; Fig. 2c–d) and miscellaneous phytoplankton (*phymisc*; Fig. 2e–f). Modelled *phydiat* overestimates satellite microphytoplankton north of 40ºN. Modelled *phymisc* underestimates satellite pico+nanophytoplankton in the SPNA but shows smaller deviations in the other regions. Both annual maps and seasonal cycles indicate an opposite bias between the two phytoplankton classes (Fig. 3d–f). As a result, total phytoplankton presents -4% of relative bias year-round in the SPNA, 8% in the Trans_Area and 13% in STNA. Despite these compensating biases, the model reproduces the latitudinal shift from a strongly seasonal, diatom-rich regime in the SPNA to a weakly seasonal, small-phytoplankton-dominated regime in the STNA.

3.1.4. Mesozooplankton carbon biomass

Mesozooplankton carbon integrated over the upper 200 m displays annual mean patterns that resemble those of NPP and sPOC stocks (Fig. 2g–h). The relative mean bias is almost 30% in the SPNA, about 90% in the Trans_Area, and around 20% in the STNA, similar to the results obtained by Clerc et al. (2024). Compared to the observational product, the model tends to exhibit a wider seasonal amplitude and, in the SPNA, a delayed peak, lagging diatoms by at least 1 month. In the observational product mesozooplankton, seasonality is better aligned with NPP, phytoplankton biomass and detrital stocks (Fig. 3a, d, g, j).

3.1.5. Small Particulate Organic Carbon (sPOC)

Annual mean sPOC stocks integrated over 0–200 m show similar large-scale patterns in the model and the G22 dataset, with decreasing magnitude and seasonal amplitude from the SPNA to the subtropical gyre (Fig. 2i–j), broadly resembling NPP patterns. The spatially averaged relative bias in the upper 200 m over the whole North Atlantic is −16% (Fig. 2j), with smaller bias in the Trans_Area and stronger underestimation in the STNA (Fig.

3i). The 0–200 m sPOC seasonal cycles are closely phase-locked to NPP in the SPNA and Trans_Area and show a high temporal correlation with G22 ($r = 0.95$ in SPNA and $r = 0.97$ in Trans_Area, both $p < 1.0 \times 10^{-6}$), although the model overestimates the seasonal amplitude in the SPNA (Fig. 3g–h).

Between 200 and 1000 m, model performance degrades. The relative mean bias in mesopelagic sPOC reaches ~50% in the Trans_Area and STNA, with widespread underestimation across most of the North Atlantic. An exception occurs in the western SPNA, which moderates the regional SPNA bias to -18%. The SPNA also exhibits the widest seasonal amplitude in mesopelagic sPOC, which is reasonably captured by the model (Fig. 3j).

Comparison with vertical profiles (Fig. 4) complements this analysis and suggests that the model (i) underestimates the vertical gradient of sPOC in the SPNA epipelagic, (ii) overestimates the sPOC attenuation gradient in the upper mesopelagic of the Trans_Area, and (iii) underestimates the magnitude and overestimates the depth of the subsurface biomass maximum in the STNA.

For completeness, modelled sPOC was also compared with estimates obtained using the algorithm of Koestner et al. (2024) in the epipelagic layer (SI text S3). K24 sPOC exhibits seasonal patterns similar to G22 but is systematically higher by around 200 mmol C m^{-2} (and up to ~400 mmol C m^{-2} in the SPNA winter, Fig.3), implying a stronger underestimation of epipelagic sPOC by the model. Comparison between G22 and K24 did not indicate systematic overperformance of either product (figure 13 in Koestner et al., 2024). Accordingly, and because G22 was specifically designed to provide consistent estimates across epi- and mesopelagic, here we retain it as the primary reference, while using the comparison with K24 to illustrate the range of algorithm-dependent observational uncertainty. A more thorough evaluation of uncertainties in the conversion from particulate backscattering to sPOC, which is beyond the scope of our study, could further refine these findings.

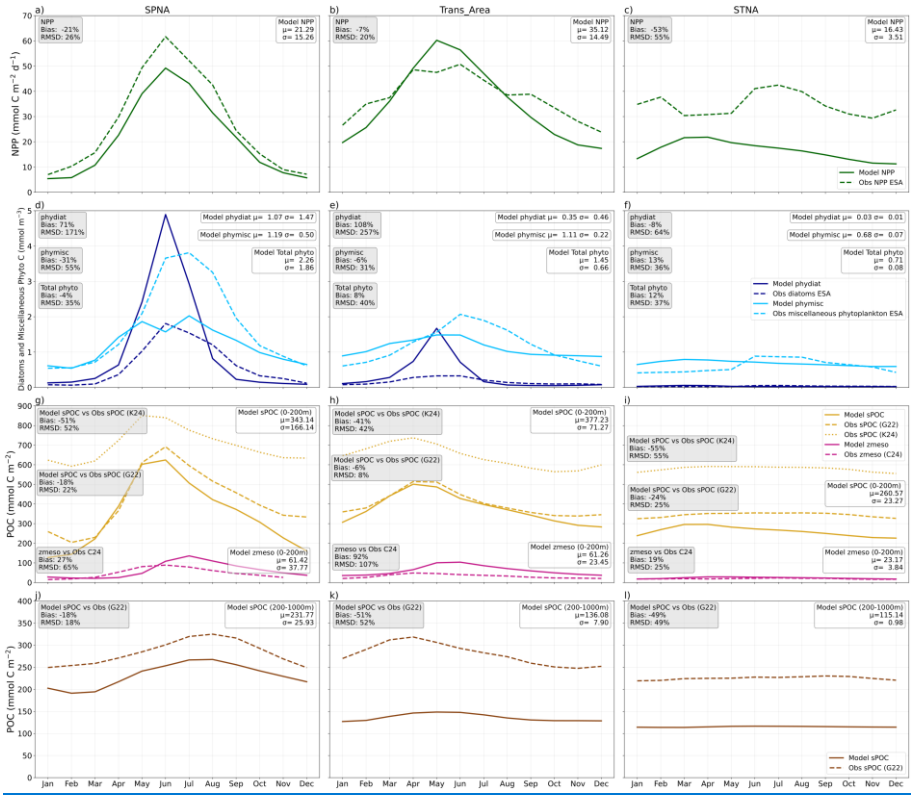

Figure 3. *Seasonal Cycle of the biogeochemical variables evaluated. Modelled variables are represented in solid lines, and the observations in dashed lines. Different colours represent different variables. Each column represents the three selected biomes: Subpolar North Atlantic (SPNA), Transitional Area (Trans_Area) and Subtropical North Atlantic (STNA). Each row shows a different seasonal cycle: NPP (a-c), Surface Carbon from phytoplankton (d-f, dark blue for diatoms and light blue for miscellaneous phytoplankton), Mesozooplankton (in pink) and Small Particulate Organic Carbon stock (sPOC- in yellow) over the 0-200m depths (g-i) and sPOC stock over the 200-1000m depths (in brown, j-l). Beige squares contain skill metrics model vs observations, and white squares include the mean and the standard deviation of the modelled variables.*

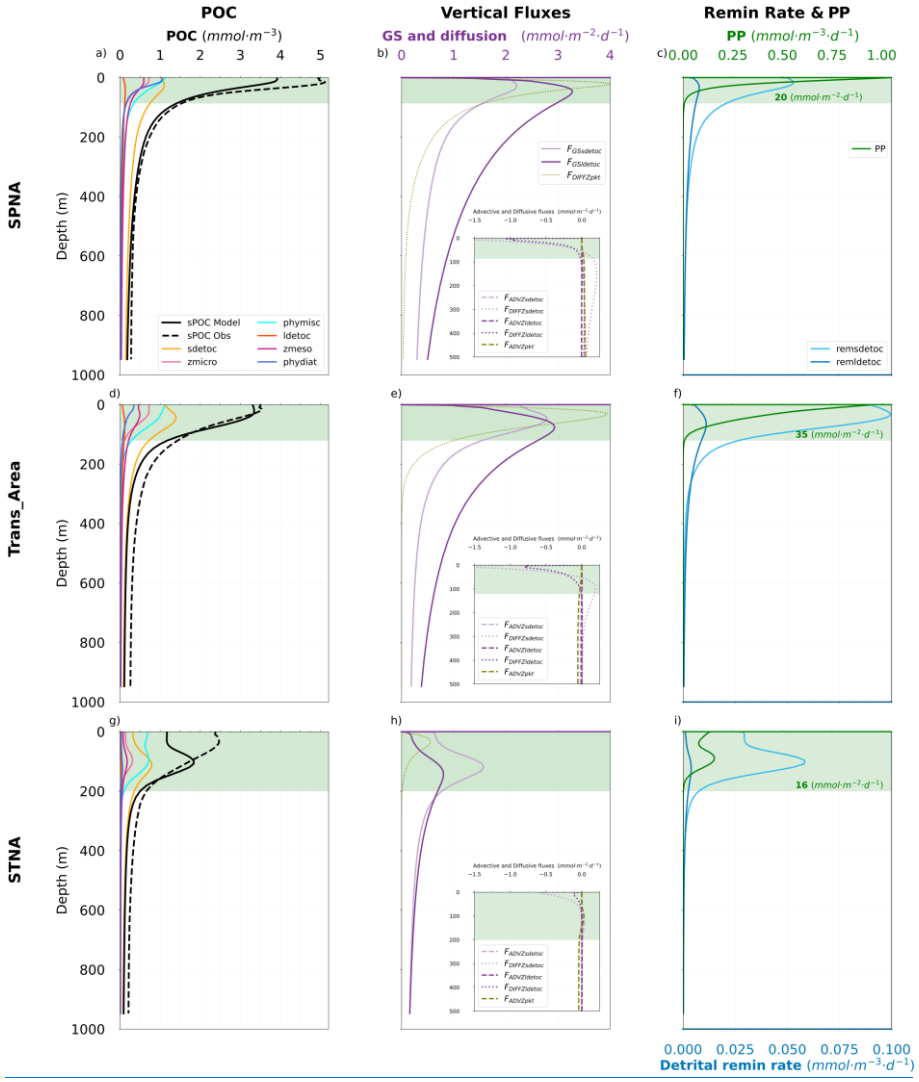

Figure 4. *Annual vertical profiles of different POC stocks (sPOC modelled and observed) and their components (first column). Vertical fluxes (second column) include gravitational sinking export fluxes only for sdetoc ($F_{GSsdetoc}$, in solid light purple) and ldetoc ($F_{GSldetoc}$, in solid dark purple), and advective (F_{ADVZ}), in dashed line style) and diffusive (F_{DIFFZ}, in dotted line style) vertical fluxes for detritus (sdetoc in light purple, and ldetoc in dark purple) and phyto-zooplankton (pkt in light green). The insets at the lower left part of the subplots in the second column contain the diffusive and advective vertical fluxes of sdetoc and ldetoc, and the advective fluxes of pkt, since their magnitudes are not comparable to the detrital gravitational sinking export fluxes and the vertical diffusive flux of pkt. Remineralisation of detritus rate (remsdetoc and remldetoc) and Primary production (PP) (third column). Green rectangles in the right column represent the productive layer (defined in Sect. 2.4); numbers at their bottom*

indicate the vertically integrated annual mean primary production (NPP) in that layer. Rows corresponds to the SPNA (a, b, c), Trans_Area (d, e, f) and STNA (g, h, i) study regions.

3.1.6. Export fluxes at 100 m and 150 m depth

To evaluate modelled POC export, we compared the monthly climatology of total vertical fluxes to ^{234}Th- and sediment trap-based estimates from the global compilations of Le Moigne (2013) and Mouw et al. (2016a). Based on the spatial distribution of the measurements, we focus this analysis on the entire subpolar North Atlantic (SPNA) and two specific study sites (Fig. 5a–b). The Porcupine Abyssal Plain (PAP) lies near the boundary between the SPNA and Trans_Area regions in the eastern Atlantic. The other study site is located near the Trans_Area–STNA boundary in the Sargasso Sea, and includes the merged datasets from the Bermuda Atlantic Time Series and the Oceanic Flux Program (BATS/OFP). In SPNA and PAP, measurements are available only from May through August in scattered years, whereas at BATS/OFP, measurements are available year-round between 1985 and 2013.

In the SPNA (Fig. 5c; Fig. 6), the model captures the observed order of magnitude of the observations, which are nevertheless extremely variable at both 100 and 150 m. This, combined with spatial and temporal sparseness, precludes drawing clear conclusions on model behaviour. At the PAP site, modelled fluxes exceed observations by about ~70% at 100 m but are in good agreement with measurements at 150 m (Fig. 5d). At BATS/OFP, where observations are available only at 150 m, the model reproduces the weak seasonality found in the observations but shows a mean positive bias of ~90%, largely driven by winter-spring months (Fig. 5e).

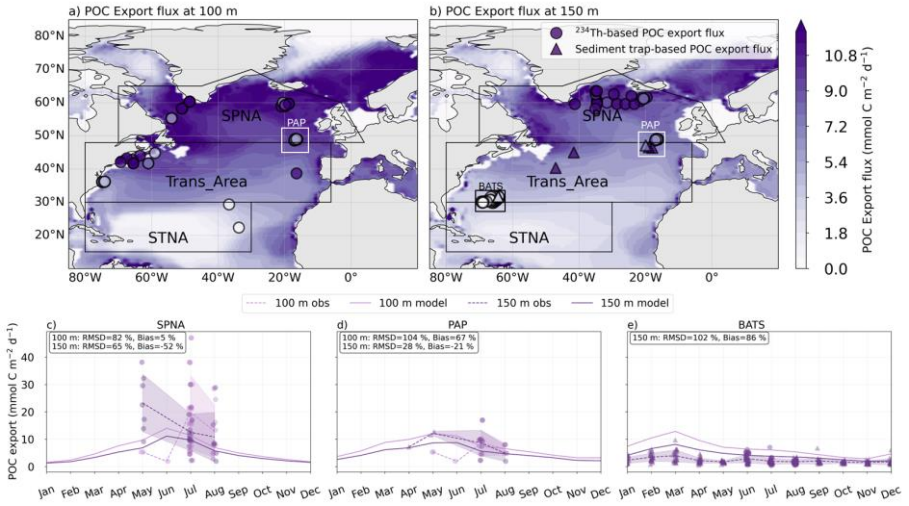

Figure 5. *Modelled annual mean (1998-2019) vertical sinking fluxes (gravitational, diffusive and advective) at 100m (a) and 150 m (b) are compared with in situ measurement compilations. Circles indicate ^{234}Th-based POC export flux, and triangles, sediment trap-based POC export flux. Modelled monthly climatologies (1998-2019) of the vertical sinking fluxes are extracted for SPNA (c), PAP (d) and BATS/OFP study sites (e) and compared with*

available observations. Light purple lines in (c-e) represent export fluxes at 100 m, and dark purple lines represent export at 150 m. Solid lines indicate modelled fluxes. Dashed lines and ribbons represent the monthly mean and standard deviation of the observations.

3.1.7. Water column export fluxes

To complete the export flux evaluation, we subsampled model output at the depth, year, month and location of data from Mouw et al. (2016a). We used data from the upper 4000 m in the North Atlantic, of which 61% was obtained at BATS/OFP, and computed model skill metrics for (i) non-binned data (n = 3388) and (ii) after binning by layer and region (n = 12). These comparisons and their corresponding metrics are shown in Fig. 6, suggesting that the model captures water-column export fluxes with small overall bias across two orders of magnitude when the data are binned. Indeed, non-binned data show substantial scatter, especially for small flux values. Crucially, different conclusions are obtained depending on whether in situ data are matched to sinking POC fluxes only or to total downward fluxes. In the first case, the comparison suggests an overall tendency for model underestimation, whereas the second case suggests a slight tendency for overestimation in the epipelagic. Patterns in the epipelagic SPNA and upper 500 m of the Trans_Area are least robust because of data scarcity.

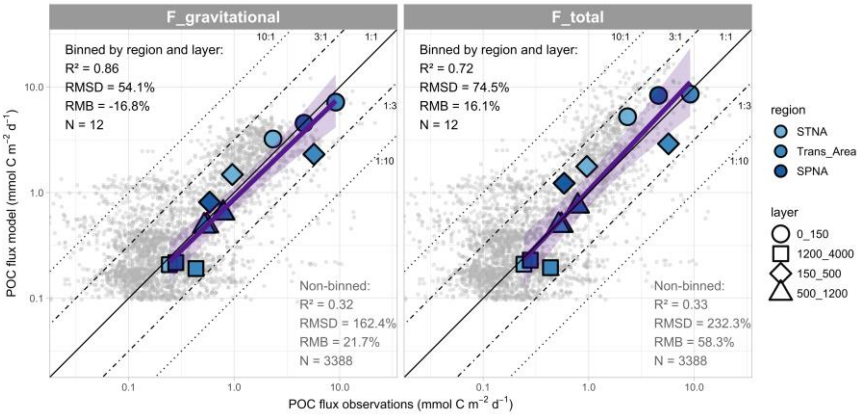

***Figure 6**. Comparison between modelled export fluxes and a compilation of in situ sediment trap measurements from Mouw et al. (2016a). Collocated data are compared directly (non-binned dataset) and after computing regional and vertical bin averages. The corresponding skill metrics are shown, along with a linear regression on binned data (purple line and envelope showing SE of the fit). Diagonal lines with different model:observation ratios are shown as visual guides. The same in situ fluxes are compared to modelled POC gravitational fluxes (left) and total fluxes (right). For this comparison, we assigned data from BATS/OFP to the STNA and data from PAP to the Trans_Area (see text and Fig. 4). Vertical boundaries were chosen to optimise data abundance in each layer while deviating minimally from the standard definitions of Zprod and the mesopelagic layer.*

Table 3. The upper part qualitatively summarises observed model biases or misfits. Arrows are used to indicate positive (↑) or negative (↓) model biases of large (2) or moderate (1) magnitude; ✓ indicates small bias, ~ indicates temporal phase shift, and "?" indicates uncertain evaluation outcome usually due to data sparseness or too-large observational uncertainties. The lower part provides interpretations based on the comparison of various bias patterns. More *speculative interpretations* are highlighted in italics and are based on insights from the modelled mesopelagic budgets.

Observed biases/misfits			
	SPNA	**Trans_Area**	**STNA**
Epipelagic	↑↑ diatoms ↓↓ misc. phytoplankton ↓ NPP ~↑ mesozooplankton ↓ sPOC stock ~? F_{POC} export Zprod	↑↑ diatoms ↓ misc. phytoplankton ~✓NPP ~↑↑ mesozooplankton ✓? sPOC stock ~? F_{POC} export Zprod	~✓diatoms ~✓misc. phytoplankton ↓↓ NPP ~↑ mesozooplankton ↓ sPOC stock ↑↑ F_{POC} export Zprod
Mesopelagic	↓ sPOC stock ✓F_{POC} lower meso	↓↓ sPOC stock ✓F_{POC} lower meso	↓↓ sPOC stock ✓F_{POC} lower meso
Interpretation in the PISCES model framework			
NPP vs. sPOC	Region-dependent NPP underestimation causes proportional biases in epipelagic sPOC stocks		
NPP vs. POC export (EE)	Modest biases suggest correct or slightly overestimated EE	Small biases suggest correct EE	Large opposite biases indicate overestimated EE

Formatted: Left

Diatoms vs. miscellaneous phyto., mesozooplankton, sPOC, and vertical POC fluxes	Diatom overgrowth at the expense of miscellaneous plankton results in mesozooplankton overestimation, with shifted seasonality. *Diatom bias likely propagates to (i) overestimation of large detritus export; (ii) excessive depletion of epipelagic sPOC by sinking; (iii) overestimation of EE.*		Small influence of model biases driven by diatoms
Epipelagic vs. mesopelagic sPOC stocks	No obvious imbalance between epipelagic and mesopelagic sPOC stocks, with moderate underestimation for both.	Increasing sPOC deficit with depth suggests excessive mesopelagic removal relative to inputs	
F_POC at Zprod vs. lower meso (TE proxy)	Large variability in export fluxes at Zprod precludes a conclusive assessment of TE.		Positive bias in export flux at Zprod suggests TE underestimation (at least at BATS/OFP)
Potential sources of TE bias, based on simulated mesopelagic budgets (non-verified)	*Excessive diatoms, hence a likely overestimation of large POC flux attenuation by zooplankton, would imply TE underestimation*		
		Mesopelagic sPOC deficit, if due to excessive removal, would imply TE underestimation	

3.2. Simulated vertical profiles of POC pools and detrital POC decay

The evaluation of model performance confirms PISCES captures the main North Atlantic biogeochemical gradients and seasonal cycles, despite some season- and region-dependent biases (Table 3). To investigate how these patterns translate into POC vertical structure, this section documents the distribution of POC components and the fluxes and remineralisation processes controlling their transformation from the epipelagic to the mesopelagic layer.

On an annual basis, total gravitational export at the base of the productive layer (Zprod) is similar in ~~S3. Note also that the dataset used herewith represents only small POC (sPOC) because $b_{bp,700}$ observations were pre-processed to filter out the optical spikes caused by large particles (Briggs et al., 2020).~~

Formatted: Font: 10 pt, Font colour: Auto

Formatted: Left

~~The vertical integrals (0–100 m and 100–500 m) of observation-based and simulated sPOC stocks were compared over the seasonal cycle (Fig. 3d-i). Only model tracers nominally smaller than 100 µm were included (*sdetoc*, *phymisc*, *phydiat* and *zmicro*). We chose the 100-500 m layer because in our implementation both algorithms give, by construction, similar estimates below 500 m. K24 estimates systematically exceed G22 by 20–60% (Table S4). In the 0-100 m layer, PISCES shows a high temporal correlation to both datasets in the SPNA ($R > 0.96$) but is biased low. In the Trans_Area, simulated sPOC is generally close to the G22 estimate. In the STNA, the model's sPOC consistently falls below both observational estimates and has wider seasonality than the observational products. In the 100-500 m layer, simulated sPOC is generally closer to G22 estimates, but slightly (SPNA, STNA) or markedly (Trans_Area) below them. Best agreement between simulated sPOC and the G22 and K24 estimates occurs in April–July in the SPNA. Overall the model exaggerates the latitudinal sPOC gradient compared to observations.~~

~~2.6.4. Export fluxes~~

~~We compared PISCES output to a compilation of in situ POC vertical fluxes measured with sediment traps (Mouw et al., 2016a). An analysis of gridded fields was not affordable because of data sparseness. Hence, we subsampled model output at the depth, time and location of the measurements, and then binned the data by layer, region and season. For fluxes measured in the top 1200 m in the North Atlantic (Fig. S7), the analysis of binned data yielded a Pearson correlation coefficient of 0.80, mean relative bias of +28% and model vs. data slope of 0.68 (p-value $< 2 \cdot 10^{-5}$).~~

Formatted: Left

3. Results

In this section, an overview of simulation results (3.1) is followed by a detailed description of mesopelagic detritus budgets (3.2) and by the analysis of POC export and transfer efficiency metrics (3.3). Besides the information shown in the figures, the quantitative data provided hereafter can be found in two summary spreadsheets included in the SM section.

3.1. Overview of simulated POC stocks and fluxes

We start by documenting the general behaviour of the POC distribution and the main factors controlling its stock in our simulation. The epipelagic POC stock shows a similar spatial pattern as NPP and gravitational export flux at 100 m ($F_{GS,100}$; Fig. 2a-c), with an increasing gradient from the Greenland coast to the southern border of the subpolar gyre, maximum values at midlatitudes (30–50°N), and a sharp decrease towards the core of the subtropical gyre. The mesopelagic POC stock shows a different pattern and decreases from the subpolar to the subtropical region. Small detritus are the most abundant POC fraction in the mesopelagic layer (cf Section 2.3 for details about the tracers composing POC), where *sdetoc* accounts for 52%, 57%, and 70% of POC in the SPNA, Trans_Area, and STNA, respectively (Fig. 4a,d,g). The *ldetoc* fraction usually is ≤10% of total POC and smaller than total zooplankton or phytoplankton (Fig. 4a,d,g).

The amplitude of the NPP seasonal cycle is similar in the subpolar and the transition and subpolar areas (Fig. 2e-f), whereas the subtropical area shows reduced seasonal variability. Peak NPP occurs in June, May, and March-April in the SPNA, Trans_Area and STNA, respectively. Gravitational export at the bottom of the productive layer (Zprod) peaks on the same month as NPP in the subpolar and transition areas, but lags NPP by ~1 month in the subtropical area. Gravitational fluxes at 1000 m lag Zprod by around 2

Formatted: Font: 10 pt, Font colour: Auto
Formatted: Heading-Main, Line spacing: 1,5 lines
Formatted: Font: 10 pt
Formatted: Font: 10 pt
Formatted: Font: 10 pt
Formatted: Left

months, with a slight increase in lag time towards lower latitudes (to the extent that such lag can be estimated with monthly data).

On an annual basis, total gravitational export at Zprod is similar in the transition and subpolar areas (3.9–4.3 mmol C m^{-2} d^{-1} or yearly, 1.4–1.6 mol C m^{-2} y^{-1}3.9–4.3 mmol C m^{-2} d^{-1}), and much lower in the subtropical area (1.3 mmol C m^{-2} d^{-1}, or 0.5 mol C m^{-2} y^{-1};) (Fig. 4b, e, h4). In addition, a largesubstantial amount of POC is exported through turbulent diffusion of plankton in the SPNA (1.4 mmol C m^{-2} d^{-1}) and the Trans_Area (0.8 mmol C m^{-2} d^{-1}). In fact, in the SPNA, the total diffusion flux of POC (including the diffusion of detritus and plankton) at Zprod, supplements by 37% the total gravitational sinking flux ($\frac{F_{DIFFZ}}{F_{GS}} \cdot 100$). Smaller exports resultarise from the diffusion of detrital POC, especially *sdetoc*. The transport of particles through, while vertical advection is negligible at the regional scale examined here.

The annualAnnual mean profile of the vertical fluxes variesflux profiles vary widely across regions, and for each tracer composing POC tracers (Fig. 4). Gravitational *sdetoc* fluxes attenuate rapidly in the upper mesopelagic and more slowly below ~400 m. By contrast, *ldetoc* shows deeper flux maxima, greater penetration through the upper mesopelagic, and unabatedgradual attenuation throughthroughout the entire mesopelagic. As a resultConsequently, the proportion of export fluxes channelledcarried by *sdetoc* increases through with depth in the lower mesopelagic. Diffusive fluxes of plankton showfluxes attenuate at shallower attenuationdepths than gravitational ones, with deeper. Yet, their penetration deepens towards the SPNA. This latitudinal pattern follows the , consistent with regional variations in maximum winter MLD, from ca. 250 m in the SPNA to ca. 70 m in the STNA (note these are regional averages; (Fig. S1 and S2).

Small detritus is the most abundant POC fraction in the mesopelagic layer, where it accounts for 52% (SPNA) to 70% (STNA) of the POC pool. The *ldetoc* fraction usually is ≤10% of total POC and smaller than total plankton (Fig. 4a, d, g).

Vertical profiles of detritus decay rates also show variationsvary by detritus type of detritus and region (Fig. 4c, f and i). The integrated decay rate of detritus (*sdetoc*+*ldetoc*) between the surface and 1000 m is highest in the Trans_Area (13.9 mmol C m^{-2} d^{-1}) compared to the other areas (8.4–8.6 mmol C m^{-2} d^{-1}), mirroring NPP. Within each layer, *sdetoc* drives patterns. Small detritus drive most of the detritus decay, with higher *sdetoc* contributions in the epipelagic (85–92%) than in

Formatted: Left
Formatted: Font: 10 pt
Formatted: Font: 10 pt
Formatted: Font: 10 pt
Formatted: Font: 10 pt
Formatted: Font: 10 pt
Formatted: Font: 10 pt
Formatted: Font: 10 pt
Formatted: Font: 10 pt
Formatted: Font: 10 pt
Formatted: Font: 10 pt
Formatted: Font: 10 pt
Formatted: Font: 10 pt
Formatted: Font: 10 pt
Formatted: Font: 10 pt
Formatted: Font: 10 pt
Formatted: Font: 10 pt
Formatted: Font: 10 pt
Formatted: Font: 10 pt
Formatted: Font: 10 pt
Formatted: Font: 10 pt
Formatted: Font: 10 pt
Formatted: Font: 10 pt
Formatted: Font: 10 pt
Formatted: Font: 10 pt
Formatted: Font: 10 pt
Formatted: Font: 10 pt
Formatted: Font: 10 pt
Formatted: Font: 10 pt
Formatted: Font: 10 pt
Formatted: Font: 10 pt
Formatted: Left
Formatted: Font: 10 pt
Formatted: Left

the mesopelagic (53–61%). To illustrate distinct ~~remineralization patterns~~remineralisation regimes, we calculated the percentage of degradation in the epipelagic layer relative to the 0-1000 m integral. In SPNA, only 58% (*sdetoc*) and 28% (*ldetoc*) of decay occurs in the epipelagic, ~~corresponding~~concurrent with low temperatures, strong *ldetoc* export and shallow Zprod. Conversely, the STNA shows 93% (*sdetoc*) and 56% (*ldetoc*) epipelagic decay, aligned with warm temperatures, reduced *ldetoc* export and deep Zprod.

Detritus decay rates result from the product of tracer concentration and the depth- and temperature-degradation rate constant *k* (see ~~2.3). While an in-depth analysis of these parameterizations is beyond the scope of this paper, an overview of simulated *k* patterns (shown~~Sect 2.2), as illustrated in Fig. ~~S8) is useful to interpret model behavior. In the case of~~7. For *sdetoc*, 0ºC-normalized *k* typically ranges 0.010–0.023 d^{-1} in the epipelagic and decreases sharply to ~0.002 d^{-1} at 1000 m; ~~the k of~~for *ldetoc*, *k* typically ranges 0.027–0.035 d^{-1} in the epipelagic and 0.015–0.020 d^{-1} at 1000 m. Thus, in PISCES, *sdetoc* becomes refractory at shallower depths than *ldetoc*~~. The differential effect of~~, explaining the limited change in *sdetoc* concentration and sinking flux below ~400 m compared to *ldetoc*.

While the change in reactivity is best described by 0ºC-normalized *k*, the actual in-situ rates are differently affected by temperature ~~on *k* depends on the thermal range~~ across regions and depths~~.~~ (Fig. 7), which here we quantify using the enhancement factor with respect to *k* at 0ºC. In the epipelagic, mean thermal enhancement factors ~~with respect to 0ºC~~ are 1.7, 3.2 and 4.5 in the SPNA, Trans_Area and STNA, respectively. Smaller thermal enhancement factors (1.5 ~~to~~ 2.5) are found in the mesopelagic. Thus, temperature exacerbates the vertical gradients in reactivity ~~(*k*) more strongly~~ at low latitudes ~~(Fig. S8).~~

Formatted: Font: 10 pt
Formatted: Font: 10 pt
Formatted: Font: 10 pt, Italic
Formatted: Font: 10 pt
Formatted: Font: 10 pt
Formatted: Font: 10 pt
Formatted: Font: 10 pt
Formatted: Font: 10 pt
Formatted: Font: 10 pt
Formatted: Font: 10 pt
Formatted: Font: 10 pt
Formatted: Font: 10 pt
Formatted: Font: 10 pt
Formatted: Left
Formatted: Font: 10 pt
Formatted: Font: 10 pt
Formatted: Font: 10 pt
Formatted: Font: 10 pt
Formatted: Font: 10 pt
Formatted: Font: 10 pt
Formatted: Font: 10 pt
Formatted: Left

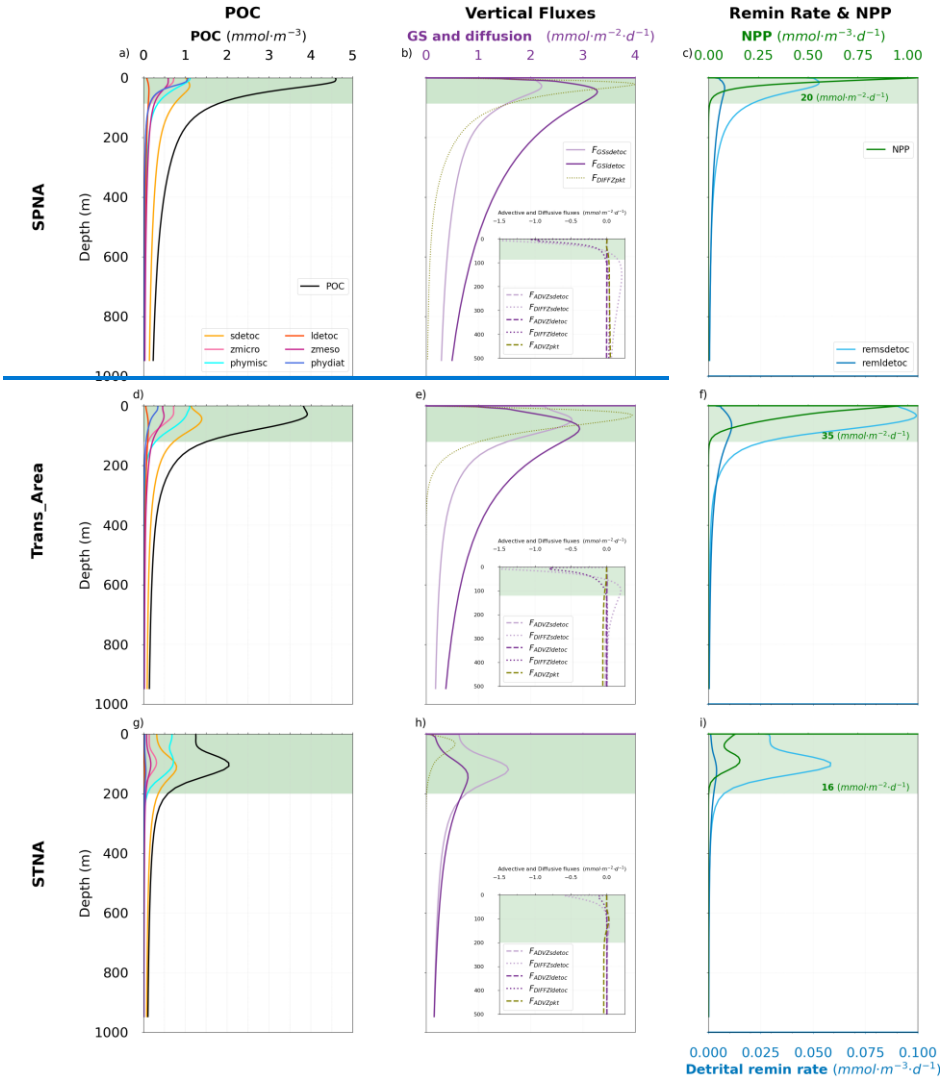

Formatted: Left

~~***Figure 4:*** *Annual vertical profiles of different POC stocks and their components (first column). Vertical fluxes (second column) include gravitational sinking export fluxes only for sdetoc ($F_{GSsdetoc}$, in solid light purple) and ldetoc ($F_{GSldetoc}$, in solid dark purple), and advective (F_{ADVZ}), in dashed linestyle) and diffusive (F_{DIFFZ}, in dotted linestyle) vertical fluxes for detritus (sdetoc in light purple, and ldetoc in dark purple) and phyto-zooplankton (pkt in light green). The insets at the lower-left part of the subplots in the second column contain the diffusive and advective vertical fluxes of sdetoc and ldetoc and the advective fluxes of pkt since their magnitudes are not comparable to the detrital gravitational sinking export fluxes and the vertical diffusive flux of pkt. Remineralization of detritus rate (remsdetoc and remldetoc) and Primary production (NPP) (third column). Green rectangles in the right column represent the productive layer (defined in section 2.4.); numbers at their bottom indicate the vertically integrated annual mean primary production in that layer. Each of the rows of this figure corresponds to one of the selected regions: SPNA (a, b, c); Trans_Area (d, e, f) and STNA (g,h,i).*~~

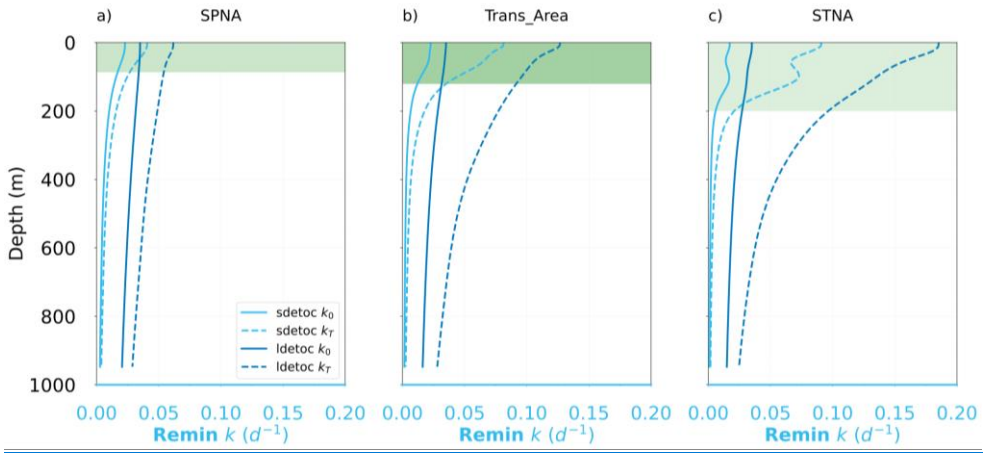

Figure 7. *Vertical profiles of the specific degradation rates of small and large detritus (sdetoc and ldetoc, respectively) at 0 degrees (k_0) and at in situ temperature (k_T) for the three regions.*

Formatted: Left

~~3.2.~~3.3. Mesopelagic detrital POC budgets: annual-mean fluxes

~~To explore the dynamics that control mesopelagic~~ Regional contrasts in POC vertical structure reflect distinct combinations of particle composition, export pathways, and remineralisation regimes (Fig. 4 and 7). To quantify how these differences arise in PISCES, we ~~computed~~now examine the annual climatological ~~budget~~budgets of detrital POC ~~pools~~ in the three regions of interest. We place particular emphasis on how regional differences in productive-layer depth, particle size structure, and export pathways translate into contrasting mesopelagic detrital budgets (Fig. 8).

~~Concerning~~For *sdetoc* ~~budgets~~, the relative contribution of gravitational inputs increases ~~towards~~toward lower latitudes (Fig. ~~5a~~8a), from 36% (SPNA) to 74% (STNA). ~~Supply~~In contrast, the supply of *sdetoc* by the mesopelagic food web shows the opposite pattern and exceeds 50% of ~~the~~ total supply in the SPNA, ~~with large contributions from~~driven primarily by mesozooplankton fragmentation of *ldetoc* (16%), plankton mortalities (20%), and microzooplankton non-assimilation (9%). ~~Plankton~~In the Trans_Area, plankton mortalities dominate biological ~~*sdetoc*~~ supply ~~in the Trans_Area~~ (14%), followed by non-assimilation (8%), bacterial breakdown of *ldetoc* (7%), and mesozooplankton fragmentation (6%). ~~Finally, in~~In the STNA, ~~inputs via~~ bacterial breakdown of *ldetoc* (7~~.3~~%) and abiotic DOC aggregation (12%) ~~are~~contribute relatively ~~larger than at higher latitudes~~more, whereas contributions from mortalities and microzooplankton non-assimilation are ~~smaller.~~ ~~Regarding *sdetoc* removal, the contribution of remineralization exceeds 70%~~reduced. Removal of *sdetoc* is dominated by remineralisation in all regions ~~and reaches~~(>70%), reaching 87% in the STNA. ~~Removal of *sdetoc* by mesozooplankton (~~"Mesozooplankton removal via phagotrophic" ingestion and flux feeding~~)~~ is also ~~important, with the highest contribution (~~significant, peaking at 17~~%)~~% in the Trans_Area~~. Removal of *sdetoc* by~~, whereas microzooplankton ~~is smaller, peaking at~~ removal remains minor (<5~~% in the SPNA.~~%).

~~Concerning~~For *ldetoc* ~~budgets~~, gravitational inputs dominate in all regions, with ~~modest~~smaller contributions from plankton mortalities and mesozooplankton non-assimilation~~.~~ (Fig. 8b). As ~~in the~~for *sdetoc* ~~budget~~, the ~~relative contribution~~importance of ~~the latter two processes~~these biological sources diminishes ~~southwards~~southward in ~~favor~~favour of ~~gravitational~~ sinking. Removal of *ldetoc* is dominated by ~~remineralization~~remineralisation, but ~~the removed percentage~~at lower fractions (50–75%) ~~is lower~~ than ~~in the case of~~ *sdetoc*. In the SPNA, nearly half of ~~the~~ *ldetoc* ~~is removed by~~ removal occurs through mesozooplankton flux feeding (30%) and fragmentation into *sdetoc* (15%). Mesozooplankton-mediated transformation rates decrease ~~towards the south~~toward lower latitudes, especially

Formatted: Font: 10 pt, Not Bold
Formatted: Font: 10 pt, Not Bold
Formatted: Heading-Main, Justified, Line spacing: 1,5 lines
Formatted ...
Formatted: Left
Formatted ...
Formatted ...
Formatted: Left

fragmentation, which in the Trans_Area contributes half as much to *sdetoc* budgets as in the SPNA. ~~The contribution of bacterial~~Bacterial disaggregation of *ldetoc* is generally ~~small and reaches~~minor, reaching 7% in the STNA.

Overall, ~~we find that~~ both ~~the processes controlling~~ *sdetoc*- and ~~the processes controlling~~ *ldetoc*-specific processes are ~~important to understand~~essential for shaping the ~~budget~~magnitude and ~~the~~ evolution of the total ~~detritus~~detrital POC stock across ~~all~~ regions~~. We note that supply processes~~ in PISCES. Supply pathways are more heterogeneous for *sdetoc* ~~than for *ldetoc*, while the opposite is true for removal processes. In fact, this is mostly explained by the~~, whereas removal pathways are more diverse for *ldetoc*. This asymmetry largely reflects *ldetoc* transformation ~~of detrital POC from *ldetoc* into *sdetoc* (cf. breakdown and~~ by fragmentation ~~of *ldetoc*),~~and disaggregation processes, which ~~acts~~act as sinks for *ldetoc* ~~but as sources for *sdetoc*.~~ while simultaneously supplying *sdetoc*. The indirect contribution of plankton diffusion also affects *sdetoc* differentially across regions (Fig. 4 b, e, i).

Formatted: Font: 10 pt
Formatted: Font: 10 pt
Formatted: Font: 10 pt
Formatted: Font: 10 pt
Formatted: Font: 10 pt
Formatted: Font: 10 pt
Formatted: Font: 10 pt
Formatted: Font: 10 pt
Formatted: Font: 10 pt
Formatted: Font: 10 pt
Formatted: Font: 10 pt
Formatted: Font: 10 pt
Formatted: Font: 10 pt
Formatted: Font: 10 pt
Formatted: Font: 10 pt, Not Italic
Formatted: Font: 10 pt
Formatted: Left

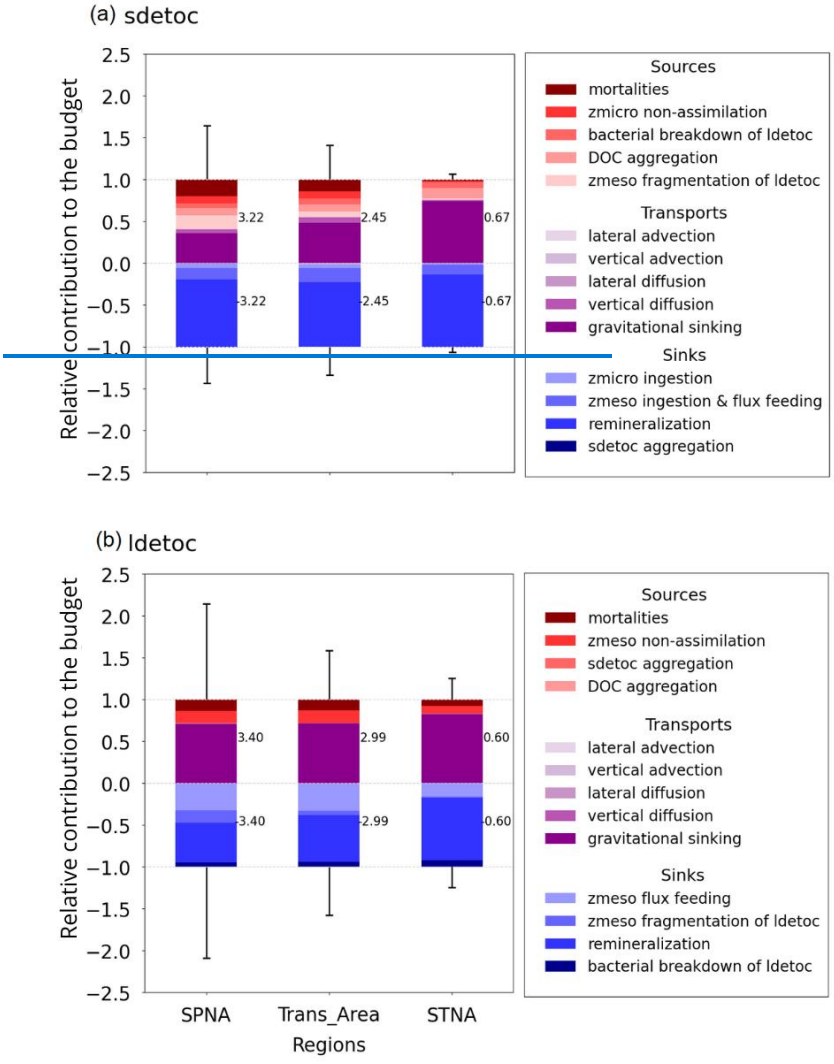

Formatted: Left

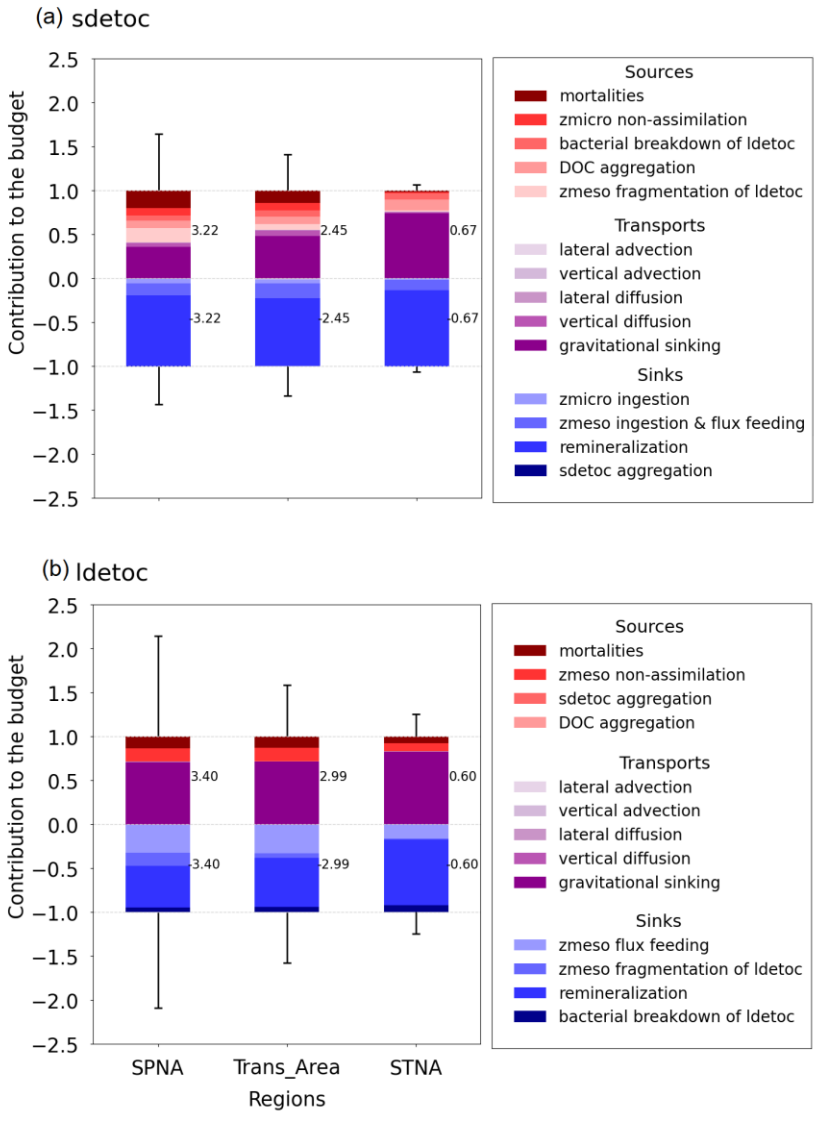

Formatted: Left

Figure ~~5~~8. *Climatological annual budget of small (a) and large (b) detrital POC over the mesopelagic layer (Zprod - 1000m) ~~for the three regions defined in Fig. 2.~~). To compare the ~~relative importance of the processes among~~contribution of each process across regions, the budget terms have been divided by the sum of the supply processes ~~for each region.~~ Numbers on the ~~left~~right of each bar indicate the sum of the inputs (positive) and outputs (negative) ~~of~~for each detrital POC tracer ~~in the mesopelagic layer.~~ Vertical ~~black~~ lines represent the temporal standard deviation of ~~the sum of the positive (top) and negative (bottom)~~ total monthly ~~budget terms~~inputs and outputs after ~~normalization~~normalisation by the annual mean value.

~~To further explore the processes controlling the mesopelagic detrital POC stock, we computed its climatological budget month by month. As expected from the seasonality of physical forcing, the~~

3.4. ~~temporal variability of~~Mesopelagic detrital POC budgets: seasonal cycle

Building on the annual-mean budgets presented in Sect. 3.3, we now examine how the processes controlling mesopelagic detrital POC vary over the seasonal cycle in PISCES. Monthly climatological budgets show that, consistent with the seasonality of physical forcing, temporal variability increases with latitude: it is ~~almost non-existent~~minimal in the STNA ~~region~~ but ~~very~~ pronounced in the SPNA ~~region (Fig. 5, 6, S8 and S9). In particular, the strong *ldetoc* seasonality in SPNA is driven by gravitational~~(Fig. 8, 9, S5 and S6).

Gravitational sinking~~, especially~~ of large detritus during the ~~spring-summer~~high-latitude bloom and post-bloom period~~,~~ is the main seasonal event. The peak in gravitational *ldetoc* supply (June) is rapidly followed by ~~inputs via sloppy feeding and mortality and by~~ maxima in *ldetoc* losses through ~~remineralization~~remineralisation, mesozooplankton flux feeding and fragmentation ~~(all of which peak in July). This contrasts with the~~. Enhanced mesozooplankton activity also generates secondary *ldetoc* sources via mortality and sloppy feeding. In contrast, *sdetoc* budgets exhibit a smoother seasonal succession ~~in biological *sdetoc* cycling. Sources of *sdetoc* shift~~, with sources shifting from mortalities and zooplankton non-assimilation in spring to *ldetoc* fragmentation in summer. ~~Succession is also observed in~~Alongside dominant removal by remineralisation, *sdetoc* sinks~~, whereby~~ transition gradually from microzooplankton ingestion ~~peaks in May, while~~to mesozooplankton ingestion and flux feeding ~~rise from April to July~~through spring and summer.

Formatted: Font: 10 pt
Formatted: Font: 10 pt
Formatted: Left
Formatted: Font: 10 pt
Formatted: Font: 10 pt
Formatted: Font: 10 pt
Formatted: Font: 10 pt
Formatted: Font: 10 pt
Formatted: Font: 10 pt
Formatted: Font: 10 pt
Formatted: Font: 10 pt
Formatted: Font: 10 pt
Formatted: Font: 10 pt
Formatted: Font: 10 pt
Formatted: Font: 10 pt, Not Bold
Formatted: Font: 10 pt
Formatted: Font: 10 pt
Formatted: Font: 10 pt
Formatted: Font: 10 pt
Formatted: Font: 10 pt
Formatted: Font: 10 pt
Formatted: Font: 10 pt
Formatted: Font: 10 pt
Formatted: Font: 10 pt
Formatted: Left
Formatted: Font: 10 pt
Formatted: Font: 10 pt
Formatted: Font: 10 pt
Formatted: Font: 10 pt
Formatted: Font: 10 pt
Formatted: Font: 10 pt
Formatted: Font: 10 pt
Formatted: Font: 10 pt
Formatted: Left

Seasonal decomposition is also necessary to understand the role of diffusive fluxes ~~in each region.~~and their contribution to detrital food webs. On an annual basis, vertical diffusion ~~results in~~represents a significant net ~~*sdetoc* supply to the~~ source of mesopelagic ~~layer~~POC in ~~all regions, with the largest contribution in~~the SPNA and the Trans_Area ~~(6.6%). In the SPNA, however, the contribution of diffusion is less apparent on an annual scale because~~, whereas in the STNA, diffusive fluxes ~~through Zprod switch sign over the seasonal cycle (Fig. 6e). Diffusion removes *sdetoc* in late autumn and early winter when deepening of the mixed layer entrains mesopelagic particles into the surface layer. Conversely, diffusion supplies *sdetoc* in late winter and early spring, when re-stratification detrains particles from the upper mixed layer.~~

~~Vertical diffusive~~primarily redistribute POC within the epipelagic layer. Diffusive fluxes of ~~plankton exceed those of *sdetoc* in all regions, supplying mesopelagic food webs (Fig.4 b,e,h). Plankton diffusion is an input to the mesopelagic in all months in the SPNA and, in April,~~ POC are, however, largely driven by plankton ~~detrainment ($5\ mmol\ m^{-2}\ d^{-1}$) is threefold the total gravitational inputs. Plankton detrainment is an indirect source of detritus, entering the~~and are therefore not included directly in detrital budgets. Instead, vertically mixed plankton enters detrital budgets through mortalities and sloppy feeding (~~eq~~Eq. 1 and 2). In the SPNA, plankton diffusion supplies POC to the mesopelagic throughout the year and peaks in April ($5\ mmol\ m^{-2}\ d^{-1}$), when it is three times larger than total gravitational inputs (SI file S2). Between December and April, when the MLD exceeds Zprod, the ratio between [mortalities + non-assimilation] and plankton diffusion is 0.70±0.27. Between May and October, this ratio increases to 7.0±5.1. Thus, ~~plankton~~ detrainment ~~supplies most~~ of plankton from the epipelagic layer dominates detritus supply (largely as *sdetoc*) before the spring bloom, ~~while the~~whereas biological processing of ~~sinking~~*sdetoc* derived from large detritus fragmentation dominates ~~budgets~~ during the ~~bloom and~~ post-bloom season. Similar, though weaker, patterns of diffusive supply occur in the Trans_Area.

Formatted: Font: 10 pt
Formatted: Font: 10 pt
Formatted: Font: 10 pt
Formatted: Font: 10 pt
Formatted: Font: 10 pt
Formatted: Font: 10 pt
Formatted: Font: 10 pt
Formatted: Font: 10 pt
Formatted: Left
Formatted: Font: 10 pt
Formatted: Font: 10 pt
Formatted: Font: 10 pt
Formatted: Font: 10 pt
Formatted: Font: 10 pt
Formatted: Font: 10 pt
Formatted: Font: 10 pt
Formatted: Font: 10 pt
Formatted: Font: 10 pt
Formatted: Font: 10 pt
Formatted: Left

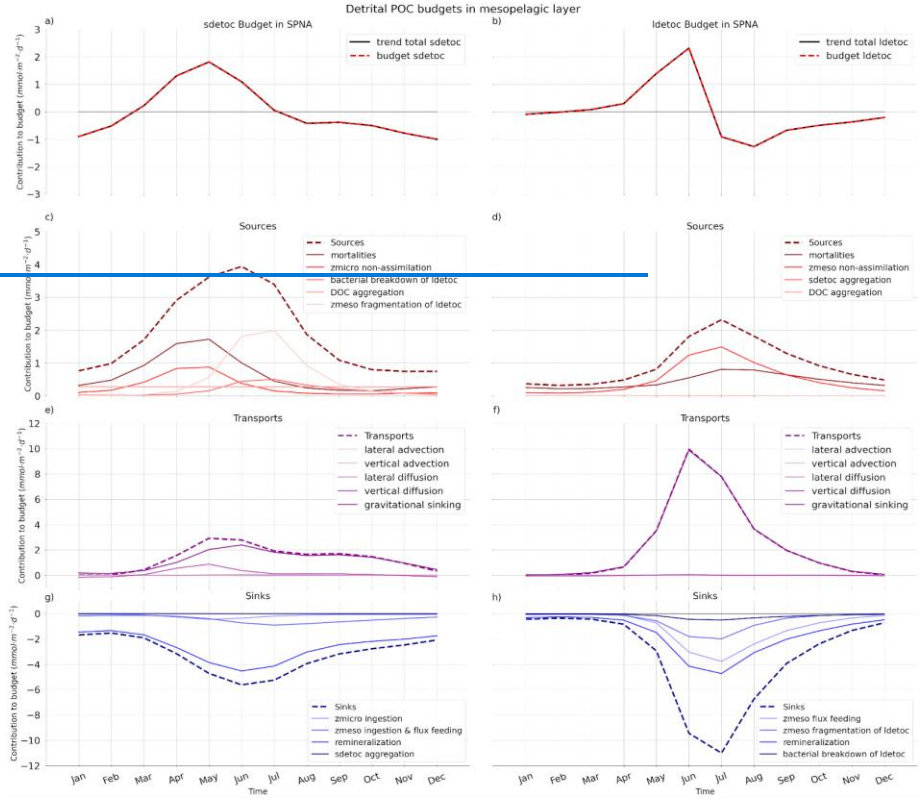

Direct diffusion of detritus is comparatively small, with the largest contribution occurring in the Trans_Area (7%). In the SPNA, diffusive fluxes of detritus switch sign over the seasonal cycle (Fig. 9e), resulting in a weak net annual supply (Fig. 8a). In late autumn and early winter, mixed-layer deepening entrains mesopelagic detritus into the epipelagic layer, whereas in spring, re-stratification promotes detrainment of detrital POC from the epipelagic to the mesopelagic layer.

Formatted: Left

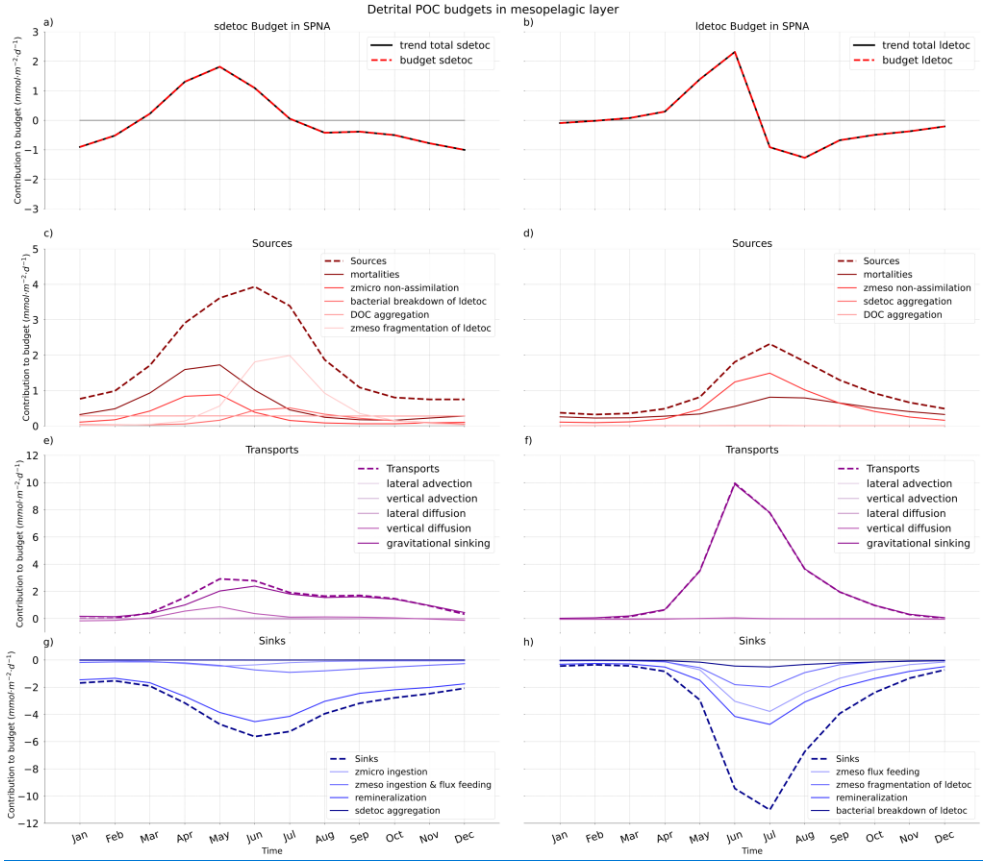

Figure 69. *Seasonal ~~Cycles~~cycles of sdetoc (left ~~column~~) and ldetoc (right ~~column~~) budgets~~; total~~ in the Subpolar North Atlantic (SPNA). Total tracer ~~trend~~trends (a, b), sources (c,d), transports (e,f) and sinks (g, h) ~~for the Subpolar North Atlantic (SPNA) region.~~are shown separately. Note the different y-axis scales ~~in the first and second rows compared to the bottom ones.~~*

Formatted: Font: 10 pt
Formatted: Font: 10 pt
Formatted: Font: 10 pt
Formatted: Font: 10 pt
Formatted: Font: 10 pt
Formatted: Left
Formatted: Font: 10 pt
Formatted: Font: 10 pt
Formatted: Font: 10 pt
Formatted: Font: 10 pt
Formatted: Left

~~3.3.~~3.5. Export and transfer efficiency metrics

~~Here we provide a synthetic description~~To synthesise the behaviour of the particulate C pump ~~through the comparison of the~~, we compare export and transfer efficiency metrics across regions (Fig. ~~7~~11). Additionally, attenuation coefficients “*b*” (Martin et al., 1987) between Zprod and 1000 m are reported in Fig. ~~8~~11. All metrics are based on annual mean fluxes.

~~Starting with the metrics based on~~Considering gravitational fluxes only, ~~we observe that~~ PISCES-simulated export efficiency (EE) decreases with latitude, from 21% in the SPNA to 8% in the STNA. ~~Interestingly, the~~In contrast, TE ~~of the gravitational flux does not change~~ varies non-monotonically with latitude and is lowest in the Trans_Area (13%), intermediate in the SPNA (17%), and highest in the subtropical area (23%). ~~The~~As a result, overall particulate C pump efficiency at 1000 m, expressed as EExTE, is ~~higher~~highest in the subpolar area (3.6%) ~~than~~and lower in the transition (1.5%) and subtropical (1.8%) areas.

Given the ~~important role~~substantial contribution of non-gravitational fluxes in ~~some regions~~NEMO–PISCES, especially plankton diffusion (Fig. ~~4b, e and h~~4), we re-computed EE and TE ~~metrics~~ for the total POC vertical flux ~~(~~, including gravitational, diffusive and advective~~).~~ components. In the subpolar and transition areas, diffusive plankton fluxes are comparable in magnitude to gravitational ones at Zprod but become negligible at 1000 m~~.~~ (Fig 4). Therefore, their inclusion increases EE but decreases TE. In the SPNA, ~~for example,~~where the ~~inclusion of~~greatest non-gravitational fluxes occur, accounting for all vertical ~~transports~~transport pathways increases EE by 8~~%, while reducing~~% but reduces TE by 3~~%. As~~%, resulting in a ~~result, the carbon pump~~modest increase in overall efficiency ~~expressed by the product~~ (EExTE ~~slightly increases~~) from 3.6% to 4.0%. ~~An analogous but smaller change is found in the Trans_Area, whereas a negligible change is found in the STNA.~~

Formatted: Font: 10 pt
Formatted: Justified, Line spacing: 1,5 lines
Formatted: Font: 10 pt
Formatted: Left
Formatted: Font: 10 pt
Formatted: Font: 10 pt
Formatted: Font: 10 pt
Formatted: Font: 10 pt
Formatted: Font: 10 pt
Formatted: Font: 10 pt
Formatted: Font: 10 pt
Formatted: Font: 10 pt
Formatted: Font: 10 pt
Formatted: Font: 10 pt
Formatted: Font: 10 pt
Formatted: Font: 10 pt
Formatted: Font: 10 pt
Formatted: Font: 10 pt
Formatted: Font: 10 pt
Formatted: Font: 10 pt
Formatted: Font: 10 pt
Formatted: Font: 10 pt
Formatted: Font: 10 pt
Formatted: Font: 10 pt
Formatted: Font: 10 pt
Formatted: Font: 10 pt
Formatted: Font: 10 pt
Formatted: Font: 10 pt
Formatted: Font: 10 pt
Formatted: Font: 10 pt
Formatted: Font: 10 pt
Formatted: Font: 10 pt
Formatted: Font: 10 pt
Formatted: Font: 10 pt
Formatted: Font: 10 pt
Formatted: Font: 10 pt
Formatted: Left

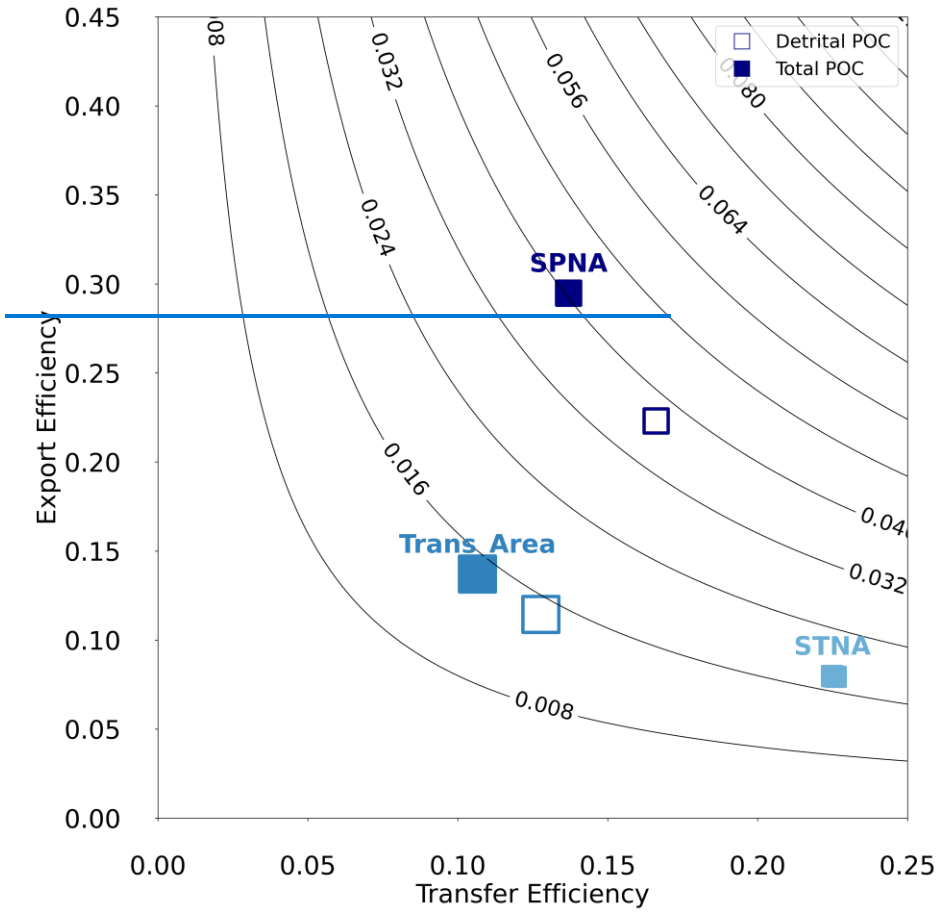

Formatted: Left

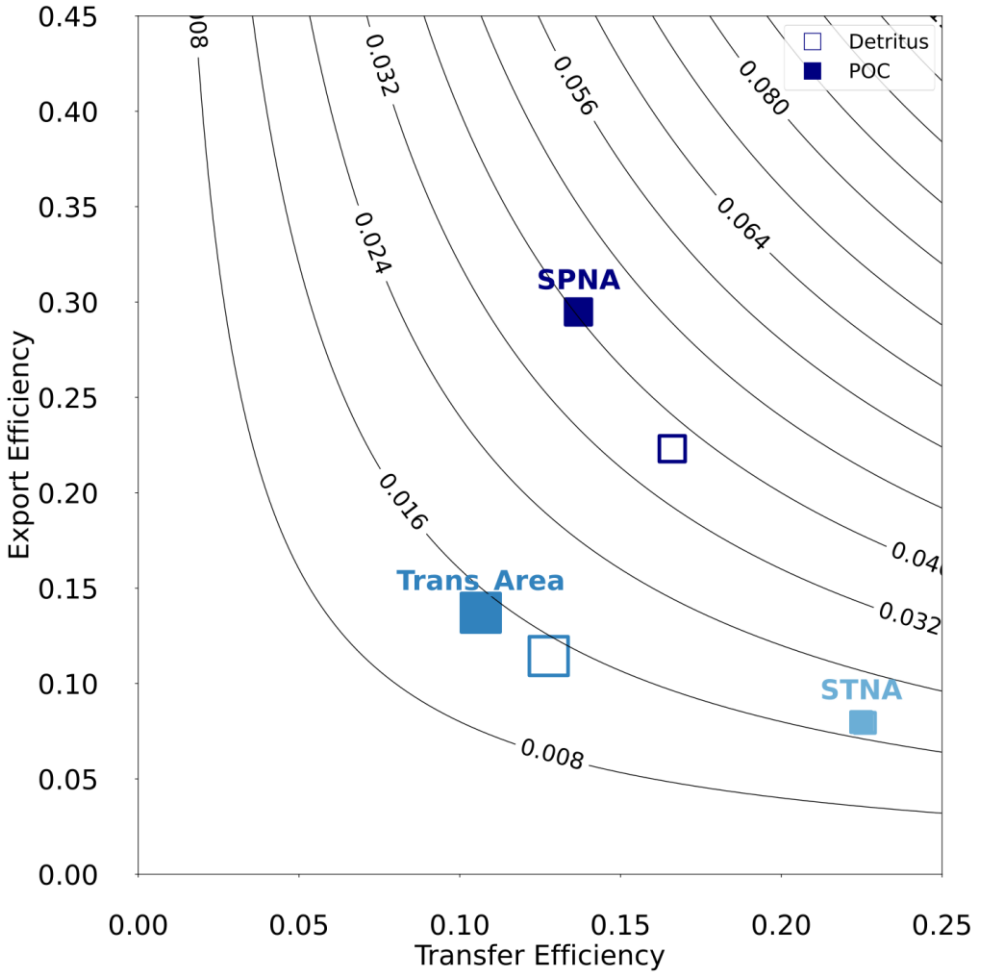

Figure 710. *Export Efficiency vs Transfer Efficiency metrics in the three regions of the North Atlantic. Empty and filled symbols indicate, respectively, if calculations account for only detrital POC or total POC (detritus and plankton). Note that*

Formatted: Font: 10 pt

Formatted: Font: 10 pt

Formatted: Left

the two symbols overlap in the STNA. Symbol size is proportional to the NPP of each region. The isolines represent overall particulate C pump strength calculated as EExTE. See ~~section~~Sect. 2.5 for details.

4 Discussion

This study provides a comprehensive analysis of POC dynamics in the ~~top~~upper 1000 m of the North Atlantic, linking ~~POC distribution~~regional and ~~seasonality with~~seasonal changes in primary production, POC stocks and export fluxes to the underlying mechanisms of detrital POC production, transport ~~and~~, transformation ~~processes. In the following discussion we address the biophysical controls on epipelagic export fluxes (4.1), the interplay between mesopelagic POC removal by bacteria~~ and ~~zooplankton (4.2), and the links between model-based efficiency metrics and real world~~ decay. By comparing the simulation to available observations ~~(4.3). To conclude, we assess the limitations of the model and propose future research pathways (4.4). A summary schematic~~, our results shed light on how interactions between ecosystem structure and the physical environment together regulate epipelagic export and mesopelagic transformation of POC.

At the basin scale, and despite significant regional biases in some variables (Fig. 2–6), PISCES-simulated productivity and gravitational export fluxes are broadly consistent with observations and previous studies. As in satellite-based assessments (Henson et al., 2012; Siegel et al., 2023), maximum export fluxes (Fig. 5a,b) are displaced northward relative to NPP (Fig. 2a), reflecting regional differences in ecosystem structure and vertical mixing. Export efficiency increases toward subpolar waters (Fig. 10), concurrent with higher diatom abundance (Mouw et al., 2016b) and an increasing contribution of fast-sinking large detritus (Fig. 11). Conversely, at lower latitudes, dominance of small organisms and detritus, together with warmer temperatures and deeper productive layers, enhances degradation within the epipelagic and limits export efficiency (Fig. 4d, 7c, 10). These large-scale patterns are consistent with early conceptual frameworks linking new production, community structure, and gravitational export (Eppley & Peterson, 1979). ~~POC fluxes and budgets is provided in Fig. 8.~~and ultimately reflect the joint influence of vertical mixing regimes (Sverdrup, 1953; Margalef, 1978) and temperature-dependent remineralisation (Cael & Follows, 2016).

~~4.1.Vertical mixing controls POC export pathways~~

~~**The productivity and gravitational export fluxes simulated by PISCES are consistent with previous studies based on diverse approaches in the STNA (Lomas et al., 2010), Trans_Arca (Giering et al., 2014) and SPNA (Wang & Fennel, 2022) (see Fig. 3 and S3, S7). Simulated spatial patterns suggest**~~

Formatted: Font: 10 pt
Formatted: Font: 10 pt
Formatted: Left
Formatted: Line spacing: 1,5 lines
Formatted: Font: 10 pt
Formatted: Font: 10 pt
Formatted: Font: 10 pt
Formatted: Font: 10 pt
Formatted: Font: 10 pt
Formatted: Font: 10 pt
Formatted: Font: 10 pt
Formatted: Justified, Line spacing: 1,5 lines
Formatted: Font: 10 pt, Not Bold
Formatted: Font: 10 pt
Formatted: Left

~~a maximum export flux displaced to the north relative to NPP (Fig. 2), in line with satellite-based assessments (Henson et al., 2012; Siegel et al., 2023). Gravitational EE increases towards subpolar waters (Fig. 7), concurrent with diatom abundance (Mouw et al., 2016b). Likewise, the fraction of gravitational export channelled through large detritus increases from 47% to 66% towards subpolar waters (Fig. 9). At lower latitudes, a higher proportion of small plankton and slow-sinking detritus, along with higher temperatures and deeper Zprod, results in more intense detritus degradation within the productive layer (Fig. 4), hence smaller EE. These patterns are well established since the early studies that linked new and regenerated production, net community production, and gravitational sinking fluxes of POC~~Building on this context, the following sections examine in detail the biophysical controls on epipelagic export fluxes (4.1), the interplay between zooplanktonic and bacterial cycling of mesopelagic POC (4.2), and how modelled processes affect POC export and transfer efficiency metrics and relate to real-world observational constraints (4.3). Since most POC fluxes and derived metrics cannot be comprehensively evaluated against gridded observational products, we compare them with sparse available observations whenever possible. To close the Discussion, we assess the limitations of the current PISCES model formulation, leveraging observed biases to outline potential pathways for improving the representation of mesopelagic POC cycling in models (4.4).

4.1. POC inputs to the mesopelagic layer: POC sinking and vertical mixing

Evaluation against ^{234}Th- and sediment trap–based estimates indicates that PISCES reproduces the order of magnitude and broad seasonality of epipelagic export fluxes in the North Atlantic, while exhibiting regionally distinct biases. In the SPNA and at PAP, model–data agreement generally improves with depth and toward summer. At BATS/OFP the model captures the weak seasonal cycle but overestimates export at 150 m, particularly in winter–spring. According to PISCES, large detritus drives 67% of the gravitational flux at 100 m in the SPNA, exceeding the range (37–64%) estimated in the western subpolar gyre by Wang and Fennel (2022). The latter study further suggests that the contribution of large detritus increases with depth, opposite to model estimates (Fig. 4). In the eastern subtropical Atlantic at 260 m, the contribution of slow-sinking (likely small) particles was >60% during most of the year (Alonso-González et al., 2010), roughly consistent with ~50% in PISCES at 200 m (Fig. 11). Model-data discrepancies possibly reflect a combination of observational uncertainties (Buesseler et al., 2007; Bishop et al., 2012) and limitations in how the model represents POC export using rigid relationships between size classes and sinking velocities (Jackson & Burd, 2015; Iversen & Lampitt, 2020; Cael et al., 2021)

Vertical gradients in simulated export are usually strongest near Zprod (Palevsky & Doney, 2018; Buesseler et al., 2020) implying intense flux attenuation in the lower epipelagic and upper mesopelagic layers. Thus, uncertainties in the mathematical representation of export and attenuation processes, together with small spatiotemporal mismatches between simulations and

Formatted: Left

observations, can lead to substantial model-data deviations. Importantly, it remains unclear whether observational export estimates from sediment traps and the ^{234}Th technique isolate gravitational sinking alone (Fig. 5) or can also intercept downward transport by diffusion and advection (and, if so, how efficiently). We therefore interpret shallow export comparisons as quantitative consistency checks rather than direct validation (Aumont et al., 2017), and analyse mesopelagic POC inputs in terms of the total simulated downward POC flux, integrating gravitational sinking of detritus with diffusive and advective transport of both detrital and living particles.

Compared to gravitational fluxes, the transport of POC by vertical mixing has received little attention until recent years. Classical formulations of the biological pump have assumed vertical particle diffusion to be negligible at large scales (Martin et al., 1987), but oscillations in mixed layer depth can effectively entrain and detrain particles (Gardner et al., 1995). In models, these transports are diagnosed as diffusive fluxes, which our results show to be quantitatively relevant at large scales, in agreement with recent research (Bellacicco et al., 2025). In the NEMO-PISCES simulation, POC diffusion amounts to 37% (25%) of annual gravitational fluxes (Fig. 4) in the SPNA (Trans_Area), in line with independent estimates. For instance, Dall'Olmo et al. (2016) inferred that the POC mixed-layer pump could represent ~23% of annual mean gravitational fluxes at high latitudes. Lacour et al. (2019) used biogeochemical Argo float profiles to quantify springtime net POC detrainment at 4.6 mmol C m^{-2} d^{-1} (55 mg C m^{-2} d^{-1}) in the SPNA. Our corresponding estimate for March–May (4.3±1.1 mmol C m^{-2} d^{-1}) is strikingly similar, despite relying on a fundamentally different approach.

Crucially, PISCES further suggests that over 85% of this diffusive POC flux is associated with living plankton rather than detritus, reflecting the sharper vertical gradient of plankton biomass and their enhanced transport during convection events (Galí et al., submitted). Altogether, gravitational and diffusive export fluxes exhibit different seasonality and deliver to the mesopelagic layer different particle mixtures in terms of size, sinking speed, and composition. Differences in supplied POC entail different transformation pathways in the mesopelagic zone (Fig. 7–9 and 11), which are examined in the next section.

Formatted: Left

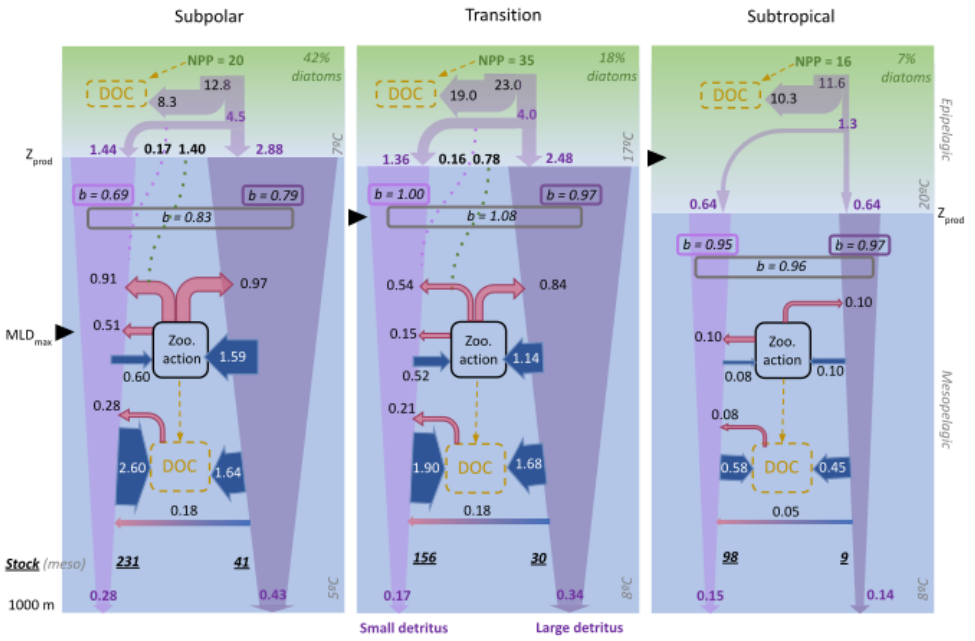

(Eppley & Peterson, 1979), ultimately reflecting the impact of different vertical mixing regimes (Sverdrup, 1953; Margalef, 1978) and temperature (Cael & Follows, 2016) on epipelagic ecosystems.

In comparison to the ecosystem drivers of gravitational fluxes, the direct transport of POC by vertical mixing has received little attention. For example, quoting the seminal paper of Martin et al. (1987), "It may be argued that vertical particle diffusion is unimportant for large spatial scales, and hence that the vertical particle distribution represents a balance between particle advection (including their gravitational sinking) and in situ production". While that is possibly the case in stagnant ocean interior waters, mixed layer depth oscillations can effectively entrain and detrain particles (Gardner et al., 1995). These transports can be diagnosed in models as diffusive fluxes, provided particle concentrations are represented realistically. For example, the lack of a suspended POC compartment precluded estimation of diffusive

Formatted: Font: 10 pt

Formatted: Left

~~POC transports in the study of Nowicki et al., (2022), which aimed at integrating all C pump mechanisms. In our NEMO-PISCES simulation, POC diffusion amounts to 37% (25%) of annual gravitational fluxes (Fig. 4) in the SPNA (Trans_Area), consistent with previous estimates. For example, Dall'Olmo et al., (2016) combined data from satellites, Argo floats and model simulations to estimate that the POC "mixed layer pump" could amount to 23% of annual mean gravitational fluxes at "high" latitudes (above 35°), regionally exceeding 100%. Lacour et al. (2019) used biogeochemical Argo float profiles to quantify net POC detrainment at 4.6 mmol C m^{-2} d^{-1} (55 mg C m^{-2} d^{-1}) in the SPNA during spring. Our mean estimate for the matching period (March-May) is 4.3±1.1 mmol C m^{-2} d^{-1}, strikingly similar given we used a completely different approach. PISCES further suggests that over 85% of this diffusive POC flux was "live" plankton. This is explained by the sharper vertical gradient of plankton compared to detritus, hence greater diffusive transport during convection events.~~

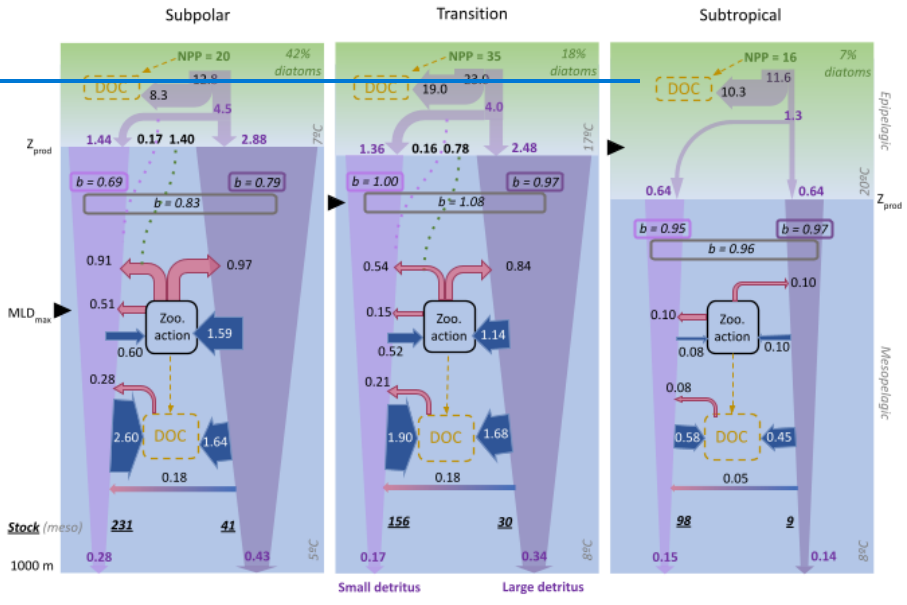

Formatted: Left

Figure ~~8~~11. *Annual budgets of detrital POC in the top km of the North Atlantic, focusing on mesopelagic transformations of small and large detritus. Epipelagic fluxes are shown more schematically, distinguishing the fraction of primary production (NPP) that flows through detrital particles and, within it, the fraction that results in gravitational (filled violet arrows) and diffusive (dotted purple lines) inputs to the mesopelagic layer. Additional particles enter the mesopelagic detrital pool via plankton vertical diffusion (dotted green lines) and subsequent conversion to detritus via mortality and zooplankton processing. Within the mesopelagic layer, blue and red arrows are used to distinguish sources and sinks, respectively, and violet arrows represent gravitational fluxes, whose narrowing represents flux attenuation. Arrow size is indicative of flux magnitude, but not to scale. All fluxes are in mmol C m^{-2} d^{-1}, and, for simplicity, fluxes smaller than 0.05 have been omitted. The vertical attenuation coefficient "b" (Martin et al., 1987), computed between Zprod and 1000 m (boxed ~~italics~~italic numbers, unitless), is shown separately for gravitational fluxes of small and large detritus and the gravitational+diffusive fluxes together. The mesopelagic vertically-integrated stocks, in mmol C m^{-2}, ~~are~~ are shown in bold italics. The percentage of diatoms ~~are~~is indicated in green at the top of each panel: 42% for SPNA, 18% for Trans_Area and 7% in the STNA.*

~~4.2. Zooplankton and bacteria jointly regulate mesopelagic detritus~~ Mesopelagic POC budgets

4.2. ~~**The *sdetoc* and *ldetoc* fluxes supplied**~~: joint regulation by ~~**the epipelagic ecosystem are differently attenuated and recycled by mesopelagic food webs in PISCES (Fig. 2-8). Zooplankton is key to detritus processing, with around half of the gravitational input flux passing through it in midlatitude and subpolar regions (Fig. 8). The influence of zooplankton on the fate of detritus has been previously emphasized by several studies (Stemmann et al., 2004a, and b; Gehlen et al., 2006; Steinberg & Landry, 2017; Stukel et al., 2019), and large sensitivity was also suggested in PISCES (see figure S3 in Aumont et al., 2017). Here we analyze in greater depth how zooplankton transformations and microbial degradation jointly shape mesopelagic detritus budgets.~~zooplankton and bacteria

Zooplankton plays a central role in detritus processing in PISCES: 50–60% of the gravitational input flux transits through zooplankton at mid and high latitudes, compared to ~20% in the subtropical area (Fig. 8 and 11). Importantly, zooplankton processing does not equate to POC flux attenuation, as a substantial and variable fraction returns to the sinking detritus pool via fragmentation, faecal pellet production and mortality (Fig. 8 and 9). As a result, POC recirculates within a mesopelagic detrital loop before final removal, primarily through bacterial decomposition (Fig. 11). In this section, we examine how

Formatted: Font: 10 pt
Formatted: Font: 10 pt
Formatted: Left
Formatted: Font: 10 pt
Formatted: Font: 10 pt
Formatted: Font: 10 pt
Formatted: Font: 10 pt, Not Bold
Formatted: Heading-Main, Left, Line spacing: 1,5 lines, Outline numbered + Level: 2 + Numbering Style: 1, 2, 3, … + Start at: 1 + Alignment: Left + Aligned at: 0,63 cm + Indent at: 1,27 cm
Formatted: Font: 10 pt, Not Bold
Formatted: Left

zooplankton transformations and microbial degradation jointly shape mesopelagic detritus budgets, and how these simulated rates compare with the limited available observations.

A stringent evaluation is provided by comparison with observations at the PAP site (see Fig. 2), where Giering et al. (2014) (G14) were able to constrain, within reasonable uncertainty, POC flux attenuation and mesopelagic metabolism. Using July–August PISCES means for the SPNA and the Trans_Area and acknowledging imperfect correspondence between model- and observations-derived rates, we find that PISCES reproduces within ±15% the magnitude of gravitational inputs, total zooplankton detritivory and bacterial degradation (Table 4). However, the model overestimates large-detritus fragmentation and the contribution of small detritus to POC decay. This discrepancy may partly reflect differences in pool definitions, as suspended POC in G14 is not fully equivalent to PISCES *sdetoc*, which accounts for suspended and slow-sinking fractions (Galí et al., 2022). Overall, this comparison is reassuring regarding simulated flux magnitudes, and further work is warranted to explore POC dynamics at the PAP site (Orihuela-García et al., *in prep*).

~~In PISCES, flux feeding and fragmentation of large detritus by mesozooplankton jointly account for 90% of the detritus fluxes through zooplankton. These processes simultaneously consume and slow down the sinking fluxes, transferring fast-sinking detritus to slow-sinking ones. The prevalence of these activities is regulated by the ratio between flux-feeding ingestion (particle interception) and total mesozooplankton ingestion (see 2.3). As a result, the flux feeder proportion increases with depth, from 20–30% in the epipelagic, above the peak of *ldetoc* sinking fluxes (see Fig. 4), to 60–85% through the mesopelagic layer (SI file 1). Seasonal export events increase zooplankton biomass and the proportion of flux feeders, which progressively enhances the removal of large sinking aggregates by mesozooplankton (Fig. 6). Ultimately, this trophic feedback limits the mesopelagic transfer efficiency during the high export season in the subpolar and transition areas.~~

~~In the SPNA, where the strongest diatom blooms occur, the enhanced fragility~~

In PISCES, flux feeding and fragmentation of large detritus by mesozooplankton critically influence the vertical transfer of gravitational fluxes (Fig. 8), consistent with previous assessments (Mayor et al., 2020). Seasonal export pulses enhance mesozooplankton biomass and the proportion of flux feeders (Sect 2.2; SI file 1), progressively intensifying removal of large sinking aggregates by mesozooplankton as the season advances (Fig. 9). Fragmentation of *ldetoc* into *sdetoc* additionally slows sinking fluxes, favouring microzooplankton consumption and microbial degradation over vertical transfer. Together, these trophic feedbacks limit mesopelagic TE during peak export periods (Fig. 9).

Formatted: Font: 10 pt
Formatted: Left
Formatted: Font: 10 pt
Formatted: Left

Although the functional representation of mesozooplankton activities in PISCES reasonably captures the magnitude of some observed process rates (Table 4), it necessarily simplifies the diversity of mesopelagic zooplankton communities and feeding strategies. In particular, the model cannot explicitly resolve the wide range of behaviours spanning flux-feeding Rhizaria to particle-attached copepods and other taxa that interact with sinking particles in distinct ways (Stukel et al., 2019; Mayor et al., 2020; Lampitt et al., 2023; Laget et al., 2024). As a result, the diagnosed trophic feedbacks should be interpreted as an emergent, functional representation of zooplankton–particle interactions rather than a taxonomically explicit description of mesopelagic food-web structure.

Large-detritus fragmentation deserves particular attention, as PISCES was the only CMIP6 model that explicitly represented this process (Henson et al., 2022). Because the model prescribes enhanced fragmentation of silica-rich aggregates ~~(see 2.3) maximizes *ldetoc*,~~ fragmentation is maximal in the SPNA (Fig. 8~~).~~ and 9; see also Fig. 3d). From May ~~through~~to July, zooplanktonic fragmentation ~~explains~~accounts for 19% of *ldetoc* flux attenuation in the SPNA, ~~and~~with bacterial disaggregation ~~causes~~contributing an additional 5~~% attenuation. Using bio-optical observations~~%. By comparison, Briggs et al. (2020) ~~found that~~attributed to fragmentation ~~explained~~ 49±22% of ~~the~~ fast-sinking particle flux attenuation during intense ~~sinking~~export events in the SPNA and the Southern Ocean~~, which is twice our estimate at the seasonal scale. Yet, their "fragmentation" estimate~~. This discrepancy likely reflects differences in process definitions and temporal averaging. In particular, the attenuation attributed to fragmentation by Briggs et al. (2020) better matches the 55% of *ldetoc* attenuation ~~not~~ explained by the sum of flux feeding, fragmentation and bacterial ~~remineralization~~disaggregation in PISCES. Further ~~comparisons between observations~~observational (Briggs et al., 2020; Wang & Fennel, 2022) and ~~models~~modelling efforts are needed to ~~reduce uncertainty in~~constrain fragmentation ~~estimates~~rates and mechanisms.

~~While~~ Despite the prominent role of zooplankton ~~plays a key role in detritus transformations~~, most ~~of the~~ flux attenuation in PISCES proceeds through microbial degradation (Fig. ~~8). The~~8, 9 and 11). Owing to the variable reactivity formulation ~~of detritus removal in PISCES yields a preferential loss of the labile fraction in~~, slow-sinking particles are degraded at ~~shallow~~shallower depths ~~(Fig. 4).~~than fast-sinking ones. Simulated ~~values of *k* (see 3.1) are~~ remineralisation rate constants (Fig. 7) fall within the wide range of ~~available~~ in situ ~~measurements, which is quite wide as a result of differences in experimental approaches, large measurement uncertainties, and inherent~~estimates, although natural and methodological variability preclude a conclusive assessment (Benner & Amon, 2015 and references therein; Belcher et al., 2016 and references therein; García-Martín et al., 2021). A more robust assessment is

obtained from vertically-integrated POC degradation rates. In the mesopelagic SPNA, decay rates in May–June (7 mmol C m^{-2} d^{-1}) resemble the GEOVIDE cruise mean (6.5 mmol C m^{-2} d^{-1}; Lemaitre et al. (2018), and summer estimates at PAP also agree within 10% (Table 4). Unfortunately, we are not aware of suitable datasets in the STNA, where available estimates reflect the respiration of POC+DOC (e.g., Ono et al., 2001) and therefore exceed simulated POC decay.

The contribution of different particle classes to community metabolism remains poorly constrained in both epipelagic (García-Martín et al., 2021) and mesopelagic waters (Table 4). In PISCES, ~~the~~ fast-sinking aggregates retain higher intrinsic reactivity ~~of large aggregates is counterbalanced by the greater~~(Fig. 7), whereas the larger stock of small detritus~~, such that *sdetoc* channels 53–61% of mesopelagic detritus degradation.~~ compensates for its lower reactivity. As a result, both particle types support comparable fractions of mesopelagic metabolism across regions (Fig. 11). Perhaps counterintuitively, ~~maximal~~the strongest *sdetoc* removal ~~rates~~, both in absolute (2.6 mmol C m^{-2} d^{-1}) ~~occur~~and relative terms (61%), occurs in the subpolar area, ~~fueled~~fuelled by particle diffusion and *ldetoc* fragmentation inputs. Overall, ~~PISCES~~these results ~~add to existing evidence for~~reinforce the ~~important role of~~emerging view that suspended and slow-sinking ~~detritus~~particles play a central role in the mesopelagic ~~metabolism~~carbon cycling (~~Arístegui et al., 2009;~~ Alonso-González et al., 2010; Baker et al., 2017; García-Martín et al., 2021; Wang and Fennel, 2022; Baumas & Bizic, 2024).

~~The increased residence time of detritus in shallow mesopelagic waters caused by *ldetoc* fragmentation further facilitates *sdetoc* ingestion by microzooplankton, resulting in a mesopelagic detrital loop that recycles particles before their terminal degradation (Fig. 8). This simulated interaction has some analogy with the microbial gardening hypothesis, which posits that zooplankton benefit from fragmenting detritus to feed on the bacterial and flagellate populations that thrive on them (Giering et al., 2014; Mayor et al., 2020).~~

Table 4. *Mesopelagic POC budgets: PISCES vs. data from Giering et al. (2014) at Porcupine Abyssal Plain (PAP, Jul-Aug). Data extracted from their Figure 2 and converted to mmol C m^{-2} d^{-1}. These budgets are not closed: some terms are omitted due to limited comparability, and a seasonal imbalance exists (at least in the model simulation).*

Process	G14 PAP	PISCES SPNA & Trans_Area	Deviation
Gravitational input	6.2	5.7	-7%

Formatted: Left
Formatted: Font: 10 pt
Formatted: Font: 10 pt
Formatted: Font: 10 pt
Formatted: Font: 10 pt
Formatted: Font: 10 pt
Formatted: Font: 10 pt
Formatted: Font: 10 pt
Formatted: Font: 10 pt
Formatted: Font: 10 pt
Formatted: Font: 10 pt
Formatted: Font: 10 pt
Formatted: Font: 10 pt
Formatted: Font: 10 pt
Formatted: Font: 10 pt
Formatted: Font: 10 pt
Field Code Changed
Formatted: Font: 10 pt, English (United Kingdom)
Formatted: Font: 10 pt, Bold, English (United Kingdom), Highlight
Formatted: Left

Process	G14 PAP	PISCES SPNA & Trans_Area	Deviation
Transformation			
Total zooplankton ingestion	3.8	3.2	-15%
of which fragmentation (*ldetoc*→*sdetoc*)	1.2	0.8	-30%
Removal			
Bacterial remineralisation (total)	5.3	5.7	+8%
of which small detritus (*sdetoc* only)	1.5	2.6	+70%

~~A stringent test for PISCES simulation results is the comparison to a study at the Porcupine Abyssal Plain (PAP) in the temperate North Atlantic (49ºN), where Giering et al. (2014) (G14) were able to match, within reasonable uncertainty, POC flux attenuation and mesopelagic metabolism. For this comparison, we use the July–August PISCES means for the SPNA and the Trans_Area (rates in mmol C m^{-2} d^{-1}). The gravitational input estimated by PISCES (G14) is 5.7 (6.2), of which 3.2 (3.8) flows through detritivorous mesozooplankton, 0.8 (1.2) is fragmented to small detritus, and 0.7 (1.0) recycled back to large detritus. Total detritus degradation by bacteria is 5.3 (5.8), with 2.6 (1.5) channelled via small detritus. It is worth noting that the suspended POC fraction in G14 may not be fully equivalent to PISCES *sdetoc*, which *de facto* accounts for the suspended and slow-sinking fractions (Galí et al., 2022) (Fig. 3). However, PISCES shows a net detritus loss of 0.8 mmol C m^{-2} d^{-1} in July–August, which in situ budgets omit. This comparison is overall reassuring with regard to PISCES skill, and further work is warranted to explore the C pump functioning at the PAP site (Orihuela-García et al., *in prep*).~~

Formatted: Font: 10 pt

Formatted: Left

Formatted: Font: 10 pt

Formatted: Left

4.3. ~~-~~Carbon pump efficiency metrics: from models to real-world measurements

~~Annual~~In PISCES, annual EE increases from 8% to 29% between subtropical and subpolar waters ~~in PISCES (Fig. 7). This~~ (Fig. 10). As found by Mouw et al. (2016b), this gradient mirrors the latitudinal ~~gradient is well~~increase in diatom abundance (Fig. 2), which in the model rises from 7% to 42% (Fig. 10). Although the modelled latitudinal EE gradient falls within the range of current estimates (Villa-Alfageme et al., 2016; Siegel et al., 2023)~~. Yet, our~~, EE is likely overestimated at mid and high latitudes because diatoms are overrepresented (Fig. 2 and 3; Table 3). Improved representation of phytoplankton functional groups and size structure in models is key to better constrain biological carbon export.

Our results ~~highlight~~further underscore the ~~need for~~importance of including non-gravitational POC fluxes in ~~C~~carbon pump ~~efficiency metrics, as current~~assessments. Neglecting these fluxes, especially those driven by vertical mixing, can substantially underestimate total POC export at high latitudes (Fig. 4 and 11). These unaccounted fluxes bias EE and TE estimates (Fig. 10) and affect interpretations of mesopelagic food-web metabolism and its seasonality (Fig. 9, S5 and S6) (Dall 'Olmo et al., 2016; Lacour et al., 2019). Current model intercomparison ~~exercises~~frameworks (e.g. CMIP) rely ~~only~~ on ~~the~~ simulated gravitational fluxes at standard depths (Palevsky & Doney, 2018; Henson et al., 2022; Wilson et al., 2022). ~~Disregarding non-gravitational fluxes, especially diffusion of plankton, distorts C pump metrics (Fig. S11) and, perhaps more importantly, our quantitative understanding of mesopelagic metabolism in relation to POC supply (Fig. 5, 6, 8 and S7).~~Thus, our findings suggest that non-gravitational POC transports, which are internally simulated by models, should be included in standard model intercomparison metrics.

~~Compared to the mechanisms that drive EE (see 4.1), the discussion about the factors controlling mesopelagic TE remains controversial. While some studies report higher TE at high latitudes (Marsay et al., 2015; DeVries & Weber, 2017) the opposite has also been found (Henson et al., 2012; Guidi et al., 2015). Noteworthy, PISCES results show a pattern that diverges from both scenarios. Instead of exhibiting a monotonic change from subtropical to subpolar oxic waters, PISCES simulates minimal TE at midlatitudes (Fig. 7), coinciding with the highest productivity (Fig. 2–4 and 8). Nevertheless, a significant TE difference between STNA and SPNA remains, consistent with findings from Henson et al. (2012) and Guidi et al. (2015). As we shall see, this pattern cannot be attributed to a single dominant factor.~~

Formatted: Font: 10 pt
Formatted: Line spacing: 1,5 lines
Formatted: Font: 10 pt
Formatted: Font: 10 pt
Formatted: Font: 10 pt
Formatted: Font: 10 pt
Formatted: Font: 10 pt
Formatted: Font: 10 pt
Formatted: Font: 10 pt
Formatted: Font: 10 pt
Formatted: Left
Formatted: Font: 10 pt
Formatted: Font: 10 pt
Formatted: Font: 10 pt
Formatted: Font: 10 pt
Formatted: Font: 10 pt
Formatted: Left

~~The lower lability of exported POC in subtropical areas, resulting from intense recycling by epipelagic food webs, was invoked to explain the latitudinal decrease in TE (Henson et al., 2012). On the other hand, the thermal control of microbial POC degradation, causing slower organic matter decay in cold waters, was used to explain the latitudinal increase in TE (DeVries & Weber, 2017). Interestingly, both phenomena occur in PISCES (Fig. S8), and their combined result is a midlatitude optimum in mesopelagic detritus degradation. To illustrate this, we computed the detritus turnover time for microbial degradation by dividing mesopelagic stocks by vertically integrated degradation rates (*sdetoc* + *ldetoc*; Fig. 8). Fastest microbial turnover occurs in the Trans_Area (52 days), followed by SPNA (64 days) and STNA (104 days). An analogous calculation for zooplanktonic detritivory also yields the shortest turnover time in the Trans_Area, concurrent with the highest proportion of flux feeders year round (which exceeds by 5–10% that in other regions, SI file S1). In all, the temperature-reactivity interaction, reinforced by zooplankton activities, results in the fastest mesopelagic detritus turnover in the Trans_Area, hence the lowest TE. Conversely, detritus recalcitrance and depressed mesopelagic mesozooplankton maximize TE in the STNA. The inverse relationship between NPP and TE found here somewhat resembles the findings of Lomas et al., (2010) who reported that, over the interannual scale, a positive trend in NPP and epipelagic export fluxes was counteracted by increased mesopelagic attenuation in the Sargasso Sea.~~

~~Considering the seasonal cycle is key when relating model results and observations (Ceballos-Romero et al., 2016) and for upscaling EE and TE from sparse measurements (De Melo Viríssimo et al., 2024). However, in this study, we refrained from reporting EE and TE at intra-annual scales. The reasons are manifold: (i) in the case of EE, there is a regionally varying time lag between NPP, detritus accumulation, and export rates (Fig. 2 and 3); (ii) in the case of TE, a distortion arises from the lagged vertical propagation of sinking fluxes. To palliate this issue, Giering et al., (2017) apply a lag correction to account for non-steady state conditions. However, complications arise when different transport mechanisms and organic carbon fractions are considered. For instance, in PISCES it would take 450 and 18 days, respectively, for *sdetoc* and *ldetoc* to travel between 100 and 1000 m if the vertical motion of those particles were only driven by gravitational sinking and no biological transformations and interconversion occurred. By contrast, vertical diffusion homogenizes tracer concentrations almost instantaneously,~~

Formatted: Left

~~reaching several hundred meters during deep convection events. These complexities jeopardize the use of simple non-steady state corrections in models and observations alike. Insights obtained from models can help assess the robustness of C pump metrics, eventually leading to improved metrics.~~

Compared to the mechanisms controlling EE (see 4.1), the factors regulating mesopelagic TE remain controversial. Mechanistic interpretations have alternately emphasised lower lability of exported POC in subtropical areas, leading to a latitudinal decrease in TE (Henson et al., 2012; Guidi et al., 2015), or reduced organic matter decay in cold mesopelagic waters, leading to a latitudinal increase in TE (DeVries & Weber, 2017). In PISCES, mesopelagic TE does not vary monotonically from subtropical to subpolar waters but instead exhibits a minimum at midlatitudes (Fig. 10). Lowest TE coincides with highest productivity (Fig. 10 and 11), broadly consistent with the climatological patterns reported by Mouw et al. (2016b). This relationship also resembles the opposite interannual trends of NPP and export versus mesopelagic transfer, reported by Lomas et al. (2010) in the Sargasso Sea. Still, TE remains higher in the STNA than in the SPNA. As we shall see, these patterns cannot be attributed to a single dominant factor.

Examination of the mechanisms driving mesopelagic TE in PISCES is informative because the model represents the interplay between variable POC reactivity and temperature-dependent decay rates (Fig. 7), as well as zooplankton detritivory. First, exported POC —especially *sdetoc*— is least reactive in the STNA, reflecting deeper and warmer Zprod (Fig. 4i), consistent with Henson et al. (2012) and Guidi et al. (2015). Second, mesopelagic POC decay rate constants also increase toward low latitudes, primarily due to temperature effects, consistent with Marsay et al. (2015) and de Vries and Weber (2017). Third, simulated detritivory rates decrease toward low latitudes (Fig. 11), but their relative importance peaks in the Trans_Area (Fig. 8), concurrent with the highest proportion of flux feeders (SI file S1). As a result of these interacting mechanisms, detritus turnover times with respect to both microbial and zooplanktonic removal (calculated as the quotient between stocks and removal rates; Fig. 11) are shortest in the Trans_Area, and much longer in the STNA. While these outcomes remain model-dependent and subject to known biases (Table 3), they help reconciling the lability- and temperature-based hypotheses, yielding a more nuanced understanding of mesopelagic TE variability (Marsay et al., 2015), and further highlight that zooplankton processes must be explicitly accounted for.

Previous studies showed that considering the seasonal cycle is key when linking EE and TE observations and models (Ceballos-Romero et al., 2016; De Melo Viríssimo et al., 2024). In this study, however, we refrain from reporting these metrics at intra-annual scale for the following reasons: (i) for EE, there is a regionally varying time lag between NPP, detritus accumulation, and export rates (Fig. 2–4); (ii) in the case of TE, distortion arises from the lagged vertical propagation of sinking POC fluxes (Giering et al., 2017), and from the lagged response of food-web processes that drive flux attenuation. In the highly seasonal SPNA, for example, sources exceed sinks by 25% in May, and sinks exceed sources by 23% in August (Fig. 9). Much larger imbalances may occur when examining smaller regions and non-climatological data. Such non-steady-state behaviour emerges

Formatted: Left

as an inherent feature of model-simulated POC budgets (Oliver et al., 2025), and explains difficulties in interpreting short-term in situ measurements (Giering et al., 2017).

4.4. Study limitations and ~~future research directions~~

4.4. ~~The regional biases shown in Fig. 2 and Table S4 indicate~~ pathways for model improvement~~. In the STNA, PISCES simulates only half of observed NPP and epipelagic sPOC stock, yet the bias of the upper mesopelagic sPOC stock is proportionally smaller. This suggests PISCES underestimates mesopelagic detritus removal, thus overestimating TE. In the Trans_Area, conversely, simulated NPP is realistic but the bias of the sPOC stock becomes more negative toward deeper waters. This may indicate an overestimation of detritus removal and an underestimation of TE. Only the SPNA shows similar biases of NPP and sPOC stocks in different layers. Thus, according to our diagnosis, improved model performance would narrow down the range of mesopelagic TE across regions.~~

~~Numerous processes are missing in the PISCES version used here: fluxes carried by zooplankton vertical migrations (Carr et al., 2008; Jónasdóttir et al., 2015; Gorgues et al., 2019); aggregate transformations by particle-associated copepods (Stemmann et al., 2004a and b; Kiørboe, 2011; Mayor et al., 2020); explicit representation of free-living and particle-attached bacteria, chemotrophic C fixation by deep-ocean prokaryotes, and bacterivory (Arístegui et al., 2009; Herndl et al., 2023). The inclusion of these processes might help close the gaps between the model and observations.~~

~~Our analysis purposely excluded some aspects of mesopelagic organic C cycling despite they are represented in PISCES. For example, we disregarded hypoxia-enhanced detritus preservation (DeVries & Weber, 2017) because oxygen minimum zones are excluded from our domain (Fig. 2). Assessment of organic C budgets is incomplete if DOC cycling and transport are not considered (Jiao et al., 2010; Nowicki et al., 2022). In PISCES, terminal detritus remineralization proceeds through DOC, reflecting that, in nature, bacteria ultimately rely on osmotrophic substrate uptake. The inclusion of DOC in the budgets would enable comparison to respiration measurements (Giering et al., 2014; García-Martín et al., 2021), fully assessing the fate of photosynthetic carbon.~~

Formatted: Font: 10 pt

Formatted: Font: 10 pt, Not Bold

Formatted: Heading-Main, Left, Space Before: 0 pt, After: 0 pt, Line spacing: 1,5 lines, Outline numbered + Level: 2 + Numbering Style: 1, 2, 3, … + Start at: 1 + Alignment: Left + Aligned at: 0,63 cm + Indent at: 1,27 cm

Formatted: Font: 10 pt, Not Bold

Formatted: Left

~~It is also important to acknowledge that the spatial patterns in TE may be sensitive to the depth bounds of the vertical domains analyzed (Fig. 4) (Marsay et al., 2015). Finally, interannual variations in the functioning of the biological C pump were overlooked here and deserve careful exploration.~~

Formatted: Left

In the previous sections, we have dissected the drivers of epipelagic export and mesopelagic POC budgets in PISCES. Here, we synthesise the resulting process-level understanding with the biases identified through model evaluation (Fig. 2–6) to provide a unified diagnosis of model performance across regions (Table 3) and outline pathways for model improvement.

In the subpolar area, simulated primary production and sPOC show small-to-moderate negative biases, while a clear bias in POC export cannot be identified (compare Fig. 5 and 6). Total phytoplankton biomass is reasonably simulated, but substantial positive biases in diatoms and mesozooplankton likely lead to an overestimation of export mediated by large detritus (Wang and Fennel, 2022). Correcting NPP underestimation would tend to increase sPOC stocks and exports. In contrast, correcting diatom overestimation would favour smaller classes of phytoplankton and detritus, lowering export efficiency. Addressing these opposing biases would likely improve model realism. In the mesopelagic SPNA, simulated sPOC stocks and export fluxes remain broadly consistent with epipelagic inputs, and the limited available observations are reasonably reproduced (Lemaitre et al., 2018), although fragmentation may be underestimated (Briggs et al., 2020). Uncertainties in the model representation of fragmentation will be addressed through sensitivity analyses in forthcoming work (Orihuela-García et al., *in prep.*).

In the midlatitude Trans_Area, epipelagic and mesopelagic biases differ in nature. Although diatoms are overrepresented at the expense of miscellaneous phytoplankton, NPP is accurately simulated, and no evident biases emerge in epipelagic sPOC stock and export fluxes, suggesting bias compensation. However, sPOC underestimation increases between epipelagic and upper mesopelagic waters, indicating excessive detritus removal. This is consistent with the overestimation of microbial POC degradation inferred from the comparison with PAP (Table 4) and would contribute to an underestimation of TE. Such a bias is not readily apparent from export flux comparisons alone, highlighting the value of evaluating models against diverse flux and stock datasets.

In the subtropical area, PISCES severely underestimates NPP, a bias that propagates to epipelagic sPOC stocks (Galí et al., 2022). Export production is instead overestimated, suggesting a strong positive bias in EE —at least according to BATS/OFP data at 150 m (Lomas et al., 2010). Below 500 m, POC fluxes are not overestimated, implying (i) an underestimation of mesopelagic TE, consistent with the increasing underestimation of sPOC with depth —also found in the Trans_Area—, and (ii) offsetting biases in EE and TE. Increasing NPP would likely exacerbate the positive bias in shallow export. This bias would further propagate vertically if mesopelagic transfer were corrected upward. Thus, PISCES' representation of POC cycling in epi- and upper mesopelagic oligotrophic waters may require revision.

Observed biases arise not only from model parameterisations but from missing biological functional groups and/or processes. Several mechanisms known to influence mesopelagic carbon cycling are not explicitly represented in the model used here, including: zooplankton vertical migrations (Carr et al., 2008; Jónasdóttir et al., 2015; Gorgues et al., 2019); the diversity of zooplankton feeding strategies (Stemmann et al., 2004b, 2004a; Kiørboe, 2011; Mayor et al., 2020; Lampitt et al., 2023; Laget

Formatted: Left

et al., 2024); and the distinct roles of free-living and particle-attached bacteria, carbon fixation by chemotrophic prokaryotes, and protist bacterivory (Arístegui et al., 2009; Herndl et al., 2023). For example, including zooplankton migration would be expected to enhance deep carbon export and likely mesopelagic sPOC stocks, while reducing NPP and epipelagic sPOC stocks (Aumont et al., 2018; Gorgues et al., 2019). These changes would entail region- and depth-dependent effects on model biases (Table 3). While incorporating missing processes might help bridge the gaps between the model and observations, it would increase model complexity and require extensive re-tuning to maintain consistency across coupled biogeochemical pathways.

~~5~~ 5. Conclusions

~~Using~~In this study, we evaluated the representation of POC dynamics in the upper 1000 m of the North Atlantic in the NEMO4-PISCESv2_RC ~~coupled~~ model ~~we obtained mechanistic~~ using diverse observational datasets. Combined with a detailed examination of detrital POC budgets extracted from the model, this approach provided insights into the processes regulating POC distribution, vertical export ~~patterns,~~ and biological ~~carbon pump efficiency across three North Atlantic~~ transformations in biogeochemically-contrasting regions. Below we summarise our main conclusions:

- ~~Gravitational~~PISCES-simulated gravitational fluxes~~, and the proportion channeled by large detritus (*ldetoc*)~~ increase with latitude (~~annual flux~~ from ~1.3 to 4.3 mmol C m^{-2} d^{-1}~~).~~ annually), whereas maximal primary production occurs in midlatitudes, in reasonable agreement with observations. Consequently, epipelagic export efficiency (EE) increases with latitude, mirroring the diatom fraction and the contribution of large, fast-sinking detrital aggregates to gravitational export. However, the model overestimates diatom biomass at mid and high latitudes, likely implying excessively large detritus export flux and removal pathways.
- In areas experiencing deep winter mixing, diffusive POC export fluxes ~~of particles (mostly~~(dominated by plankton biomass) peak in early spring, ~~before~~preceding the ~~season of intense~~ summertime peak in gravitational export~~, supplementing gravitational fluxes by up to 37% in the SPNA annually. Thus,~~. Model-derived diffusive fluxes ~~must be considered in C pump assessments~~are consistent with independent observational estimates, and supply ~1.6 mmol C m^{-2} d^{-1} to the mesopelagic subpolar Atlantic annually. Neglecting non-gravitational fluxes substantially underestimates EE in this region (21% vs. 29%) and obscures the coupling between primary production and mesopelagic metabolism.
- ~~Annual mesopelagic budgets in PISCES reveal distinct latitudinal regimes. Gravitational sinking is a major source in detrital budgets, but its contribution decreases northward as other sources, such as mortalities, sloppy feeding, large detritus fragmentation, and DOC aggregation, become more important. This shift is particularly pronounced in the small detritus (*sdetoc*) budget. Although bacterial degradation remains the primary removal mechanism for *sdetoc* (70–87%), its dominance decreases with latitude while zooplankton ingestion slightly increases. This pattern is most evident in the large detritus (*ldetoc*) budget, where removal by zooplankton accounts for up to 47% of *ldetoc* flux attenuation in the SPNA. These findings highlight the spatial heterogeneity of biogeochemical processes affecting particle dynamics.~~
- ~~Small detritus dominate particle degradation in all regions and drive between a third (Trans_Area) and half (STNA) of the gravitational fluxes at 1000 m. The variable reactivity scheme (Aumont et al., 2017) is the unique feature~~

Formatted: Font: Bold
Formatted: Normal, No bullets or numbering
Formatted: Font: 10 pt
Formatted: Left
Formatted: Font: 10 pt
Formatted: Font: 10 pt
Formatted: Font: 10 pt
Formatted: Font: 10 pt
Formatted: Font: 10 pt
Formatted: Font: 10 pt
Formatted: Font: 10 pt, Not Bold
Formatted: Left, Bulleted + Level: 1 + Aligned at: 0,63 cm + Indent at: 1,27 cm
Formatted: Font: Not Bold
Formatted: Left

~~enabling PISCES to capture the dynamics and stocks of small detritus, *de facto* accounting for both suspended and slow-sinking fractions. Moreover, PISCES is the only CMIP-class model featuring zooplankton fragmentation (Henson et al. 2022), which critically influences POC budgets by attenuating fast-sinking fluxes and boosting *sdetoc* turnover. Given the reasonable match with available observations (e.g., Giering et al., 2014), we prompt inclusion of these processes in other models, while refining their parameterization.~~

- ~~Mesopelagic trophic feedbacks triggered by seasonal gravitational supply drive the increased attenuation of POC fluxes in productive conditions. In PISCES, contrasting with previous studies, annual TE is minimal in the midlatitudes, the region with highest annual NPP, reflecting synergistic effects of temperature, detritus reactivity, and zooplankton attenuation.~~

- In the subtropical area, bias compensation between underestimated primary production and overestimated POC export leads to overestimation of modelled EEE (8%). In the lower mesopelagic, however, the model reproduces observed gravitational fluxes, suggesting that model-diagnosed transfer efficiency (23%) may be underestimated. Negative biases in mesopelagic small POC further indicate an increasing imbalance in modelled detritus supply and removal toward low latitudes. These biases warrant further examination, given the large contribution of oligotrophic regions to global POC export.
- Mesopelagic POC budgets are jointly regulated by zooplankton transformations and microbial degradation. A large fraction of the gravitational POC supply —up to 60% in the subpolar region— transits through zooplankton. Much of this material is recycled via fragmentation, faecal pellet production, and mortality, rather than being immediately attenuated. This mesopelagic detrital loop modulates particle size, sinking speed, and residence time, thereby shaping microbial remineralisation pathways and rates that ultimately drive POC decay. Modelled mesopelagic decay rates agree within ±15% with scarce observations at mid-to-high latitudes.
- In PISCES, mesopelagic transfer efficiency is lowest in midlatitudes and coincides with maximal productivity, consistent with some observational assessments. This pattern arises from interacting mechanisms: (i) increasing lability of exported POC toward higher latitudes; (ii) increasing temperature-driven mesopelagic decay rates toward low latitudes; (iii) seasonal trophic feedback between aggregate export and zooplankton, by which enhanced export of large aggregates triggers zooplankton detritivory and fragmentation, limiting transfer efficiency in productive regions. These modelled mechanisms reconcile apparently contradictory hypotheses and highlight the essential role of zooplankton in regulating mesopelagic POC transfer.
- Small slow-sinking detritus supports 50–61% of mesopelagic POC decay across regions and drives 33–50% of the export flux at 1000 m. Key modelled responses enabling these contributions are (i) diverse sources for small detritus —such as zooplankton fragmentation and bacterial disaggregation of large aggregates, plankton mortality, and sloppy feeding— and (ii) the refractory nature of small particles reaching the lower mesopelagic in PISCES. Further research is needed to clarify functional links between small and large POC fractions and their model representation.

Formatted: Left

- Overall, this study demonstrates the value of a mechanistic, budget-based approach to evaluating models of the biological carbon pump. Detailed POC budget analysis reveals model-specific drivers of export and transfer efficiency and provides a reproducible method to diagnose inter-model biases. This approach can guide model tuning and the development of parameterisations for missing processes. Ultimately, biases in modelled POC budgets can inform assessments of biogenic DIC sequestration fluxes.

Formatted: Left

Appendices

Supplementary information with supplementary text, tables and figures is included in a pdf document. In addition, there are two files (S1 and S2) with the post-processed model output data in the supplementary information section.

Code, data, or code and data availability

Post-processed data are available as annexes in the supplementary information section and additional detailed information on the raw outputs will be provided upon request. The open-source Autosubmit workflow manager (https://autosubmit.readthedocs.io/en/master/) was used to ensure simulation reproducibility. All analyses and plots were developed through open-source code: Python3 (https://python.org/, last access: 12 February 2026), ESMValCore (https://doi.org/10.5281/zenodo.3387139, last access: 26 March 2025), and R version 4.3.3 (https://cran.r-project.org/bin/, April 2024). The codes used for the analysis and plots, including Jupyter notebooks, will be made available upon request to the MAOG. All observational data used for model evaluation are publicly available.

Author contributions

Conceptualisation: MAOG, MG, YRR, RB
Methodology: MAOG, MG, YRR, VL, MC, SL, MSC, PAB
Investigation: MAOG, MG, YRR
Visualisation: MAOG, MG
Funding acquisition: MG, YRR
Project administration: MG, YRR
Supervision: MG, YRR
Writing – original draft: MAOG
Writing – review & editing: MAOG, MG, YRR, RB.

Competing interests.

Authors declare that they have no competing interests

Acknowledgements & Financial support

We thank the Barcelona Supercomputing Center team (Eneko Martín-Martínez, Marcus Falls, Victòria Agudetse, Eric Ferrer, Elisa Bergas-Massó, Joan Llort and Valentina Sicardi) for their help in developing the experiment set-up and/or postprocessing

Formatted: Font: 10 pt, Font colour: Black
Formatted: Font: 10 pt
Formatted: Heading 1, Space Before: 0 pt, Line spacing: single, Pattern: Clear
Formatted: Font: 10 pt, Not Bold, Font colour: Auto
Formatted: Left

and plotting results, and Olivier Aumont for useful discussions. The Spanish Sciences and Universities Ministry funded this work through a personal FPI grant (PRE2020-093628, to M.A.O-G.) and the OPERA project (PID2019-107952GA-I00, to M.G. and Y.R-R.). ~~-~~M.G. acknowledges financial support through a Junior Leader Fellowship from "La Caixa" Banking Foundation (ORCAS project; LCF/BQ/PI18/11630009). The ICM-CSIC is supported by a "Severo Ochoa" Centre of Excellence grant (CEX2019-000928-S). We thank ~~the~~two anonymous reviewers for their comments, which helped improve the manuscript.

~~**Open Research**~~

~~Post-processed data are available as annexes in the supplementary materials section and additional detailed information on the raw outputs will be provided upon request. The simulations in this study were performed in MareNostrum4 using the Autosubmit workflow manager (https://autosubmit.readthedocs.io/en/master/). All analyses and plots were developed through open-source code: Python3 (https://python.org/, last access: 26 March 2025) and ESMValCore, a community tool for pre-processing data from Earth system models and running analysis script (https://doi.org/10.5281/zenodo.3387139, last access: 26 March 2025). The codes used for the analysis and plots, including Jupyter notebooks, will be available upon request to the corresponding author. All observational data used in model evaluation are publicly available on their websites.~~

References

Alonso-González, I. J., Arístegui, J., Lee, C., Sanchez-Vidal, A., Calafat, A., Fabrés, J., Sangrá, P., Masqué, P., Hernández-Guerra, A., & Benítez-Barrios, V. (2010). Role of slowly settling particles in the ocean carbon cycle. *Geophysical Research Letters*, *37*(13), 2010GL043827. https://doi.org/10.1029/2010GL043827

Formatted: Font: 10 pt, Not Bold, Font colour: Auto
Formatted: Font: 10 pt, Not Bold, Font colour: Auto
Formatted: Font: 10 pt, Font colour: Black
Formatted: Font: 10 pt, Font colour: Auto
Formatted: Left, Line spacing: single, Pattern: Clear
Formatted: Font: 10 pt, Font colour: Black
Formatted: Font: 10 pt, Not Bold, Font colour: Auto
Formatted: Left

Alonso-González, I. J., Arístegui, J., Vilas, J. C., & Hernández-Guerra, A. (2009). Lateral POC transport and consumption in surface and deep waters of the Canary Current region: A box model study. *Global Biogeochemical Cycles*, *23*(2), 2008GB003185. https://doi.org/10.1029/2008GB003185

Arístegui, J., Gasol, J. M., Duarte, C. M., & Herndld, G. J. (2009). Microbial oceanography of the dark ocean's pelagic realm. *Limnology and Oceanography*, *54*(5), 1501–1529. https://doi.org/10.4319/lo.2009.54.5.1501

Aumont, O., Ethé, C., Tagliabue, A., Bopp, L., & Gehlen, M. (2015). PISCES-v2: An ocean biogeochemical model for carbon and ecosystem studies. *Geoscientific Model Development*, *8*(8), 2465–2513. https://doi.org/10.5194/gmd-8-2465-2015

Aumont, O., Maury, O., Lefort, S., & Bopp, L. (2018). Evaluating the Potential Impacts of the Diurnal Vertical Migration by Marine Organisms on Marine Biogeochemistry. *Global Biogeochemical Cycles*, *32*(11), 1622–1643. https://doi.org/10.1029/2018GB005886

Aumont, O., Van Hulten, M., Roy-Barman, M., Dutay, J.-C., Éthé, C., & Gehlen, M. (2017). Variable reactivity of particulate organic matter in a global ocean biogeochemical model. *Biogeosciences*, *14*(9), 2321–2341. https://doi.org/10.5194/bg-14-2321-2017

Baker, C. A., Henson, S. A., Cavan, E. L., Giering, S. L. C., Yool, A., Gehlen, M., Belcher, A., Riley, J. S., Smith, H. E. K., & Sanders, R. (2017). Slow-sinking particulate organic carbon in the Atlantic Ocean: Magnitude, flux, and potential controls. *Global Biogeochemical Cycles*, *31*(7), 1051–1065. https://doi.org/10.1002/2017GB005638

Baumas, C., & Bizic, M. (2024). A focus on different types of organic matter particles and their significance in the open ocean carbon cycle. *Progress in Oceanography*, *224*, 103233. https://doi.org/10.1016/j.pocean.2024.103233

Belcher, A., Iversen, M., Giering, S., Riou, V., Henson, S. A., Berline, L., Guilloux, L., & Sanders, R. (2016). Depth-resolved particle-associated microbial respiration in the northeastAtlantic. *Biogeosciences*, *13*(17), 4927–4943. https://doi.org/10.5194/bg-13-4927-2016

Bellacicco, M., Marullo, S., Dall'Olmo, G., Iudicone, D., & Buongiorno Nardelli, B. (2025). The oceanic physical injection pump of organic carbon. *Nature Communications*, *16*(1), 7100. https://doi.org/10.1038/s41467-025-62363-z

Formatted: Left

Benner, R., & Amon, R. M. W. (2015). The Size-Reactivity Continuum of Major Bioelements in the Ocean. *Annual Review of Marine Science*, *7*(1), 185–205. https://doi.org/10.1146/annurev-marine-010213-135126

Berger, W. H., & Wefer, G. (1990). Export production: Seasonality and intermittency, and paleoceanographic implications. *Global and Planetary Change*, 3(3), 245-254.

Bishop, J. K. B., Lam, P. J., & Wood, T. J. (2012). Getting good particles: Accurate sampling of particles by large volume in-situ filtration. *Limnology and Oceanography: Methods*, *10*(9), 681–710. https://doi.org/10.4319/lom.2012.10.681

Bol, R., Henson, S. A., Rumyantseva, A., & Briggs, N. (2018). High-Frequency Variability of Small-Particle Carbon Export Flux in the Northeast Atlantic. *Global Biogeochemical Cycles*, *32*(12), 1803–1814. https://doi.org/10.1029/2018GB005963

Boudreau, B. P., & Ruddick, B. R. (1991). On a reactive continuum representation of organic matter diagenesis. *American Journal of Science*, *291*(5), 507–538. https://doi.org/10.2475/ajs.291.5.507

Boyd, P. W., Claustre, H., Levy, M., Siegel, D. A., & Weber, T. (2019). Multi-faceted particle pumps drive carbon sequestration in the ocean. *Nature*, *568*(7752), 327–335. https://doi.org/10.1038/s41586-019-1098-2

Brabson, E. K., Doyle, L. F., Acosta, R. P., Fedorov, A. V., Hull, P. M., & Burls, N. J. (2025). *A Revised Temperature-Dependent Remineralization Scheme for the Community Earth System Model (v1.2.2)*. Climate and Earth system modeling. https://doi.org/10.5194/egusphere-2025-3808

Bressac, M., Laurenceau-Cornec, E. C., Kennedy, F., Santoro, A. E., Paul, N. L., Briggs, N., Carvalho, F., & Boyd, P. W. (2024). Decoding drivers of carbon flux attenuation in the oceanic biological pump. *Nature*, *633*(8030), 587–593. https://doi.org/10.1038/s41586-024-07850-x

Briggs, N., Dall'Olmo, G., & Claustre, H. (2020). Major role of particle fragmentation in regulating biological sequestration of CO_2 by the oceans. *Science*, *367*(6479), 791–793. https://doi.org/10.1126/science.aay1790

Brun, P., Stamieszkin, K., Visser, A. W., Licandro, P., Payne, M. R., & Kiørboe, T. (2019). Climate change has altered zooplankton-fuelled carbon export in the North Atlantic. *Nature Ecology & Evolution*, *3*(3), 416–423. https://doi.org/10.1038/s41559-018-0780-3

Formatted: Left

Buesseler, K. O. (1998). The decoupling of production and particulate export in the surface ocean. *Global Biogeochemical Cycles*, *12*(2), 297–310. https://doi.org/10.1029/97GB03366

Buesseler, K. O., Boyd, P. W., Black, E. E., & Siegel, D. A. (2020). Metrics that matter for assessing the ocean biological carbon pump. *Proceedings of the National Academy of Sciences*, *117*(18), 9679–9687. https://doi.org/10.1073/pnas.1918114117

Buesseler, K. O., Lamborg, C. H., Boyd, P. W., Lam, P. J., Trull, T. W., Bidigare, R. R., Bishop, J. K. B., Casciotti, K. L., Dehairs, F., Elskens, M., Honda, M., Karl, D. M., Siegel, D. A., Silver, M. W., Steinberg, D. K., Valdes, J., Van Mooy, B., & Wilson, S. (2007). Revisiting Carbon Flux Through the Ocean's Twilight Zone. *Science*, *316*(5824), 567–570. https://doi.org/10.1126/science.1137959

Burd, A. B., Hansell, D. A., Steinberg, D. K., Anderson, T. R., Arístegui, J., Baltar, F., Beaupré, S. R., Buesseler, K. O., DeHairs, F., Jackson, G. A., Kadko, D. C., Koppelmann, R., Lampitt, R. S., Nagata, T., Reinthaler, T., Robinson, C., Robison, B. H., Tamburini, C., & Tanaka, T. (2010). Assessing the apparent imbalance between geochemical and biochemical indicators of meso- and bathypelagic biological activity: What the @$♯! is wrong with present calculations of carbon budgets? *Deep Sea Research Part II: Topical Studies in Oceanography*, *57*(16), 1557–1571. https://doi.org/10.1016/j.dsr2.2010.02.022

Cael, B. B., Cavan, E. L., & Britten, G. L. (2021). Reconciling the Size-Dependence of Marine Particle Sinking Speed. *Geophysical Research Letters*, *48*(5), e2020GL091771. https://doi.org/10.1029/2020GL091771

Cael, B. B., & Follows, M. J. (2016). On the temperature dependence of oceanic export efficiency. *Geophysical Research Letters*, *43*(10), 5170–5175. https://doi.org/10.1002/2016GL068877

Carr, S. D., Capet, X. J., Mcwilliams, J. C., Pennington, J. T., & Chavez, F. P. (2008). The influence of diel vertical migration on zooplankton transport and recruitment in an upwelling region: Estimates from a coupled behavioral-physical model. *Fisheries Oceanography*, *17*(1), 1–15. https://doi.org/10.1111/j.1365-2419.2007.00447.x

Ceballos-Romero, E., Le Moigne, F. A. C., Henson, S., Marsay, C. M., Sanders, R. J., García-Tenorio, R., & Villa-Alfageme, M. (2016). Influence of bloom dynamics on Particle Export Efficiency in the North Atlantic: A

Formatted: Left

comparative study of radioanalytical techniques and sediment traps. *Marine Chemistry*, *186*, 198–210. https://doi.org/10.1016/j.marchem.2016.10.001

Claustre, H., Legendre, L., Boyd, P. W., & Levy, M. (2021). The Oceans' Biological Carbon Pumps: Framework for a Research Observational Community Approach. *Frontiers in Marine Science*, *8*, 780052. https://doi.org/10.3389/fmars.2021.780052

Dall'Olmo, G., Dingle, J., Polimene, L., Brewin, R. J. W., & Claustre, H. (2016). Substantial energy input to the mesopelagic ecosystem from the seasonal mixed-layer pump. *Nature Geoscience*, *9*(11), 820–823. https://doi.org/10.1038/ngeo2818

De Boyer Montégut, C. (2023). *Mixed layer depth climatology computed with a density threshold criterion of 0.03kg/m3 from 10 m depth value* [~~Dataset~~Data set]. SEANOE. https://doi.org/10.17882/91774

De Melo Viríssimo, F., Martin, A. P., & Henson, S. A. (2022). Influence of Seasonal Variability in Flux Attenuation on Global Organic Carbon Fluxes and Nutrient Distributions. *Global Biogeochemical Cycles*, *36*(2), e2021GB007101. https://doi.org/10.1029/2021GB007101

De Melo Viríssimo, F., Martin, A. P., Henson, S. A., & Wilson, J. D. (2024). Seasonality in Carbon Flux Attenuation Explains Spatial Variability in Transfer Efficiency. *Geophysical Research Letters*, *51*(4), e2023GL107050. https://doi.org/10.1029/2023GL107050

DeVries, T., & Weber, T. (2017). The export and fate of organic matter in the ocean: New constraints from combining satellite and oceanographic tracer observations. *Global Biogeochemical Cycles*, *31*(3), 535–555. https://doi.org/10.1002/2016GB005551

Doléac, S., Lévy, M., El Hourany, R., & Bopp, L. (2025). Toward more robust net primary production projections in the North Atlantic Ocean. *Biogeosciences*, *22*(4), 841–862. https://doi.org/10.5194/bg-22-841-2025

Doney, S. C., Mitchell, K. A., Henson, S. A., Cavan, E., DeVries, T., Gruber, N., Hauck, J., Mouw, C. B., Müller, J. D., & Primeau, F. W. (2024). Observational and Numerical Modeling Constraints on the Global Ocean Biological Carbon Pump. *Global Biogeochemical Cycles*, *38*(7), e2024GB008156. https://doi.org/10.1029/2024GB008156

Formatted: Left

Eppley, R. W., & Peterson, B. J. (1979). Particulate organic matter flux and planktonic new production in the deep ocean. *Nature*, *282*(5740), 677–680. https://doi.org/10.1038/282677a0

Fennel, K., Mattern, J. P., Doney, S. C., Bopp, L., Moore, A. M., Wang, B., & Yu, L. (2022). Ocean biogeochemical modelling. *Nature Reviews Methods Primers*, *2*(1), 76. https://doi.org/10.1038/s43586-022-00154-2

Francois, R., Honjo, S., Krishfield, R., & Manganini, S. (2002). Factors controlling the flux of organic carbon to the bathypelagic zone of the ocean. *Global Biogeochemical Cycles*, *16*(4). https://doi.org/10.1029/2001GB001722

Frenger, I., Landolfi, A., Kvale, K., Somes, C. J., Oschlies, A., Yao, W., & Koeve, W. (2024). Misconceptions of the marine biological carbon pump in a changing climate: Thinking outside the "export" box. *Global Change Biology*, *30*(1), e17124. https://doi.org/10.1111/gcb.17124

Galí, M., Falls, M., Claustre, H., Aumont, O., & Bernardello, R. (2022). Bridging the gaps between particulate backscattering measurements and modeled particulate organic carbon in the ocean. *Biogeosciences*, *19*(4), 1245–1275. https://doi.org/10.5194/bg-19-1245-2022

García-Martín, E. E., Sanders, R., Evans, C. D., Kitidis, V., Lapworth, D. J., Rees, A. P., Spears, B. M., Tye, A., Williamson, J. L., Balfour, C., Best, M., Bowes, M., Breimann, S., Brown, I. J., Burden, A., Callaghan, N., Felgate, S. L., Fishwick, J., Fraser, M., … Mayor, D. J. (2021). Contrasting Estuarine Processing of Dissolved Organic Matter Derived From Natural and Human-Impacted Landscapes. *Global Biogeochemical Cycles*, *35*(10), e2021GB007023. https://doi.org/10.1029/2021GB007023

Gardner, W. D., Chung, S. P., Richardson, M. J., & Walsh, I. D. (1995). The oceanic mixed-layer pump. *Deep Sea Research Part II: Topical Studies in Oceanography*, *42*(2–3), 757–775. https://doi.org/10.1016/0967-0645(95)00037-Q

Gasol, J. M., Del Giorgio, P. A., & Duarte, C. M. (1997). Biomass distribution in marine planktonic communities. *Limnology and Oceanography*, *42*(6), 1353–1363. https://doi.org/10.4319/lo.1997.42.6.1353

Gehlen, M., Bopp, L., Emprin, N., Aumont, O., Heinze, C., & Ragueneau, O. (2006). *Reconciling surface ocean productivity, export fluxes and sediment composition in a global biogeochemical ocean model*.

Formatted: Left

Giering, S. L. C., Sanders, R., Lampitt, R. S., Anderson, T. R., Tamburini, C., Boutrif, M., Zubkov, M. V., Marsay, C. M., Henson, S. A., Saw, K., Cook, K., & Mayor, D. J. (2014). Reconciliation of the carbon budget in the ocean's twilight zone. *Nature*, *507*(7493), 480–483. https://doi.org/10.1038/nature13123

Giering, S. L. C., Sanders, R., Martin, A. P., Lindemann, C., Möller, K. O., Daniels, C. J., Mayor, D. J., & St. John, M. A. (2016). High export via small particles before the onset of the ~~N orth A tlantic~~North Atlantic spring bloom. *Journal of Geophysical Research: Oceans*, *121*(9), 6929–6945. https://doi.org/10.1002/2016JC012048

Gorgues, T., Aumont, O., & Memery, L. (2019). Simulated Changes in the Particulate Carbon Export Efficiency due to Diel Vertical Migration of Zooplankton in the North Atlantic. *Geophysical Research Letters*, *46*(10), 5387–5395. https://doi.org/10.1029/2018GL081748

Guidi, L., Legendre, L., Reygondeau, G., Uitz, J., Stemmann, L., & Henson, S. A. (2015). A new look at ocean carbon remineralization for estimating deepwater sequestration. *Global Biogeochemical Cycles*, *29*(7), 1044–1059. https://doi.org/10.1002/2014GB005063

Henson, S. A., Laufkötter, C., Leung, S., Giering, S. L. C., Palevsky, H. I., & Cavan, E. L. (2022). Uncertain response of ocean biological carbon export in a changing world. *Nature Geoscience*, *15*(4), 248–254. https://doi.org/10.1038/s41561-022-00927-0

Henson, S. A., Sanders, R., & Madsen, E. (2012). Global patterns in efficiency of particulate organic carbon export and transfer to the deep ocean. *Global Biogeochemical Cycles*, *26*(1), 2011GB004099. https://doi.org/10.1029/2011GB004099

Henson, S. A., Yool, A., & Sanders, R. (2015). Variability in efficiency of particulate organic carbon export: A model study. *Global Biogeochemical Cycles*, *29*(1), 33–45. https://doi.org/10.1002/2014GB004965

Henson, S., Bisson, K., Hammond, M. L., Martin, A., Mouw, C., & Yool, A. (2024). Effect of sampling bias on global estimates of ocean carbon export. *Environmental Research Letters*, *19*(2), 024009. https://doi.org/10.1088/1748-9326/ad1e7f

Formatted: Left

Hernández-León, S., Calles, S., & Fernández De Puelles, M. L. (2019). The estimation of metabolism in the mesopelagic zone: Disentangling deep-sea zooplankton respiration. *Progress in Oceanography*, *178*, 102163. https://doi.org/10.1016/j.pocean.2019.102163

Herndl, G. J., Bayer, B., Baltar, F., & Reinthaler, T. (2023). Prokaryotic Life in the Deep Ocean's Water Column. *Annual Review of Marine Science*, *15*(1), 461–483. https://doi.org/10.1146/annurev-marine-032122-115655

Honjo, S. (1980). Material fluxes and modes of sedimentation in the mesopelagic and bathypelagic zones. *Journal of Marine Research 38, (1)*. https://elischolar.library.yale.edu/journal_of_marine_research/1499

Iversen, M. H., & Lampitt, R. S. (2020). Size does not matter after all: No evidence for a size-sinking relationship for marine snow. *Progress in Oceanography*, *189*, 102445. https://doi.org/10.1016/j.pocean.2020.102445

Jackson, G. A. (1993). Flux feeding as a mechanism for zooplankton grazing and its implications for vertical particulate flux ~~t~~. *Limnology and Oceanography*, *38*(6), 1328–1331. https://doi.org/10.4319/lo.1993.38.6.1328

Jackson, G. A., & Burd, A. B. (2015). Simulating aggregate dynamics in ocean biogeochemical models. *Progress in Oceanography*, *133*, 55–65. https://doi.org/10.1016/j.pocean.2014.08.014

Jiao, N., Herndl, G. J., Hansell, D. A., Benner, R., Kattner, G., Wilhelm, S. W., Kirchman, D. L., Weinbauer, M. G., Luo, T., Chen, F., & Azam, F. (2010). Microbial production of recalcitrant dissolved organic matter: Long-term carbon storage in the global ocean. *Nature Reviews Microbiology*, *8*(8), 593–599. https://doi.org/10.1038/nrmicro2386

Johnson, W. M., Longnecker, K., Kido Soule, M. C., Arnold, W. A., Bhatia, M. P., Hallam, S. J., Van Mooy, B. A. S., & Kujawinski, E. B. (2020). Metabolite composition of sinking particles differs from surface suspended particles across a latitudinal transect in the South Atlantic. *Limnology and Oceanography*, *65*(1), 111–127. https://doi.org/10.1002/lno.11255

Jónasdóttir, S. H., Visser, A. W., Richardson, K., & Heath, M. R. (2015). Seasonal copepod lipid pump promotes carbon sequestration in the deep North Atlantic. *Proceedings of the National Academy of Sciences*, *112*(39), 12122–12126. https://doi.org/10.1073/pnas.1512110112

Kharbush, J. J., Close, H. G., Van Mooy, B. A. S., Arnosti, C., Smittenberg, R. H., Le Moigne, F. A. C., Mollenhauer, G., Scholz-Böttcher, B., Obreht, I., Koch, B. P., Becker, K. W., Iversen, M. H., & Mohr, W. (2020). Particulate Organic

Formatted: Left

Carbon Deconstructed: Molecular and Chemical Composition of Particulate Organic Carbon in the Ocean. *Frontiers in Marine Science*, *7*, 518. https://doi.org/10.3389/fmars.2020.00518

Kiørboe, T. (2011). How zooplankton feed: Mechanisms, traits and trade-offs. *Biological Reviews*, *86*(2), 311–339. https://doi.org/10.1111/j.1469-185X.2010.00148.x

Kiørboe, T., Tang, K., Grossart, H.-P., & Ploug, H. (2003). Dynamics of Microbial Communities on Marine Snow Aggregates: Colonization, Growth, Detachment, and Grazing Mortality of Attached Bacteria. *Applied and Environmental Microbiology*, *69*(6), 3036–3047. https://doi.org/10.1128/AEM.69.6.3036-3047.2003

Kobayashi, S., Ota, Y., Harada, Y., Ebita, A., Moriya, M., Onoda, H., Onogi, K., Kamahori, H., Kobayashi, C., Endo, H., Miyaoka, K., & Takahashi, K. (2015). The JRA-55 Reanalysis: General Specifications and Basic Characteristics. *Journal of the Meteorological Society of Japan. Ser. II*, *93*(1), 5–48. https://doi.org/10.2151/jmsj.2015-001

Koestner, D., Stramski, D., & Reynolds, R. A. (2024). Improved multivariable algorithms for estimating oceanic particulate organic carbon concentration from optical backscattering and chlorophyll-a measurements. *Frontiers in Marine Science*, *10*, 1197953. https://doi.org/10.3389/fmars.2023.1197953

Kulk, G., Platt, T., Dingle, J., Jackson, T., Jönsson, B., Bouman, H., Babin, M., Brewin, R., Doblin, M., Estrada, M., Figueiras, F., Furuya, K., González-Benítez, N., Gudfinnsson, H., Gudmundsson, K., Huang, B., Isada, T., Kovač, Ž., Lutz, V., … Sathyendranath, S. (2020). Primary Production, an Index of Climate Change in the Ocean: Satellite-Based Estimates over Two Decades. *Remote Sensing*, *12*(5), 826. https://doi.org/10.3390/rs12050826

Kwon, E. Y., Primeau, F., & Sarmiento, J. L. (2009). The impact of remineralization depth on the air–sea carbon balance. *Nature Geoscience*, *2*(9), 630–635. https://doi.org/10.1038/ngeo612

Lacour, L., Briggs, N., Claustre, H., Ardyna, M., & Dall'Olmo, G. (2019). The Intraseasonal Dynamics of the Mixed Layer Pump in the Subpolar North Atlantic Ocean: A Biogeochemical-Argo Float Approach. *Global Biogeochemical Cycles*, *33*(3), 266–281. https://doi.org/10.1029/2018GB005997

Lacour, L., Llort, J., Briggs, N., Strutton, P. G., & Boyd, P. W. (2023). Seasonality of downward carbon export in the Pacific Southern Ocean revealed by multi-year robotic observations. *Nature Communications*, *14*(1), 1278. https://doi.org/10.1038/s41467-023-36954-7

Formatted: Left

Laget, M., Drago, L., Panaïotis, T., Kiko, R., Stemmann, L., Rogge, A., Llopis-Monferrer, N., Leynaert, A., Irisson, J.-O., & Biard, T. (2024). Global census of the significance of giant mesopelagic protists to the marine carbon and silicon cycles. *Nature Communications*, *15*(1), 3341. https://doi.org/10.1038/s41467-024-47651-4

Lampitt, R. S., Briggs, N., Cael, B. B., Espinola, B., Hélaouët, P., Henson, S. A., Norrbin, F., Pebody, C. A., & Smeed, D. (2023). Deep ocean particle flux in the Northeast Atlantic over the past 30 years: Carbon sequestration is controlled by ecosystem structure in the upper ocean. *Frontiers in Earth Science*, *11*, 1176196. https://doi.org/10.3389/feart.2023.1176196

Le Quéré, C., Andrew, R. M., Canadell, J. G., Sitch, S., Korsbakken, J. I., Peters, G. P., Manning, A. C., Boden, T. A., Tans, P. P., Houghton, R. A., Keeling, R. F., Alin, S., Andrews, O. D., Anthoni, P., Barbero, L., Bopp, L., Chevallier, F., Chini, L. P., Ciais, P., … Zaehle, S. (2016). Global Carbon Budget 2016. *Earth System Science Data*, *8*(2), 605–649. https://doi.org/10.5194/essd-8-605-2016

Legendre, L. (2024). Jigsaw puzzle of the interwoven biologically-driven ocean carbon pumps. *Progress in Oceanography*, *229*, 103338. https://doi.org/10.1016/j.pocean.2024.103338

~~Lévy, M., Estublier, A., & Madec, G. (2001). Choice of an advection scheme for biogeochemical models. *Geophysical Research Letters*, *28*(19), 3725–3728. https://doi.org/10.1029/2001GL012947~~

Lemaitre, N., Planquette, H., Planchon, F., Sarthou, G., Jacquet, S., García-Ibáñez, M. I., Gourain, A., Cheize, M., Monin, L., André, L., Laha, P., Terryn, H., & Dehairs, F. (2018). Particulate barium tracing of significant mesopelagic carbon remineralisation in the North Atlantic. *Biogeosciences*, *15*(8), 2289–2307. https://doi.org/10.5194/bg-15-2289-2018

Lévy, M., Bopp, L., Karleskind, P., Resplandy, L., Ethe, C., & Pinsard, F. (2013). Physical pathways for carbon transfers between the surface mixed layer and the ocean interior. *Global Biogeochemical Cycles*, *27*(4), 1001–1012. https://doi.org/10.1002/gbc.20092

Lindeman, R. L. (1942). *The Trophic-Dynamic Aspect of Ecology*.

~~Lomas, M. W., Steinberg, D. K., Dickey, T., Carlson, C. A., Nelson, N. B., Condon, R. H., & Bates, N. R. (2010). Increased ocean carbon export in the Sargasso Sea linked to climate variability is countered by its enhanced mesopelagic~~

Formatted: Left

attenuation. *Biogeosciences*, *7* Bulletin of Mathematical Biology, 53(1), 57–70. https://doi.org/10.5194/bg-7-57-2010167-191.

Madec, G. (2008). *NEMO ocean engine* (27) [Project Report]. Institut Pierre-Simon Laplace (IPSL). https://eprints.soton.ac.uk/64324/

Margalef, R. (1978). Life-forms of phytoplankton as survival alternatives in an unstable environment. *Oceanologica Acta*, *1*(4), 493–509.

Marinov, I., Gnanadesikan, A., Sarmiento, J. L., Toggweiler, J. R., Follows, M., & Mignone, B. K. (2008). Impact of oceanic circulation on biological carbon storage in the ocean and atmospheric *p* CO_2. *Global Biogeochemical Cycles*, *22*(3), 2007GB002958. https://doi.org/10.1029/2007GB002958

Marsay, C. M., Sanders, R. J., Henson, S. A., Pabortsava, K., Achterberg, E. P., & Lampitt, R. S. (2015). Attenuation of sinking particulate organic carbon flux through the mesopelagic ocean. *Proceedings of the National Academy of Sciences*, *112*(4), 1089–1094. https://doi.org/10.1073/pnas.1415311112

Martin, J. H., Knauer, G. A., Karl, D. M., & Broenkow, W. W. (1987). VERTEX: Carbon cycling in the northeast Pacific. *Deep Sea Research Part A. Oceanographic Research Papers*, *34*(2), 267–285. https://doi.org/10.1016/0198-0149(87)90086-0

Mayor, D. J., Gentleman, W. C., & Anderson, T. R. (2020). Ocean carbon sequestration: Particle fragmentation by copepods as a significant unrecognised factor?: Explicitly representing the role of copepods in biogeochemical models may fundamentally improve understanding of future ocean carbon storage. *BioEssays*, *42*(12), 2000149. https://doi.org/10.1002/bies.202000149

Mayor, D. J., Sanders, R., Giering, S. L. C., & Anderson, T. R. (2014). Microbial gardening in the ocean's twilight zone: Detritivorous metazoans benefit from fragmenting, rather than ingesting, sinking detritus: Fragmentation of refractory detritus by zooplankton beneath the euphotic zone stimulates the harvestable production of labile and nutritious microbial biomass. *BioEssays*, *36*(12), 1132–1137. https://doi.org/10.1002/bies.201400100

Morel, A., Huot, Y., Gentili, B., Werdell, P. J., Hooker, S. B., & Franz, B. A. (2007). Examining the consistency of products derived from various ocean color sensors in open ocean (Case 1) waters in the perspective of a multi-sensor approach. Remote Sensing of Environment, 111(1), 69–88.

Formatted: Left

~~Mouw, C. B., Barnett, A., McKinley, G. A., Gloege, L., & Pilcher, D. (2016a 10 20). Global ocean particulate organic carbon flux merged with satelliteparameters. *Earth System Science Data*, *8*(2), 531–541. https://doi.org/10.5194/essd-8-531-2016~~

Mouw, C. B., Barnett, A., McKinley, G. A., Gloege, L., & Pilcher, D. (10/2016b). Phytoplankton size impact on export flux in the global ocean. *Global Biogeochemical Cycles*, *30*(10), 1542–1562. https://doi.org/10.1002/2015GB005355

NEMO System Team. (2019). *NEMO Ocean Engine* (No. 27; Version ~~v4~~v5.0, Scientific Notes of Climate Modelling Center). ~~Institut Pierre-Simon Laplace (IPSL).~~Zenodo. https://zenodo.org/doi/10.5281/zenodo.1464816

NEMO TOP Working. (2018). *TOP – Tracers in Ocean Paradigm – The NEMO Tracers engine*. https://doi.org/10.5281/ZENODO.1471700

Neukermans, G., Bach, L. T., Butterley, A., Sun, Q., Claustre, H., & Fournier, G. R. (2023). Quantitative and mechanistic understanding of the open ocean carbonate pump—Perspectives for remote sensing and autonomous in situ observation. *Earth-Science Reviews*, *239*, 104359. https://doi.org/10.1016/j.earscirev.2023.104359

~~Nowicki, M., DeVries, T., & Siegel, D.~~Oliver, S., Yool, A~~. (2022). Quantifying~~., Henson, S. A., & Martin, A. P. (2025). Where and When the Mesopelagic Carbon ~~Export and Sequestration Pathways of the Ocean's Biological Carbon Pump. *Global Biogeochemical Cycles*, *36*(3), e2021GB007083.~~Budget Balances, if at All. *Geophysical Research Letters*, *52*(7), e2024GL111667. https://doi.org/10.1029/~~2021GB007083~~2024GL111667

Ono, S., Ennyu, A., Najjar, R., & Bates, N. (1998). Shallow remineralization in the Sargasso Sea estimated from seasonal variations in oxygen, dissolved inorganic carbon and nitrate. *Deep Sea Research Part II: Topical Studies in Oceanography*, *48*(8–9), 1567–1582.

Palevsky, H. I., & Doney, S. C. (2018). How Choice of Depth Horizon Influences the Estimated Spatial Patterns and Global Magnitude of Ocean Carbon Export Flux. *Geophysical Research Letters*, *45*(9), 4171–4179. https://doi.org/10.1029/2017GL076498

Pomeroy, L. R. (1974). The Ocean's Food Web, A Changing Paradigm. *BioScience*, *24*(9), 499–504. https://doi.org/10.2307/1296885

Formatted: Left

Ricour, F., Guidi, L., Gehlen, M., DeVries, T., & Legendre, L. (2023). Century-scale carbon sequestration flux throughout the ocean by the biological pump. *Nature Geoscience*, *16*(12), 1105–1113. https://doi.org/10.1038/s41561-023-01318-9

Rodgers, K. B., Aumont, O., Toyama, K., Resplandy, L., Ishii, M., Nakano, T., Sasano, D., Bianchi, D., & Yamaguchi, R. (2024). Low-latitude mesopelagic nutrient recycling controls productivity and export. *Nature*, *632*(8026), 802–807. https://doi.org/10.1038/s41586-024-07779-1

Sathyendranath, S., Brewin, R., Brockmann, C., Brotas, V., Calton, B., Chuprin, A., Cipollini, P., Couto, A., Dingle, J., Doerffer, R., Donlon, C., Dowell, M., Farman, A., Grant, M., Groom, S., Horseman, A., Jackson, T., Krasemann, H., Lavender, S., … Platt, T. (2019). An Ocean-Colour Time Series for Use in Climate Studies: The Experience of the Ocean-Colour Climate Change Initiative (OC-CCI). *Sensors*, *19*(19), 4285. https://doi.org/10.3390/s19194285

Sauzède, R., Claustre, H., Uitz, J., Jamet, C., Dall'Olmo, G., D'Ortenzio, F., Gentili, B., Poteau, A., & Schmechtig, C. (2016). A neural network-based method for merging ocean color and Argo data to extend surface bio-optical properties to depth: Retrieval of the particulate backscattering coefficient. *Journal of Geophysical Research: Oceans*, *121*(4), 2552–2571. https://doi.org/10.1002/2015JC011408

Siegel, D. A., DeVries, T., Cetinić, I., & Bisson, K. M. (2023). Quantifying the Ocean's Biological Pump and Its Carbon Cycle Impacts on Global Scales. *Annual Review of Marine Science*, *15*(1), 329–356. https://doi.org/10.1146/annurev-marine-040722-115226

Steinberg, D. K., & Landry, M. R. (2017). Zooplankton and the Ocean Carbon Cycle. *Annual Review of Marine Science*, *9*(1), 413–444. https://doi.org/10.1146/annurev-marine-010814-015924

Stemmann, L., & Boss, E. (2012). Plankton and Particle Size and Packaging: From Determining Optical Properties to Driving the Biological Pump. *Annual Review of Marine Science*, *4*(1), 263–290. https://doi.org/10.1146/annurev-marine-120710-100853

Stemmann, L., Jackson, G. A., & Gorsky, G. (~~7~~2004a). A vertical model of particle size distributions and fluxes in the midwater column that includes biological and physical processes—Part II: Application to a three year survey in the

Formatted: Left

NW Mediterranean Sea. *Deep Sea Research Part I: Oceanographic Research Papers*, *51*(7), 885–908. https://doi.org/10.1016/j.dsr.2004.03.002

Stemmann, L., Jackson, G. A., & Ianson, D. (~~7~~/2004b). A vertical model of particle size distributions and fluxes in the midwater column that includes biological and physical processes—Part I: Model formulation. *Deep Sea Research Part I: Oceanographic Research Papers*, *51*(7), 865–884. https://doi.org/10.1016/j.dsr.2004.03.001

Stukel, M. R., Ohman, M. D., Kelly, T. B., & Biard, T. (2019). The Roles of Suspension-Feeding and Flux-Feeding Zooplankton as Gatekeepers of Particle Flux Into the Mesopelagic Ocean in the Northeast Pacific. *Frontiers in Marine Science*, *6*, 397. https://doi.org/10.3389/fmars.2019.00397

Sverdrup, H. U. (1953). On Conditions for the Vernal Blooming of Phytoplankton. *ICES Journal of Marine Science*, *18*(3), 287–295. https://doi.org/10.1093/icesjms/18.3.287

Takeuchi, M., Doubell, M. J., Jackson, G. A., Yukawa, M., Sagara, Y., & Yamazaki, H. (2019). Turbulence mediates marine aggregate formation and destruction in the upper ocean. *Scientific Reports*, *9*(1), 16280. https://doi.org/10.1038/s41598-019-52470-5

Tsujino, H., Urakawa, S., Nakano, H., Small, R. J., Kim, W. M., Yeager, S. G., Danabasoglu, G., Suzuki, T., Bamber, J. L., Bentsen, M., Böning, C. W., Bozec, A., Chassignet, E. P., Curchitser, E., Boeira Dias, F., Durack, P. J., Griffies, S. M., Harada, Y., Ilicak, M., … Yamazaki, D. (2018). JRA-55 based surface dataset for driving ocean–sea-ice models (JRA55-do). *Ocean Modelling*, *130*, 79–139. https://doi.org/10.1016/j.ocemod.2018.07.002

Uchimiya, M., Fukuda, H., Wakita, M., Kitamura, M., Kawakami, H., Honda, M. C., Ogawa, H., & Nagata, T. (2018). Balancing organic carbon supply and consumption in the ocean's interior: Evidence from repeated biogeochemical observations conducted in the subarctic and subtropical western North Pacific. *Limnology and Oceanography*, *63*(5), 2015–2027. https://doi.org/10.1002/lno.10821

Uitz, J., Claustre, H., Morel, A., & Hooker, S. B. (2006). Vertical distribution of phytoplankton communities in open ocean: An assessment based on surface chlorophyll. *Journal of Geophysical Research: Oceans*, *111*(C8), 2005JC003207. https://doi.org/10.1029/2005JC003207

Formatted: Left

Uitz, J. U., Huot, Y., Bruyant, F., Babin, M., & Claustre, H. (2008). Relating phytoplankton photophysiological properties to community structure on large scales. *Limnology and Oceanography*, *53*(2), 614–630. https://doi.org/10.4319/lo.2008.53.2.0614

Vancoppenolle, M., Fichefet, T., Goosse, H., Bouillon, S., Madec, G., & Maqueda, M. A. M. (2009). Simulating the mass balance and salinity of Arctic and Antarctic sea ice. 1. Model description and validation. *Ocean Modelling*, *27*(1–2), 33–53. https://doi.org/10.1016/j.ocemod.2008.10.005

Villa-Alfageme, M., De Soto, F. C., Ceballos, E., Giering, S. L. C., Le Moigne, F. A. C., Henson, S., Mas, J. L., & Sanders, R. J. (2016). Geographical, seasonal, and depth variation in sinking particle speeds in the North Atlantic. *Geophysical Research Letters*, *43*(16), 8609–8616. https://doi.org/10.1002/2016GL069233

Volk, T., & Hoffert, M. I. (1985). Ocean Carbon Pumps: Analysis of Relative Strengths and Efficiencies in Ocean-Driven Atmospheric CO_2 Changes. In E. T. Sundquist & W. S. Broecker (Eds~~.~~), *Geophysical Monograph Series* (pp. 99–110). American Geophysical Union. https://doi.org/10.1029/GM032p0099

Walker, B. D., Beaupré, S. R., Guilderson, T. P., McCarthy, M. D., & Druffel, E. R. M. (2016). Pacific carbon cycling constrained by organic matter size, age and composition relationships. *Nature Geoscience*, *9*(12), 888–891. https://doi.org/10.1038/ngeo2830

Walker, S. L., & Palevsky, H. I. (2025). Ocean carbon export flux projections in CMIP6 Earth System Models across multiple export depth horizons. *Global Biogeochemical Cycles*, 39(4), e2024GB008329.

Wang, B., & Fennel, K. (2022). Biogeochemical-Argo data suggest significant contributions of small particles to the vertical carbon flux in the subpolar North Atlantic. *Limnology and Oceanography*, *67*(11), 2405–2417. https://doi.org/10.1002/lno.12209

Wang, B., & Fennel, K. (2024). Distinct sources of uncertainty in simulations of the ocean biological carbon pump at different depths. *Communications Earth & Environment*, *5*(1), 395. https://doi.org/10.1038/s43247-024-01561-x

Weber, T., Cram, J. A., Leung, S. W., DeVries, T., & Deutsch, C. (2016). Deep ocean nutrients imply large latitudinal variation in particle transfer efficiency. *Proceedings of the National Academy of Sciences*, *113*(31), 8606–8611. https://doi.org/10.1073/pnas.1604414113

Formatted: Left

Wilson, J. D., Andrews, O., Katavouta, A., De Melo Viríssimo, F., Death, R. M., Adloff, M., Baker, C. A., Blackledge, B., Goldsworth, F. W., Kennedy-Asser, A. T., Liu, Q., Sieradzan, K. R., Vosper, E., & Ying, R. (2022). The biological carbon pump in CMIP6 models: 21st century trends and uncertainties. *Proceedings of the National Academy of Sciences*, *119*(29), e2204369119. https://doi.org/10.1073/pnas.2204369119

Formatted: Left, Space Before: 0 pt, Line spacing: single, Pattern: Clear

Formatted: Left